Spring 2018

Simultaneous enhancement of fluidity and thixotropy of vibration-free concrete

Piyush Rajendra Lunkad

SIMULTANEOUS ENHANCEMENT OF FLUIDITY AND THIXOTROPY OF VIBRATION-FREE CONCRETE

by

PIYUSH RAJENDRA LUNKAD

A THESIS

Presented to the Faculty of the Graduate School of the

MISSOURI UNIVERSITY OF SCIENCE AND TECHNOLOGY

In Partial Fulfillment of the Requirements for the Degree

MASTER OF SCIENCE IN CIVIL ENGINEERING

2018

Approved by

Dr. Dimitri Feys, Advisor
Dr. Kamal H. Khayat
Dr. Aditya Kumar

ABSTRACT

This research articulates the development of a vibration-free concrete for slip-form paving enabling a simple and rapid construction process. To achieve this, properties such as rheology including thixotropy, shape stability, and workability loss with time are mainly investigated. Concrete mixture with high thixotropic strength and its shape holding ability, flowability, and workability retention with time is evaluated. This study consists of two phases: (1) selection of paste component from rheology of cement paste incorporating various micro- and nano- sized particles (2) study of fresh properties of concrete mixtures using the excess paste layer concept.

From the cement paste study, it has been concluded that the structural build-up method provides a better understanding to assess the thixotropy development. A water-to-binder (w/b) ratio of 0.35 and PCE based superplasticizer were selected. The results showed that materials such as silica fume, slag and attapulgite clay are considered effective binder materials showing higher thixotropic build-up compared to other materials.

In the development of VFC, on decreasing the paste layer thickness, the workability loss increases and thixotropy development decreases significantly, which can mostly likely be attributed to the dispersing admixture. The binary concrete mixtures incorporating attapulgite clay showed low workability loss resulting consistent thixotropic buildup in early and extended time period. The ternary mixture with slag and attapulgite clay showed high thixotropic buildup suitable for the early and extended transportation time. The dosage of superplasticizer controls the workability loss but also affects the structural build up rate or thixotropy in both the cement paste and concrete mixture incorporating SCMs and mineral fillers.

ACKNOWLEDGEMENT

My profound thanks to my advisor Dr. Dimitri Feys, for benefactioning me with the opportunity to participate in a very unique and interesting research project which added valuable information to my knowledge and experience. I am also grateful for his patient guidance, valuable suggestions, time and enormous encouragement, which made my graduate experience at Missouri S&T more meaningful and exploring.

I would like to express my gratitude towards RE-CAST for the financial support of this project.

I would like to thank my committee members Dr. Kamal H. Khayat and Dr. Aditya Kumar for their scrutiny, over my project and improving my thesis wherever needed. Also, I would like to thank John Bullock, Jason Cox, Margarita Ley Hernandez, Andrew Bryde, Alexis Salinas, TJ Daniels, Arthur Graesser, Alexandra Wehar for helping on this research project. A big thanks to Daniel Galvez Moreno for his great guidance and significant assistance in this project.

I am very grateful to my Parents and beloved Uncle Mr. Hukmichand Lunkad for believing in me and my abilities, my brother and my sister in law for being so supportive and loving, and also my other all family members for their strong support and continuous encouragement throughout my years of study. This accomplishment would not have been possible without them. Cheers to my both nieces, nephew, siblings and friends for the entertainment in my life. Also, a big thanks to two wonderful personalities Anushka and Antriksh in my life. Love you all!

TABLE OF CONTENTS

Page

LIST OF FIGURES

Page

LIST OF TABLES

Page

1. INTRODUCTION

1.1 BACKGROUND

In today's developing transportation and infrastructure world, concrete roadways and pavements construction methods yielding faster, more durable and more economical pavement have always been widely appreciated by federal and state transportation authorities (or concrete paving industry). For instance, larger scale projects require accelerated construction processes in order to be profitable or to reduce negative economical impacts caused by traffic delays. Slip form paving originated in the 1940s in the Midwest, with production rates generally in the range of 65-100 m^3/hr [1]. Due to its higher production rate, lower labor requirement, and economy, compared to conventional fixed-form paving, it has been widely acclaimed as an efficient construction method in the modern concrete paving industry. Slip form pavers differ from conventional fixed form pavers as no fixed forms are required because slip form pavers have side forms moving with the machine.

Slip form paving is a continuous extrusion type process simultaneous involving the placement, consolidation, and finishing of fresh concrete. As shown in Figure 1.1, an auger spreads the pile of concrete in front of the strike off plate and the strike off plate bring the slab to its desired thickness or elevation by removing excess concrete. Then, concrete is consolidated by a series of vibrators (Figure 1.2) and a tamper forces large aggregate particle into the slab to prevent them from striking out from the surface. Finally, a slip form mold consists of a profile pan and a side form to level off the slab and to produce a finished surface. In this process, a concrete mixture is used with slump value less than 50 mm. Due to the lower workability of the mixture, an extensive amount of vibration energy is required to remove entrapped air during consolidation of the concrete. The vibration energy needs to be maintained to control the air void system

in order to provide resistance to freezing and thawing. The position of the vibrators, one next to another, is specific to overlap their influence zones by 50-75 mm [2].

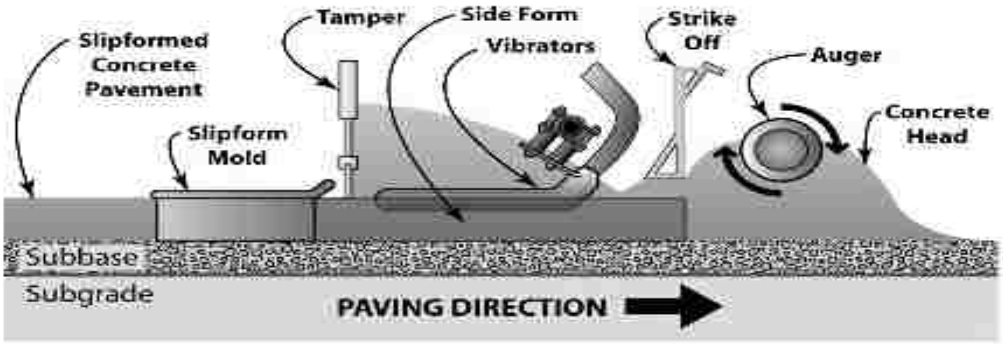

Figure 1.1 Slip form equipment setup [3]

Figure 1.2 Vibrators on the underside of a paving machine [4]

However, an improper setting of the vibration frequency leads to over-consolidation or insufficient consolidation of the concrete mixture and poor influence zones [2], [5]. The poor influence zones are observed as longitudinal trails along the finished pavement,

which are also called vibrator trails, as shown in Figure 1.3, spaced similarly to the vibrators spacing in the machine. This may also lead to a decrease in the entrained air content, as well as an increase in bleeding and segregation which may cause cracking along the vibrator trail under heavy traffic load [6]. In addition, a decrease in air content of fresh concrete makes hardened concrete susceptible to reduced freeze-thaw durability and scaling of pavement [5]. The scaling is also amplified by the action of the tamper, placed next to vibrators, due to its purpose to force the coarse aggregate below the surface and as such creating a mortar-rich surface [7].

Figure 1.3 Longitudinal vibrator trails [4]

To eliminate such problems, a concrete mixture requiring no vibration energy should be sufficiently flowable during the placement process and have stable shape after the extrusion process. Recently, large scale studies of the feasibility of a new type of self-consolidating concrete (SCC), or slip-form SCC (SFSCC), have been conducted by Iowa State University and Northwestern University.

1.2 WHAT IS SLIP-FORM SELF-CONSOLIDATING CONCRETE (SFSCC)?

The concept of SFSCC was originated from the development of SCC mixtures suitable for the slip form paving. SCC has gained a significant amount of interest from precast and cast-in-place construction industry due to its excellent flowability, stability (segregation and bleeding resistance), high production capacity and improved concrete surface quality. Wang et al. [8] indicated that flow behavior of SFSCC is between conventional slip form concrete and SCC. Conventional slip form concrete has good shape stability with less workability whereas regular SCC has excellent flowability with no shape stability. From the slump test results, it has been observed that potential SFSCC mixtures has slump value of approximately 200 mm and slump flow value is about 325-375 mm. Pekmezci et al. [9] indicated that SFSCC has the ability to self-consolidate and hold its shape with minimal consolidation energy. Moreover, in order to achieve the two conflicting phenomena of flowability and shape stability, concrete with acceptable stiffness and green strength has been developed [8]. Green strength is defined as the maximum stress that a fresh concrete can sustain until collapse. In a feasibility study for SFSCC [8], the rheological response of mixtures with various fine minerals (e.g. nano-clays), supplementary cementitious materials (SCMs) or chemical admixtures were studied to evaluate the workability and green strength development of SFSCC. It has been observed that rheological properties play a significant role in the follow-up study [10] for the selection of materials, the mix proportioning and understanding the flowability and green strength of SFSCC. In addition, to further validate the performance of the developed SFSCC, hardened properties should be comparable to those of conventional slip form pavement concrete in terms of strength, durability, and sustainability. The results indicated that properties such as heat of hydration, porosity, rapid chloride ion permeability and freeze-thaw durability were

comparable to those of conventional concrete, while properties such as compressive strength and shrinkage were more elevated than for the conventional concrete [10].

The field implementation conducted by Wang et al. [10] shows that SFSCC can be prepared in a batching plant. Wang et al. [10] proposed that modifications in the paver machine during the placement and extrusion process are required for the proper distribution of the SFSCC mixture along the width, and a horizontal leg to mold and hold the fresh concrete mixture for a sufficiently long duration until it develop adequate green strength. The field implementation study also shows on-site modifications of water and high-range water reducer (HRWR) agent to achieve target workability. This may be necessary to reduce a loss of workability with transport time and the influence of addition of other rheology-modifying agents. Thus, a focus of this research is to study the time dependent characteristics such as green strength development which can also be related to thixotropy development [8] and workability loss, to achieve a better understanding to develop concrete mixtures suitable for slip-form paving application.

1.3 OBJECTIVES

The final goal of this research project is to develop a vibration-free concrete (VFC) with balanced flowability and shape stability (green strength) for slip form paving without any consolidation energy. In the development of VFC, flowability, thixotropy, structural buildup, and workability loss will be focused upon, to assess the suitability of the mixture. Detailed objectives of the research are explained below:

- To investigate the influence of w/b ratio, superplasticizer (SP) type, SCMs and mineral fillers on factors such as instant structural build-up, high thixotropy rate, and workability loss in cement paste.

- To investigate the influence of excess paste layer thickness, binder materials and SP consumption on slip-form paving performance-based characteristics. While assuring a slump flow of 500 ± 50 mm to ease the concrete placement process with low workability loss and its immediate shape holding ability where fresh concrete can sustain its self-weight without any formwork support in slip-form paving.
- To obtain a correlation between static yield stress measurement and green strength test using Roussel and Coussot model.

1.4 SCOPE OF THESIS

This thesis is divided into four sections. Section two describes the rheology of the paste component of VFC including previous experimental work, the influence of mineral and chemical admixture on the rheology of paste and concrete component of SCC and SFSCC, the materials and experimental program adopted in this research task, and the analysis and conclusions. Similarly, section three focuses on the fresh properties of VFC. Section four discusses key hardened properties studied in this project. Section five concludes this thesis, providing a summary of important findings and recommendations for future work.

1.5 RESEARCH SIGNIFICANCE

It can be observed from the field application [10] of SFSCC, on-site modifications in mix proportion were conducted in order to achieve the targeted workability of the mixtures. This modification required due to loss of workability is difficult to control. For instance, in one of the field applications (bike path at the south 4thstreet, Ames, IA), even though after on-site addition of HRWR admixture and water,

the workability of mixture did not meet the selected criteria when the paving was executed [10]. This may have led to less consolidation and air entrapped at surface as mentioned by Wang et al. [10]. Moreover, the authors also recommended studying different admixtures to maintain or increase the yield stress to improve green strength as well as to provide better flowability during the extrusion process.

Hence, in this research, the development of a concrete mixture with high thixotropic strength and its shape holding ability, flowability, and workability retention with time imitating transportation and delivery practices will be determined. In addition, for a given application, this research can provide the understanding of the rheological properties of cement paste incorporating micro- and nano- sized particles and a new methodology to measure and quantify thixotropy.

2. PASTE COMPONENT OF VIBRATION-FREE CONCRETE (VFC)

This section describes briefly how the rheological parameters relating to the flowability and shape holding ability are important in the selection of constituent materials of SFSCC. In recent years, modifications in rheology, including thixotropy and structural breakdown of SCC, have been identified as effective parameters to obtain properties and characteristics required for the proposed application. For a slip form paving process, concrete mixtures with limited flowability and high green strength development, the yield stress can be related to the shape stability of concrete in a moving slip form [10]. During the mixing process, i.e. at high shear rates, concrete becomes more flowable due to a reduction in yield stress and viscosity. However, during the extrusion process, i.e. at low shear rates, concrete becomes less flowable and can develop green strength due to its thixotropic nature [8]. The thixotropic behavior of concrete has a significant role in the green strength development process. Therefore, rheological properties such as the steady state flow curve (dynamic properties) and thixotropy are mainly discussed.

In the subsequent sections, a literature review on measuring procedures for rheological properties and the influence of paste components on rheological properties is provided. Furthermore, the adopted experimental program and the obtained results are discussed in detail.

2.1 EVALUATION OF RHEOLOGICAL PROPERTIES

This section discusses the fundamentals of flow curve and thixotropy, and measurement techniques involved in obtaining those.

2.1.1 Flow Curve. The flow curve is an important measurement to understand the flow behavior of the material. The flow curve of a liquid material is obtained by

plotting shear stress versus shear rate [11]. A viscosity curve can also be plotted from these same data as a function of shear stress or shear rate. Typical flow curves of different types of fluids are shown in Figure 2.1.

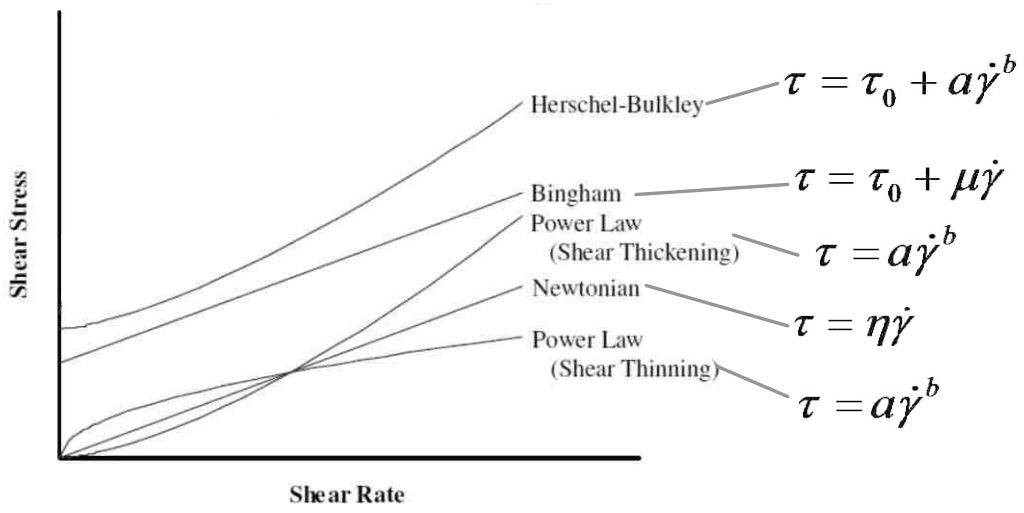

Figure 2.1 Typical flow curves of different fluids [12]

Cement paste or concrete materials are generally expressed by means of Bingham model in equation (2.1) i.e.

$$\tau = \tau o + \mu_p \dot{\gamma} \tag{2.1}$$

Where, τ = shear stress (Pa)

τ_o = dynamic yield stress (Pa)

μ_p = plastic viscosity (Pa s)

$\dot{\gamma}$ = shear rate (s^{-1})

The dynamic yield stress can be simply defined as the minimum stress to maintain or initiate flow and plastic viscosity is defined as the resistance to flow once the yield stress is exceeded. Therefore, the flow curve is typically plotted to calculate the dynamic properties of a liquid. The flow curve or viscosity can be determined by increasing or decreasing the shear rate and calculating the corresponding shear stress,

or vice versa. From the flow curve measurements, the values of the rheological parameters, dependent on the model employed, can be derived as a function of the rheometer geometry. As there is no standard procedure available to conduct rheological measurements, it is crucial to set shear rate wisely, corresponding to the shear rate the material will be subjected to in practice. Careful study of the limitations of the rheometer, its geometry, and each rheological model, should be conducted prior to the measurement and analysis of rheological data.

2.1.2 Thixotropy. Thixotropy can be defined as a decrease in viscosity under constant shear stress or shear rate while recovering the viscosity after the removal of shear stress or shear rate [13]–[19]. More details about thixotropy can be found in review articles [13], [20]–[22]. Thixotropic behavior exists in heterogeneous materials, cement paste is one of the examples. In cement paste, once cement particles come in contact with the water, flocs form rapidly and lead to the formation of a three dimensional networked structure [23]. During shearing, the flocs are broken and viscosity of the cement paste is decreasing. On the other hand, at rest, the (re-)formation of these flocs and consequent internal structure leads to a rebuild and viscosity of the cement paste increases with time. This reversible build-up of internal structure due to (de-)flocculation of cement particles is significant in cement particles with size up to 40 µm, according to J.E. Wallevik [24]. However, the reversible nature of cement pastes or concrete influenced by an additional time-dependent action i.e., hydration process. In other words, the reversible nature of cement or cementitious particle tends to decrease with time due to formation of a permanent structure. This formation of permanent connections due to strong flocculation or chemical reactions is referred to as workability loss [25], [26]. Overall, because of the change in microstructure due to (de-)flocculation and change in cement phases and products due to hydration with time, the

physical characterization of thixotropy of cement solely is difficult to perform with extended resting time.

A simple physical description of thixotropy was developed by Coussot [27] by means of an energy well concept as shown in Figure 2.2. In figure (a), cement particles are held together in a position with the smallest potential energy. When a small amount of external energy is applied to the materials or the suspension, the particle will move back to its original position, corresponding to elastic solid behavior. That is if ΔE is insufficient to move the particle outside the energy well as shown in (b). Whereas, when higher external energy, higher than the threshold value is applied, the particle will leave the energy well, as shown in (c) and flow will occur. For thixotropic behavior of cementitious materials, at rest, the depth of the energy well or the energy required to move the particle out of the well, increases with time due to Brownian motion, colloidal interactions, and the hydration mechanism. At last, as shown in figure (d), the depth of energy well varies with time due to thixotropy effect.

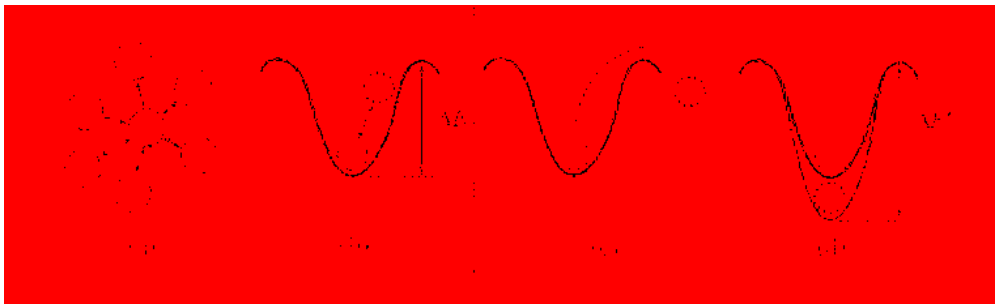

Figure 2.2 A simple physical description of thixotropic yield stress behavior of cementitious materials [27]

Ferron et al. [16] described the structural buildup phase as follows: In cementitious materials, structural buildup is directly related to reversible structural changes from thixotropy and irreversible structural changes due to hydration process and age of specimen. A significant buildup in structure was observed from hysteresis

loop measurements with increased resting time [16]. The particle size of cementitious materials is also an important factor in understanding of thixotropy and workability loss. The distinction of thixotropy, workability loss, and structural breakdown based on cement particle size is explained by J.E. Wallevik [24].

2.1.2.1 Measurement techniques. This part will give an overview of the most common methods used to measure thixotropy of cementitious materials.

2.1.2.1.1 Stepwise change in shear rate or shear stress. In this method, the sample is subjected to stepwise changes in shear rate or shear stress until the steady state or equilibrium state is reached [21]. Khayat et al. [17], [28]–[31] developed this method, also known as the structural breakdown area method, where variations of shear stresses over time were obtained at a given set of rotational speeds. The thixotropy is quantified by the difference between the maximum initial stress and shear stress at equilibrium for a given time duration. This difference of initial stress and equilibrium stress is an indication of the magnitude of structural modifications inside the material, as suggested by Lapasin et al. [32]. In this method, the initial peak yield stress (τ_i) corresponds to the initial structural condition and, with maintained shear rate, the shear stress decreases with time reaching equilibrium (τ_e). The structural breakdown area (A_b) is the area covered between initial stress values and equilibrium stress values for different rotational speeds, as shown in Figure 2.3. Ahari et al. [33] also used the structural breakdown area method to evaluate thixotropic properties of SCC mixtures containing various supplementary cementitious materials. In this method, two varying parameters, namely time and shear rate provide good understanding in analyzing thixotropic models [15], [21]. However, the value of the breakdown area has no physical meaning and the result is dependent on the measurement procedure employed [15].

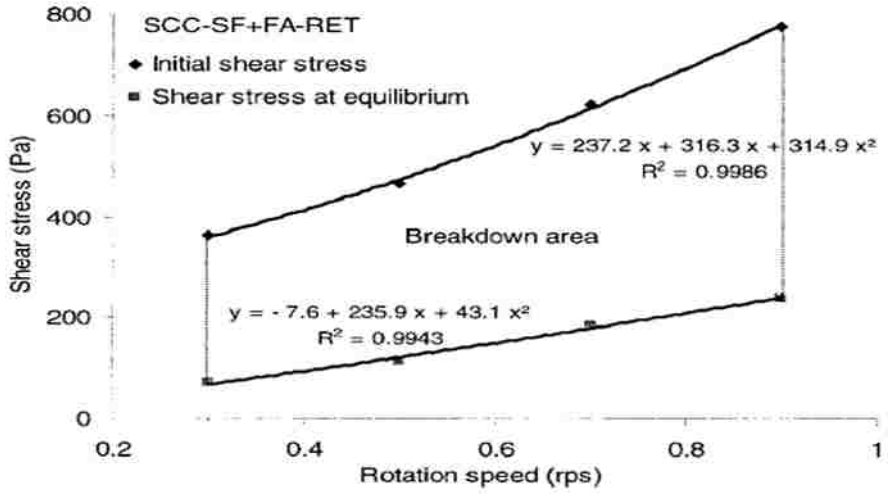

Figure 2.3 Determination of breakdown area obtained by initial torque responses at each rotational velocity and the equilibrium torque values [17]

2.1.2.1.2 <u>Hysteresis loop curve.</u> One of the more popular ways to quantify thixotropy of cement paste is to conduct a hysteresis loop test. In this method, a hysteresis loop is formed by increasing the shear rates and decreasing the shear rates as shown in Figure 2.4. The area enclosed by both the up and the down curve, as shown in Figure 2.5 relates to the energy required to break the flocculated structure and to measure thixotropy [13], [18], [21], [22]. However, the area and shape of the loop can vary significantly according to the material, shear history, and procedure [13], [15], [21], [22].

Roussel [18] stated that this method does not provide an intrinsic value of any physical rheological parameter. Barnes [13] and Mewis [21] also mentioned that the test procedure and response are both based on the chosen time and shear rate, making the outcome dependent on the procedure. More uncertainties and inaccuracies of hysteresis loop method have been explained in detail in [13], [15], [18], [21], [34].

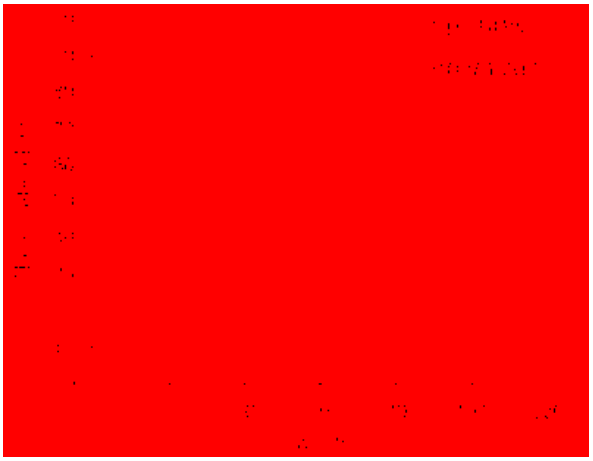

Figure 2.4 Shear rate history for hysteresis loop curve test [10]

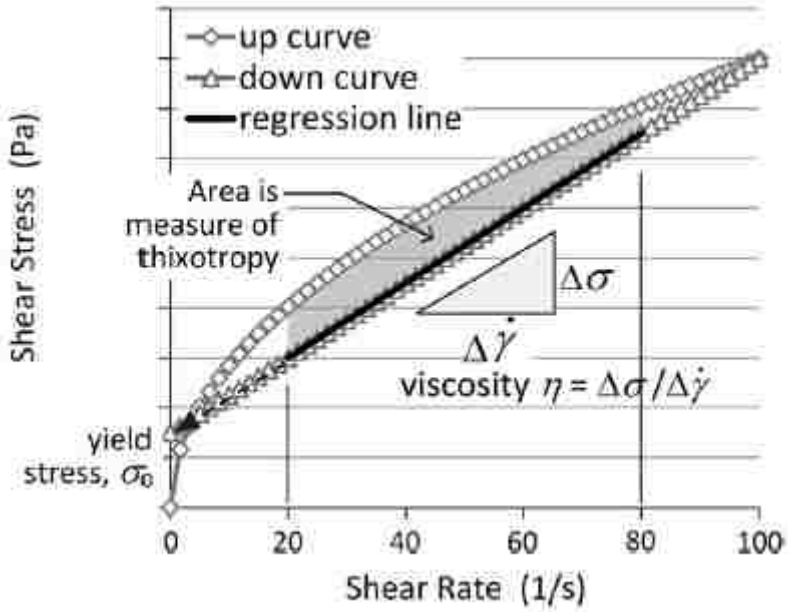

Figure 2.5 Cement paste hysteresis loop [10]

2.1.2.1.3 <u>Static yield stress measurement.</u> Thixotropy can be easily assessed by the increase in static yield stress with resting time due to build-up of structure in the material [15], [18], [22], [35]. To understand the influence of thixotropy on formwork pressure, multi-layer casting, and static stability, Roussel [18], [36] indicated that flocculation at rest is more important than de-flocculation under flow. Billberg [22] introduced a unique method to determine thixotropy of SCC by measuring the dynamic

rheology (flow curve) before and after the resting period and measuring static yield stress in every 10 min interval. This method separates the irreversible loss of workability from reversible thixotropic behavior. This phenomenon can also be explained by means of Figure 2.6 [22]. The static yield stress increases linearly under a resting condition, whereas the dynamic yield stress showed negligible change. Similar behavior was also observed by Ovarlez and Roussel.

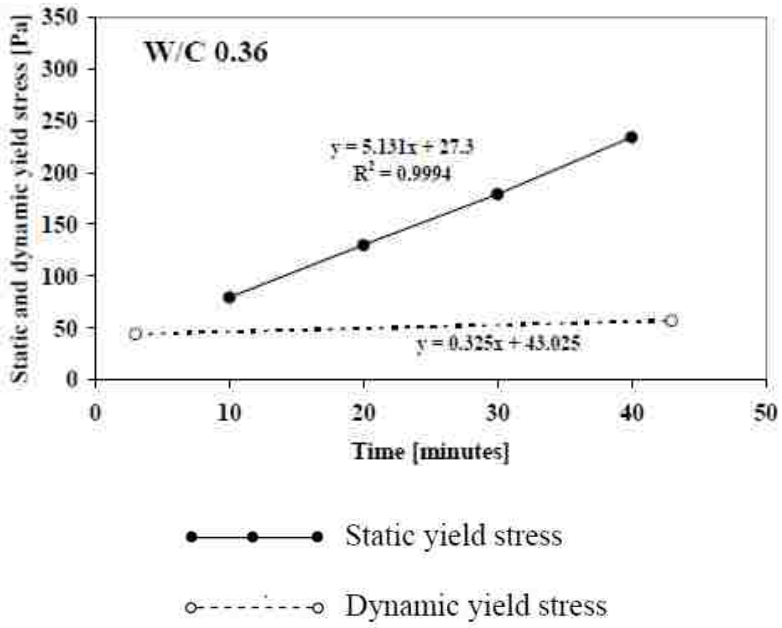

Figure 2.6 Linear increment in static yield stress over a time under a rest [22]

This linear increment in static yield stress of cement paste and flowable concrete is transformed into a simple equation by Roussel [18], in which, at rest, shear rate is zero and the growth of the apparent yield stress is according to the following equation (2.2).

$$\tau = \tau_0 + A_{thix} \cdot t \quad (2.2)$$

Where, τ = shear stress (Pa)

τ_0 = static yield stress (Pa)

A_{thix} = characteristic time for structuration of cement paste or concrete (Pa/s)

t = time (s)

2.1.3 Summary. In this section (Section 2.1), a brief background of thixotropy, workability loss and different measurement techniques to measure these properties was described. Thixotropy is the reversible nature of a material to deflocculate under shear and flocculate at rest. In cement paste or flowable concrete, the pure reversible nature of thixotropy, thus avoiding non-reversible aspects, is only visible for a relatively short duration after initial contact between cement and water. However, the evaluation of thixotropy is influenced by structural breakdown and workability loss with longer intervals or longer resting time due to the hydration process. Thus, the measurement of thixotropy of cement-based materials is significantly influenced by its microstructure changes induced by the shear history and hydration mechanism.

The three most commonly used techniques for measurement of thixotropy of cement-based materials were discussed. Firstly, applying a stepwise change in the shear rate was employed by Khayat and associates. However, the outcome is dependent on measurement parameters such as time of rest and difference between the rotational velocities. Secondly, the hysteresis loop method, one of the fastest and easiest measurement procedures, quantifies thixotropy by breakdown area. On the other hand, it is often dependent on shear history protocol. This might lead to erroneous and inconsistent interpretation of the data.

Thirdly, the structural buildup method, developed by Roussel and Billberg provides a better and simplified meaning of thixotropy, as it is characterized as an increase in static yield stress during rest. The influence of viscosity in the measurement process is considered negligible due to the very low shear rate applied. This method has been applied to study the influence of thixotropy on multi-layer casting and formwork pressure. On the other hand, as shape stability is required, the concrete mixture must develop a sufficiently high yield stress shortly after placement, to ensure it can withstand the stress generated by its own weight. Sufficient fluidity and high thixotropy are thus simultaneously required.

In this research, the development of a concrete having an excellent balance between the flowability during the placement and shape stability after the extrusion process without any consolidation energy is intended. In rheological terms, this can be reflected as follows: a mix with low initial yield stress to ease the placement procedure and significant thixotropic development shortly after the placement, to hold its own weight and shape is required. Thus, structural buildup determined with the increase in static yield stress method is an effective way to measure thixotropy and will be used for the selection of paste components for the VFC. More details about the measurement procedure are given in section 2.4**.**

2.2 INFLUENCE OF CONSTITUENT ELEMENTS ON RHEOLOGY INCLUDING THIXOTROPY

In this section, factors affecting the rheological properties of concrete are discussed in detail. The rheology of fresh concrete is mainly influenced by its constituent materials. In SFSCC, the thixotropic behavior of concrete has a significant role in the green strength development progress. It is well established in the literature that the rheological properties, including thixotropy, are strongly

dependent on a large number of factors, including cement content and binder composition [17], [37], water/binder (w/b) ratio [35-37], aggregate type and content [40] and the type and dosage of HRWR [38], [41] VMA [31], [42] or other chemical admixtures. Tattersall and Banfill [43] reported that the cement characteristics such as the packing density, fineness, and chemical composition have a significant role on thixotropy. All chemical admixtures, as well as a large number of supplementary cementitious materials, were reported to affect the rheological behavior of cement-based systems [33], [37], [44]. In addition, the influence of clays and nanoparticles on the rheological properties was also investigated recently [42-45]. Thus, for further selection of materials in the research task focusing on cement paste, it is very important and valuable to review previous studies focused on modifying the rheology by the incorporation of various mineral fillers and chemical admixtures.

2.2.1 Effect of Water to Binder Ratio (w/b). Topcu and Uygunoglu [38] investigated effect of different binders with varying w/b ratio and superplasticizer (SP) content on yield stress of self-consolidating mortar. They reported that yield stress decreases and flowability increases with an increase in w/b ratio and SP content. Billberg [22] has also reported that with an increase in w/b ratio from 0.34 to 0.42 the structural build-up, i.e. consequences of thixotropy, decreases by almost 80%. He mentioned that w/b ratio is related to the particle concentration and decreasing w/b lowers the interparticle distance, resulting in quicker structural build-up. Furthermore, Rahman et al. [37] stated that thixotropy increases with an increase in binder content when sand and coarse aggregate content is low. Also, w/b ratio influences the average distance between the particle and their interaction level, leading to increase in thixotropy with decrease in w/b ratio. Roby [49] indicated that an increase in w/b ratio increases the lubrication of cement paste and decreases the cohesiveness of the mixture.

Assad and Khayat [39], [50] further stated that mixtures with higher w/b ratio and lower coarse aggregate proportion show a reduction in internal friction and increase the mobility of the mixture, yielding higher initial lateral pressure and slower thixotropy development. Thus, it is obvious that on increasing w/b ratio, thixotropy of concrete mixture decreases.

2.2.2 Effect of Cement Properties. According to Nunes et al. [51], the workability is influenced by different cement deliveries and cement-superplasticizer interaction should be studied for different cement deliveries in SCC mixtures. The authors further mentioned that changes in rheological properties are mainly caused by differences in cement fineness and the sulphate amount of cement. Juvas et al. [52] reported the workability of mortars with superplasticizer is substantially more sensitive than for mortars without superplasticizer. Quanji [53] stated that cement pastes with high alkali content yield faster structural rebuilding rate potentially due to the increase in bond strength of particles by the pore solution chemistry. Also, it enhances prismatic crystal formation ability which enhances interlocking of microstructure and increases the structural rebuilding rate.

2.2.3 Effect of SCMs and Mineral Fillers. A small addition of nanoclay, which is a thixotropy enhancing material, has the ability to improve thixotropy [54] and shape stability [9], [45] of SFSCC. Wang et al. [10] studied the thixotropy of cement paste with an increase in attapulgite clay (0.5%, 1%, 2%, 3%), a nanoclay, using a hysteresis loop method. Results showed that increasing the amount of attapulgite clay increases thixotropic development with time. The addition of attapulgite clay also increased thixotropy of cement paste combined with fly ash or in presence of HRWR or AEA (air-entraining agent). Ferron et al. [16] mentioned that nano-sized particles create a more stable microstructure in concrete and work as a filler material by filling

the gaps between the cement particles. Quanji et al [47] showed that increase in dosage of attapulgite clay not only increased the yield stress and viscosity but also enhanced the thixotropy with time. This study also confirms the beneficial effect of nanoclay on thixotropy and the effective relationship between flow percent reduction and structural rebuilding of cement paste. It was concluded that the optimum dosage of nanoclay for the effective thixotropic behavior would be a 1.3% addition by mass of cement [47]. Many researchers attributed the influence of nanoclay on improvement of thixotropy due to its surface charge [47], ability to absorb water [47], irregular microstructure [54], smaller size [16], [47] and specific surface area [16]. However, Kawashima et al. [46] reported that nanoclay has immediate effect on thixotropy due to flocculation mechanism but, this effect diminishes over a time.

Hassan et al. [55] compared the influence of metakaolin (MK) and silica fume (SF) on the rheological properties of SCC. Their results indicated that the replacement of metakaolin (up to 25%) increased the plastic viscosity and yield stress significantly by 2.4 times and 3.2 times of the reference mixture respectively (at a constant HRWR dosage 3460 ml/m^3). They also reported that 8% SF had less effect on viscosity but, 8% SF had more influence on yield stress compared to 8% MK. Topcu and Uygunoglu [38] investigated the factors affecting the yield stress of self-consolidating mortar such as the addition of mineral additives, the water-to-binder (w/b) ratio, and the dosage of chemical admixture. Their results showed that when increasing the w/b and increasing the superplasticizer (SP) content, the yield stress decreased in self-consolidating mortars containing different mineral additives (limestone powder, waste marble powder, brick powder). Güneyisi and Gesoğlu [44] investigated the influence of binary and ternary mixtures using fly ash (FA) and MK on the rheology of self-compacting mortar. The addition of MK enhanced the viscosity while FA decreased the viscosity.

They also mentioned that combination of both FA and MK can be modified to achieve required yield stress and viscosity. The cement pastes studied by Wang et al. [8] showed that fly ash (class C and F) decreased the yield stress and viscosity compared to a mixture with 100% cement, whereas 30% slag replacement increased both the viscosity and yield stress. Rahman et al. [37] studied the thixotropic behavior of SCC containing mineral additives and SCMs such as limestone powder (LSP), silica fume (SF), and fly ash (FA) by means of the static yield stress method proposed by Roussel [18]. They found a significant increase in thixotropy (A_{thix}) with an increase in the amount of fly ash amount from 5% to 10% whereas silica fume showed the opposite trend. LSP had less impact on thixotropy. All binary mixtures in the study [37] showed higher thixotropy index than the reference SCC mix because of higher fineness and structuration rate.

Rahman et al. [37] further showed that A_{thix} can be used to determine the suitability of mix designs for particular SCC applications. SF mixtures could be applied for horizontal construction and FA mixtures could be selected for the construction of walls. Assaad and Khayat [17] investigated the thixotropic and rheological properties of SCC using silica fume (SF), fly ash (FA) and blast furnace slag (BFS). They reported that binary (PC + SF), ternary (PC + SF + FA) and quaternary systems (PC+SF+BFS+FA) showed lower plastic viscosity and higher thixotropy values compared to plain SCC mix during the initial 30 min. Later, after re-mixing a decrease in thixotropy was noticed in the quaternary mixture until 150 min. They also reported that mixtures incorporating more cementitious materials and low aggregate contents displayed lower thixotropy values. Lately, Ahari et al. [33] reported that SCMs such as FA and MK led to an increase in plastic viscosity irrespective of the w/b ratio, whereas SF and BFS led to decrease in plastic viscosity.

2.2.4 Effect of Chemical Admixtures. In this section, influence of chemical admixture such as superplasticizer and viscosity-modifying agent on rheology of paste and concrete component of SCC is discussed.

2.2.4.1 Effect of superplasticizer (SP). There are some research studies available regarding the influence of superplasticizer on the development of thixotropy. Ore et al. [56] have shown the limited influence of incorporating a water-reducing agent on thixotropy. However, Ferron et.al [16] reported that the use of superplasticizer for adoption of a lower w/c in pastes is the most effective method to enhance the rate of structural build-up. Billberg [22] found that electrostatic hindrance mechanism of melamine SP showed more structural buildup than steric hindrance mechanism of PCE (poly carboxylate ether)-SP. Adding a HRWRA to enhance workability was reported to increase formwork pressure and thus decrease thixotropy [49-50], while for a given slump, reducing w/c ratio by using HRWRA developed similar formwork pressure as that of concrete made without HRWRA [49-50]. Wang et al. [10] indicated that the addition of HRWR and AEA in cement paste made with FA and attapulgite clay decreases thixotropy and viscosity. Roussel et al. [36] have indicated that for a polycarboxylate-based superplasticizer, by increasing the amount of superplasticizer in the mixture, the structuration rate (A_{thix}) decreased.

2.2.4.2 Effect of viscosity modifying admixtures (VMA). Viscosity-enhancing admixtures are mostly used along with a high-range water reducing agents to control cohesiveness and increase the stability [59]. The thixotropic behavior of cement pastes is related to the interactions between solid particles and the water medium containing chemical admixtures such as HRWRA and VMA [37], [51-52]. Thixotropic properties were measured by considering the influence of HRWRA and VMA combinations on concrete-equivalent-mortar with equivalent fluidity and by

using a parallel plate rheometer [41]. Results [41] showed that powder or liquid polysaccharide-based VMAs develop greater initial static shear stress needed to breakdown the structure after resting time compare to cellulose-based VMA. On the other hand, a higher degree of flocculation has been reported in mixtures containing combinations of VMA with naphthalene-based HRWRA compared to combinations of VMA with polycarboxylate-based HRWRA [41]. In addition, Assaad and Khayat [39] indicated that in SCC made with w/b of 0.36 and ternary cement (6% silica fume, 22% Class F fly ash, and 72% Type 10 (GU) portland cement), combining cellulose based VMA with PCE-HRWRA led to higher thixotropy compared to mixtures containing polysaccharide-based VMA and poly-naphthalene sulfonate (PNS) HRWRA.

Assad and Khayat [31] concluded that combination of cellulose-based VMA along with polycarboxylate-based HRWRA increased the degree of thixotropy of SCC compared to mixtures containing powder or liquid polysaccharide-based VMA and naphthalene-based HRWRA. However, the SCC mixtures containing cellulose-based VEA with polycarboxylate-based HRWRA showed a lower rate of increase in thixotropy with time due to its fluidity retention property [31]. Van der Vurst et al. [61] investigated the influence of four different VMAs (attapulgite clay, diutan gum, corn starch, and propylene carbonate) on the robustness of SCC mortars. Their results showed that maximum robust yield stress was found in mixtures without VMA and mixtures with attapulgite clay. Also, diutan gum had highest plastic viscosity while attapulgite clay and corn starch displayed no effect on the plastic viscosity. Helnan-Moussa et.al [60] presented a semi-empirical procedure to evaluate the structural breakdown of fresh cement pastes with different amounts of viscosity-modifying admixture (VMA). A stepwise decreasing shear rate sequence has been applied after a constant high pre-shear. Results indicated that, beyond a maximum value of VMA,

cement pastes form tri-dimensional networks that are significantly flocculated and thus show more difficulty to deflocculate by shearing [60].

2.2.5 Summary. Thixotropy decreases with an increase in w/b ratio due to less interparticle interactions. The cement-superplasticizer interaction should be investigated for different deliveries or sources of cement. Various SCMs and nanomaterials have been used in the past to improve the rheology of SCC mixtures for formwork pressure, pumping, cast-in place, and slip form paving applications. The physical and chemical characteristics of the incorporated micro- or nano-sized fillers play an important role in attributing the influence of materials to the development of rheological properties. Nanoclays, such as attapulgite clay, turned out as very effective thixotropy enhancing materials having good shape stability and fluidity.

Material such as fly ash, silica fume, metakaolin and limestone dust show no proper trend with thixotropy development, which may be due to factors such as different physical and chemical properties of the materials, replacement rate employed, intended application, and method or model used for analyzing the rheology of a mixture. The performance of SCMs and mineral fillers also changes with the addition of different types of chemical admixtures. In general, the study of SCMs and nanoparticles is also advantageous for reducing concrete production cost without sacrificing its fresh and hardened properties. More details about materials and methods can be found in the next section.

2.3 EXPERIMENTAL PROGRAM

The workability of vibration-free concrete (VFC) for slip-form paving must be close to self-consolidating to ensure a proper compaction and to minimize the entrapped air content. On the other hand, as shape stability is required, the concrete mixture must

develop a sufficiently high yield stress shortly after placement, to ensure it can withstand its own weight. Sufficient fluidity and high thixotropy are thus simultaneously required. To minimize material use, as the origin of thixotropy lies in the cement paste, and as aggregates are generally considered to amplify the rheological properties of the paste, the first task of this research is performed on paste level.

2.3.1 Materials and Methods. In this section, physical and chemical properties of materials employed, mixture design, and testing procedures are discussed in detail.

2.3.1.1 Cement, SCMs, and mineral fillers. The chemical composition and physical properties of all materials such as cement, SCMs, and mineral fillers employed to investigate their suitability for VFC for slip forming are listed below in Table 2.1.

2.3.1.2 Dispersing admixture. Two commercially available dispersing admixtures (SP) were employed: one polycarboxylate-based (PCE) having density of 1.03 g/cm^3 and with solid content of 35.2% and one polynaftalene-based (PNS) superplasticizer having density of 1.20 g/cm^3 with solid content of 55%. The dosage of the admixture was varied to assure a mini-slump flow diameter of 300 ± 20 mm.

2.3.2 Mix Design and Mixing Procedure. The investigation on the cement pastes was divided into two subtasks. For both dispersing admixtures, the influence of w/b was evaluated, in absence of any SCM or filler. Consecutively, the PCE dispersant and a w/b = 0.35 was retained for the investigation on the SCMs and fillers.

2.3.2.1 Mix design. Table 2.2 represents the mix designs evaluated. All cement pastes were prepared in a small Hobart mixer. The volume of cement paste produced is 750 ml for each mixture. The replacement of SCMs and mineral fillers by percentage mass of cement can be seen in first column.

2.3.2.2 Mixing procedure. All mixtures were prepared in a small Hobart mixer. Table 2.3 shows the different steps in the procedure, in which mixing and

Table 2.1 Chemical and physical properties of cement, SCMs, and mineral fillers

Basic compounds (%)	Cement (REF)	Cement-(REF-New)	Slag (SL)	Fly ash (FA)	Silica fume (SF)	Meta-kaolin (MK)	Kaolin (Ka)	Attapulgite clay (AC)
Na_2O	-	-	-	3.28	0.03	0.05	-	0.39
MgO	2.77	1.46	8.10	7.93	0.43	0.29	0.36	10.30
Al_2O_3	3.35	3.53	6.84	17.47	0.81	42.90	40.05	11.60
SiO_2	16.68	17.34	34.69	37.56	96.98	53.45	53.05	63.93
SO_3	3.25	3.40	2.19	-	0.32	0.23	0.52	0.35
K_2O	0.57	0.58	0.37	-	0.73	0.14	0.09	0.65
CaO	69.01	69.63	45.70	25.33	0.29	0.02	0.02	5.84
TiO_2	0.25	0.26	0.47	1.42	-	2.18	3.21	0.65
Mn_2O_3	0.17	0.06	0.74	-	0.01	-	-	0.08
Fe_2O_3	3.62	3.47	0.55	7.02	0.11	0.56	2.04	5.02
Specific gravity	3.17	3.16	2.90	2.95	2.39	2.68	2.94	2.29
Mean particle size (μm)	15.4	14.5	14.2	13.5	0.35	1.31[1]	0.3[1]	0.3[1]

[1] *It should be noted that mean particle size obtained from commercially available data*

Table 2.2 Mix designs of investigated cement pastes (in grams 750 ml of paste)

Paste	Cement	Water	SCM	Dispersant	w/b
PCE 0.30	1218	365		PCE: 4.4	0.30
PCE 0.35	1126	394		PCE: 3.0	0.35
PCE 0.40	1048	419		PCE: 2.0	0.40
PCE 0.45	979	441		PCE: 1.5	0.45
PNS 0.30	1218	365		PNS: 12.2	0.30
PNS 0.35	1126	394		PNS: 8.8	0.35
PNS 0.40	1048	419		PNS: 4.1	0.40
PNS 0.45	979	441		PNS: 2.2	0.45
FA-C 25	838	391	Fly ash: 279	PCE: 1.9	0.35
Slag 25	836	390	Slag: 279	PCE: 2.6	0.35
LF 10	1006	391	Limestone: 112	PCE: 2.8	0.35
SF 5	1062	391	Silica fume: 56	PCE: 4.9	0.35
MK 25	827	386	Metakaolin: 276	PCE: 11.2	0.35
Ka 1	1115	394	Kaolin: 11	PCE: 3.6	0.35
NS 1	1114	394	Nanosilica: 11	PCE: 6.1	0.35
AC 0.5	1120	394	Attapulgite clay*[2]: 6	PCE: 10.7	0.35
SL 25 – SF 5	774	387	Slag: 277 Silica fume: 55	PCE: 4.0	0.35

[2] *It should be noted that the Attapulgite clay is delivered in slurry form. The reported values are the mass of active ingredient. The added water of the mixture has been compensated for the water in the slurry. The amount of water reported is the total amount of water in the cement paste.*

Table 2.2 Mix designs of investigated cement pastes (in grams 750 ml of paste) cont.

SL 25 – AC 0.5	830	390	Slag: 278 Attapulgite clay: 6	PCE: 9.8	0.35
SF 5 – AC 0.5	1055	391	Silica fume: 56 Attapulgite clay: 6	PCE: 23.3	0.35
SL 25 – SF 5 – AC 0.5	768	387	Slag: 276 Silica fume: 55 Attapulgite clay: 6	PCE: 14.9	0.35

scraping are altered to ensure the homogeneity of the sample. The contact time between cement and water is taken as the reference time. The starting time of the rheological measurements is relative to this reference time. The dispersing admixture (SP) is added in delayed fashion. The desired quantity is determined through preliminary tests, evaluating the mini-slump flow for different dosages.

Table 2.3 Mixing procedure

Time	Duration	Action	Addition
-0.5 min	30 s	Mixing	Dry materials
0 min	60 s	Mixing	Water
1 min	60 s	Scraping	
2 min	30 s	Mixing	
2.5 min	120 s	Mixing	SP
4.5 min	30 s	Scraping	
5 min	60 s	Mixing	

2.4 RHEOLOGY

In this section, the measurement procedures involved in evaluation of rheological properties and parameters considered in determination of thixotropy are discussed in detail.

2.4.1 Measurement Procedure. The rheological properties of the mixtures were evaluated with the Anton Paar MCR 302, in parallel plate configuration as shown in Figure 2.7. The plates are 50 mm in diameter and are sandblasted to minimize slip between the plates and the sample. The gap was maintained at 1 mm, and temperature was kept constant at 23°C. The temperature-controlling hood was placed on top of the system in an attempt to minimize the evaporation of water from the sample. Immediately after mixing and the evaluation of the mini-slump flow, a small sample of cement paste is placed on the paste is bottom plate. The lowering of the upper plate squeezes the sample in between both plates, filling up all space in between the plates. The edges of the plates were trimmed to avoid the edge effects.

The sample was evaluated using two different procedures: a flow curve, and static yield stress measurements at rest. The flow curve is measured by imposing a linearly decreasing shear rate with time, ranging from 100 s^{-1} to 5 s^{-1} in a 30 s timeframe (interval 2 in Figure 2.8). The flow curve is preceded by a 90 s pre-shear period, during which the shear rate is kept constant at 100 s^{-1} (interval 1 in Figure 2.8). This pre-shear is imposed to bring all samples to the same reference state (corresponding to this shear rate), in an attempt to eliminate the shear history (mixing, placing and rest) from the sample prior to the measurements. The flow curve is used to determine the dynamic yield stress and plastic viscosity (if the material obeys the Bingham model), or the modified Bingham model was imposed in case the sample was severely shear-thickening.

Figure 2.7 Anton Paar MCR 302 equipment

The static yield stress method is used to measure the thixotropy, but it shows sensitivity to the shear history. Yuan et al. [62] investigated the effect of different shear rate (0.001, 0.003, 0.005, 0.008, 0.01, and 0.02 s^{-1}) on static yield stress test. The authors concluded that 0.005 s^{-1} is a suitable shear rate for cement paste with and without HRWRA. Also, shear rates higher than 0.005 s^{-1} require less time to reach the peak value, potentially disturbing the structure of cement more. However, a low shear rate value of 0.001 s^{-1} requires significant time to reach the peak value and can influence the test results [62]. Thus, to determine the thixotropic properties, the sample was subjected to a constant shear rate of 0.005 s^{-1} (exaggerated in Figure 2.8). The corresponding shear stress evolution of the sample is monitored over a 60 s time period. When the thixotropic properties were evaluated immediately after obtaining the flow curve (interval 3 in Figure 2.8), a steady increase in shear stress is monitored. This increase in shear stress is a reflection of the thixotropic properties immediately after mixing. This thixotropic measurement is then repeated four times at 5 minute intervals, each time giving the sample 4 min rest while measuring the shear stress response in the 5^{th} minute (intervals 5, 7, 9 and 11 in Figure 2.8). For these profiles, as a larger static

yield stress is developed, the shear stress shows, potentially, a steep slope with time until it reaches a peak, followed by a descending curve. The first part of the curve corresponds to the elastic deformation, while the peak corresponds to the static yield stress: the stress needed to initiate flow after rest.

The pre-shear prior to the flow curve tests starts at 15 min after contact between water and cement. The first flow curve is determined between 16.5 and 17 min, and in the 17th, 22nd, 27th, 32nd and 37th minute, the stress response to a very small shear rate is determined, as discussed above. The entire procedure: pre-shear, flow curve and 5 thixotropy tests, is repeated on the same sample, 45 min after contact between cement and water. By comparing both flow curves at 15 and 45 min, an indication is given on the contribution of workability loss (mainly caused by strong C-S-H connections between the particles) to the stress development. Roussel et al. [19] reported that short

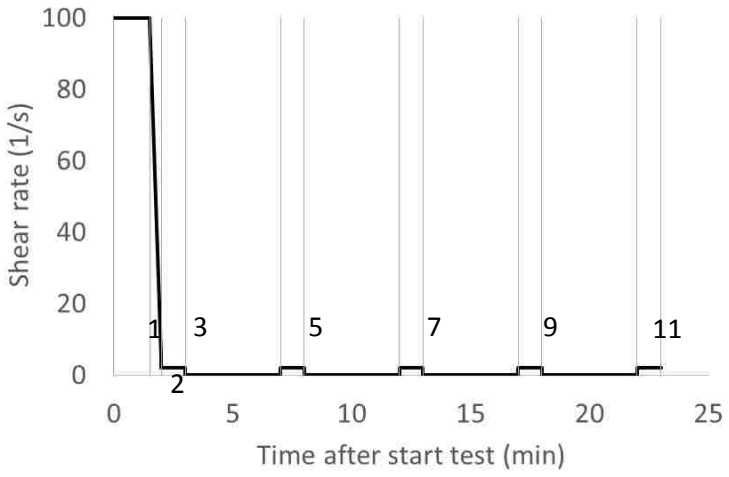

Figure 2.8 Shear rate profile. Interval 1 is the pre-shear, interval 2 represents the flow curve. During intervals 3, 5, 7, 9 and 11, the sample is sheared at 0.005 s^{-1} during 1 minute (the figure is exaggerated to enhance visibility). In between intervals 3, 5, 7, 9 and 11, the sample is at rest.

term (few seconds) thixotropy is due to initial colloidal flocculation while a long term thixotropy is due to continuing nucleation process of hydration products. For practical applications, the workability loss is less favorable in case of prolonged transportation times. Roussel et al. [19] further mentioned that C-S-H nucleation is the main driving factor in the development of thixotropy and hydration accelerating materials, such as silica fume and limestone filler, can be useful for the production of highly thixotropic concrete without any workability loss [19]. In this paper [19], cement pastes were not plasticized (paste with superplasticizer or dispersant), which may lead to enhanced precipitation of the hydrates and influence the development of thixotropy with the hydration accelerating material. However, in plasticized pastes, even in presence of hydration accelerating materials, the dissolution of ions and the precipitation of the hydration products may be slowed down and may affect the thixotropic build-up.

2.4.2 Determination of Rheological Properties. Figure 2.9 shows a typical result of the flow curve measurement. The measured torque (T) is expressed as a function of the angular velocity (Ω) as shown in equation (2.3) By means of a Reiner-Riwlin type of equation for parallel plate rheometers, the intercept of the T-Ω curve (G) is transformed into the yield stress, and the slope of the curve (L) can be used to calculate the viscosity (equations (2.4) and (2.5)).

$$T = G + L\Omega \tag{2.3}$$

$$\tau_o = \frac{3G}{2\pi R^3} \tag{2.4}$$

$$\mu_p = \frac{2HL}{\pi R^4} \tag{2.5}$$

τ_o = yield stress (Pa)

R = radius of plate (m)

μ_p = plastic viscosity (Pa s)

H = gap between the plates (m)

For the example shown below, the yield stress is 5.1 Pa, and the plastic viscosity is 0.72 Pa s at 15 min. The evolution of the obtained (dynamic) yield stress from 15 to 45 min is used to evaluate the workability loss of the mixture. Figure 2.10 shows the typical stress response at a constant shear rate of 0.005 s^{-1}, immediately measured after the flow curve. In total, 100 data points are determined in 60 s. The shear stress profile shows a continuously increasing shear stress with time, attributed to the restructuring of the material under very small shear. The average of the last 10 data points is taken as one of the parameters studied: it indicates how much yield stress the sample can develop immediately after shearing.

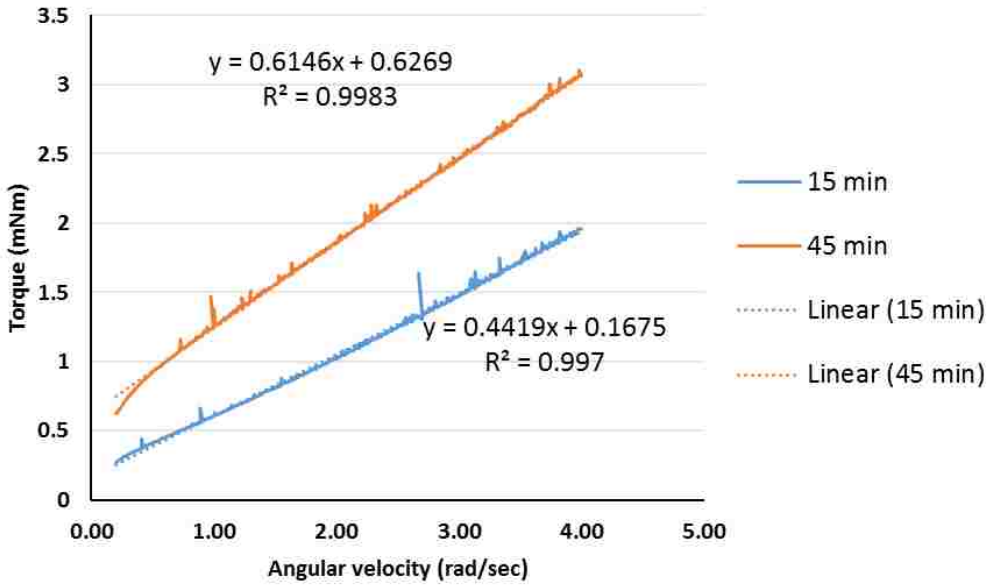

Figure 2.9 Flow curves at 15 and 45 min for the PCE 0.35 mixture

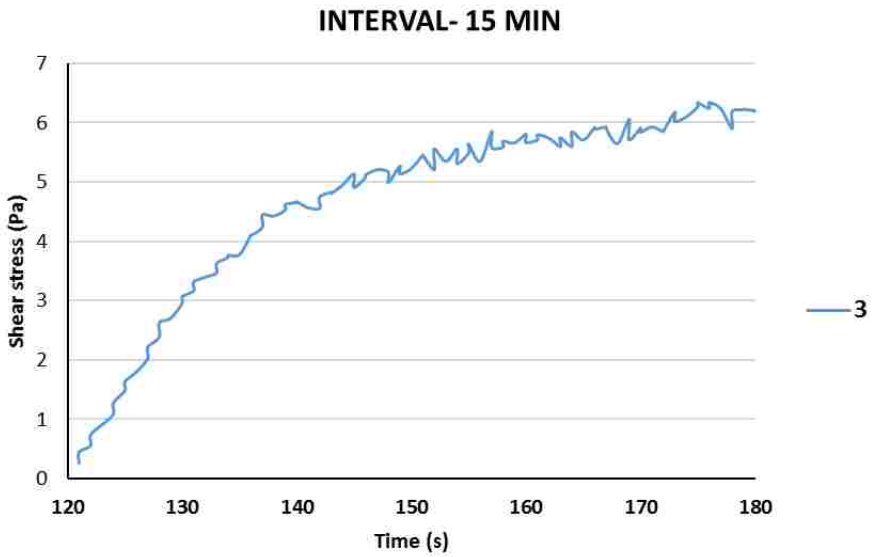

Figure 2.10 Typical result of the increase in shear stress at a constant shear rate of 0.005 s^{-1}, immediately after obtaining the flow curve. Result shown is for the PCE 0.35 mixture at 17 min.

Figure 2.11 shows the remaining static yield stress responses. The legend indicates the measurement intervals in the rheometer. For intervals 5, 7, 9 and 11, the maximum values are considered the static yield stress. The thixotropy is further evaluated by the average increase in static yield stress with time ($\Delta\tau_{0,s}$: static yield stress minus shear stress at end of interval 3 / elapsed time since the end of the flow curve), as well as the individual value of the 5th interval, corresponding to a 5 min rest (in fact, 1 min at 0.005 s^{-1}: interval 3, and 4 min rest) as shown in equation (2.6).

$$\Delta\tau_{0,s} = \frac{\tau_{0,s,x} - \tau_{0,s,3}}{t_x - t_3} \tag{2.6}$$

Where:
$\Delta\tau_{0,s}$ = the increase of static yield stress (Pa/min)

$\tau_{0,s,x}$ = the static yield stress measured in interval x (Pa) (x = 5, 7, 9, or 11)

t_x = time at which $\tau_{0,s,x}$ is measured (min)

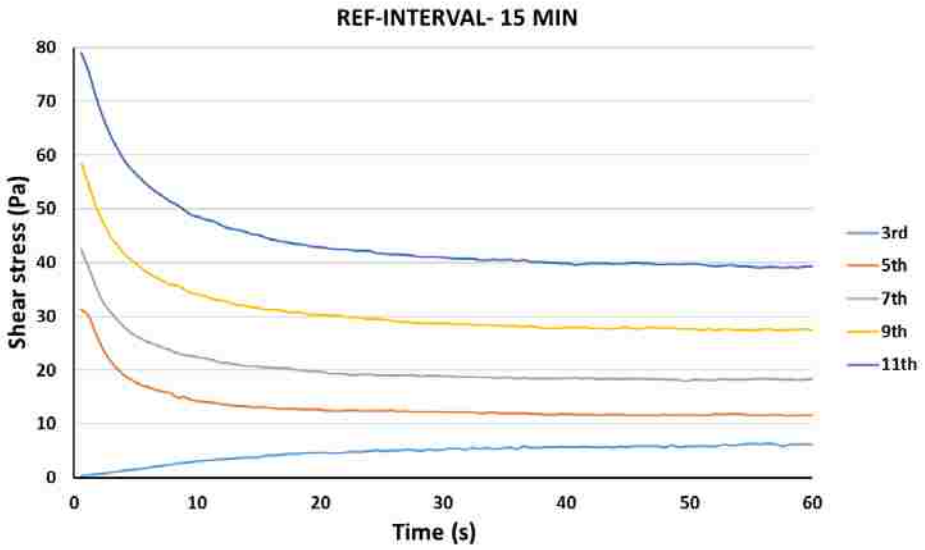

Figure 2.11 Static yield stress measurements. The colors represent the measurement intervals in the rheometer. Results for the PCE 0.35 mixture at 15 min.

To summarize: the following parameters are used for the evaluation of the rheological properties:

- Increase in dynamic yield stress, obtained from the flow curves between 15 and 45 min, to determine the workability loss
- The average shear stress at the end of the third interval, just after the flow curve, which corresponds to the immediate development of internal structure.
- The increase in static yield stress over 5 min of rest, taken as the maximum shear stress value at interval 5 minus the value at the end of interval 3.
- The average increase in static yield stress with time, taken as the average of the maximum shear stress (minus shear stress at the end of interval 3) divided by the elapsed time since the end of the flow curve, for intervals 5, 7, 9 and 11.

2.5 RESULTS AND DISCUSSION

In this section, influence of w/b ratio, SP type, SCMs and mineral fillers on thixotropy and fluidity of cement paste is discussed in detail.

2.5.1 Influence of Water-to-Binder Ratio and Dispersant Type. The influence of and the dispersant type on the rheology, and in particular thixotropic build-up, has been investigated based on the first eight mixtures mentioned in Table 2.2. Table 2.4 shows the detailed results of all measurements. The first three columns represent the flow curve results, in terms of (dynamic) yield stress and viscosity, both at 15 and 45 min. The change in dynamic yield stress is an indication of the workability loss of the sample. The last three columns are reflecting the thixotropic build-up of the pastes. The static yield stress in interval 3 is measured 1 min after the determination of the flow curve. The static yield stress increase with time in the following intervals is calculated by means of the $\Delta\tau_{0,s}$ in equation (2.6) above.

The results in Table 2.4 and in Figure 2.12 to Figure 2.14 clearly show, as expected, that all rheological properties are directly dependent on w/b, regardless of the dispersant type. The lower w/b, the more thixotropic the mixtures are. An efficient way to increase thixotropy of cement pastes is to decrease w/b, especially for values of w/b below 0.40. In fact, at w/b = 0.40, no significant thixotropy in the pastes has been noticed. Regarding the dispersant type, the PNS superplasticizer delivers the largest increase in static yield stress in the first minute (Figure 2.14), but in the longer term, the increase in static yield stress for the PNS is lower than that for the PCE (Table 2.4, Figure 2.14). Furthermore, the mixtures with PNS show a larger workability loss, based on the dynamic yield stress obtained from the flow curves (Figure 2.12). This is also reflected in a larger static yield stress values for the second measurement (starting at 45 min), compared to the first measurement (starting at 15 min). In case a long workability

Table 2.4 Rheological results for the pastes with different w/c and different dispersant type.

Note that YS stands for the yield stress, ΔYS is the change in dynamic yield stress between the 15 and 45 min flow curve measurements. The static yield stress in interval 3 is the increase in shear stress (at 0.005 s-1) during 1 minute immediately after determining the flow

Mixture	Dynamic YS (Pa)	Viscosity (Pa s)	ΔYS (Pa/min)	Static YS Interval 3 (Pa/min)	Static YS Interval 5 (Pa/min)	Average Static YS (Pa/min)
PCE 0.30	*15'*: 8.1 *45'*: 30.7	*15'*: 1.01 *45'*: 1.40	0.76	*15'*: 20.0 *45'*: 53.0	*15'*: 11.6 *45'*: 15.2	*15'*: 6.4 *45'*: 8.7
PCE 0.35	*15'*: 5.1 *45'*: 19.2	*15'*: 0.72 *45'*: 1.00	0.47	*15'*: 6.2 *45'*: 22.4	*15'*: 5.0 *45'*: 12.0	*15'*: 3.9 *45'*: 7.2
PCE 0.40	*15'*: 2.4 *45'*: 7.4	*15'*: 0.25 *45'*: 0.38	0.17	*15'*: 0.5 *45'*: 3.6	*15'*: 0.7 *45'*: 3.1	*15'*: 1.2 *45'*: 2.9
PCE 0.45	*15'*: 2.9 *45'*: 6.5	*15'*: 0.13 *45'*: 0.20	0.12	*15'*: 0.9 *45'*: 2.5	*15'*: 1.1 *45'*: 1.7	*15'*: 1.0 *45'*: 1.5
PNS 0.30	*15'*: 12.3 *45'*: 40.7	*15'*: 0.90 *45'*: 1.14	0.95	*15'*: 20.4 *45'*: 60.4	*15'*: 7.2 *45'*: 13.5	*15'*: 4.1 *45'*: 8.2
PNS 0.35	*15'*: 13.3 *45'*: 37.0	*15'*: 0.25 *45'*: 0.36	0.79	*15'*: 10.7 *45'*: 42.7	*15'*: 2.1 *45'*: 11.6	*15'*: 2.2 *45'*: 7.5
PNS 0.40	*15'*: 6.3 *45'*: 14.5	*15'*: 0.17 *45'*: 0.26	0.27	*15'*: 0.3 *45'*: 4.8	*15'*: 0.1 *45'*: -	*15'*: 0.2 *45'*: 0.9
PNS 0.45	*15'*: 0.3 *45'*: 0.8	*15'*: 0.05 *45'*: 0.06	0.02	*15'*: 0.1 *45'*: 0.0	*15'*: 0.1 *45'*: 0.0	*15'*: 0.1 *45'*: 0.0

retention is desired (e.g. in case of long transportation times), this workability loss is disadvantageous. To reduce the workability loss, the PCE dispersing agent is selected for the next series of experiments.

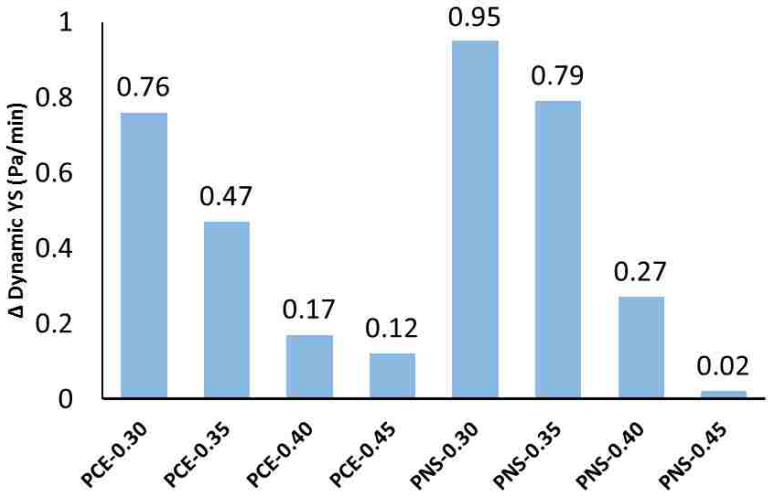

Figure 2.12 Increase in dynamic yield stress

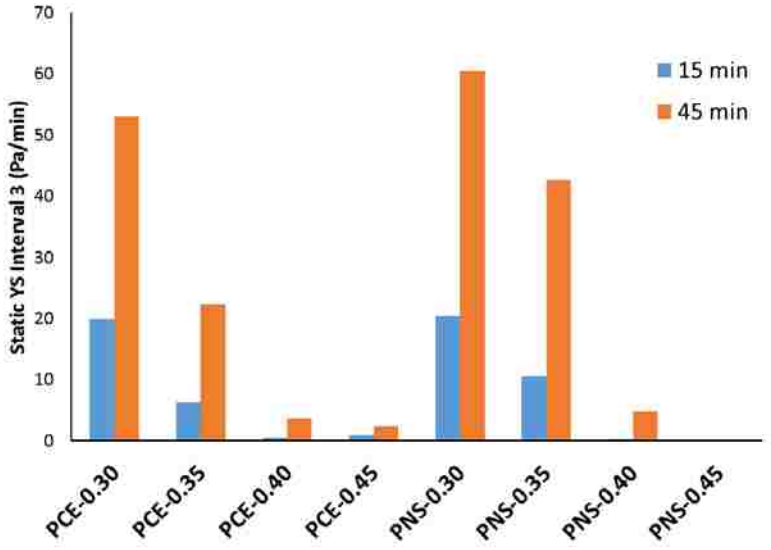

Figure 2.13 Static yield stress for interval 3

As thixotropy is largely dependent on w/b, the most logical choice to maximize thixotropy would be w/b = 0.30. However, detailed analysis of the static yield stress curves learns that the static yield stress does not substantially increase beyond 5 min of rest for the mixtures with w/b = 0.30. It appears that the static yield stress plateaus and any subsequent increase, especially for the measurements after 45 min, could be attributed to the hydration mechanism. This reduction in static yield stress can be clearly observed when comparing the last three columns in Table 2.4 The average increase in static yield stress over 20 min is approximately 65% smaller compared to the increase in the first minute for the PCE 0.30 system. The difference between the average increase in static yield stress and the increase in static yield stress in the first minute is less than 50% for the PCE 0.35 mixture, indicating a more prolonged increase in thixotropic properties (and hydration). The mixture with w/b = 0.35 also has a lower workability loss, and therefore, the PCE 0.35 mixture is selected as reference for the remaining part of the work on cement-pastes.

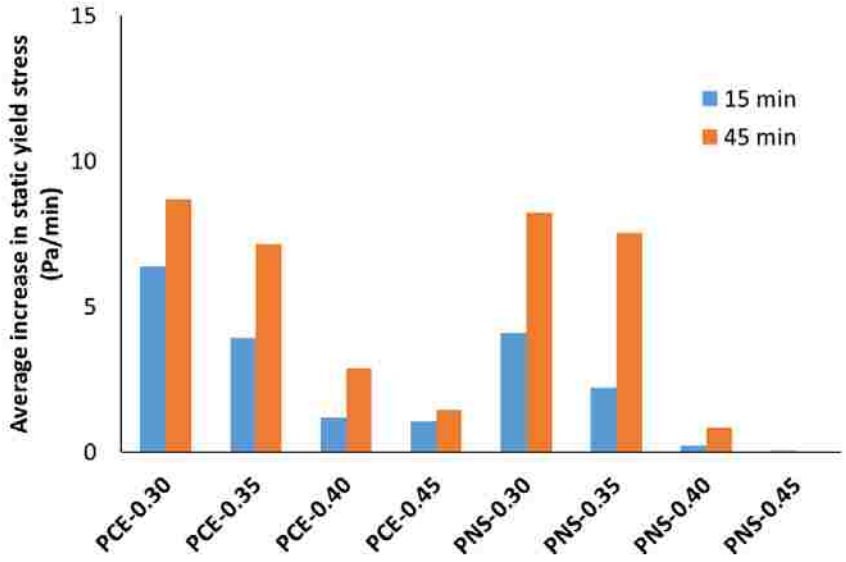

Figure 2.14 Average increase in static yield stress

2.5.2 Influence of Supplementary Cementitious Materials and Mineral Fillers. In this section, influence of evaluated binder materials on thixotropy and workability loss of paste is discussed.

2.5.2.1 Binary binder systems. After the selection of the PCE dispersant and the 0.35 water-to-binder ratio, a number of different supplementary cementitious materials (SCMs) and mineral fillers were evaluated. Detailed results are presented in Table 2.5, and in Figure 2.15 to Figure 2.17. Figure 2.18 shows the SP consumption to reach the desired mini-slump flow (as reported in Table 2.2). Fly ash required low amount of SP, whereas metakaolin required high amount of SP. From Figure 2.15 it can be seen that nearly all added SCMs or fillers cause a less important increase in dynamic yield stress compared to the reference mixture, except for the mixture with

Table 2.5 Rheological properties of cement pastes with binary composition (cement + SCM or filler)

Paste	Dynamic YS (Pa)	Viscosity (Pa s)	ΔYS (Pa/min)	Static YS Interval 3 (Pa/min)	Static YS Interval 5 (Pa/min)	Average Static YS (Pa/min)
REF	*15'*: 5.1 *45'*: 19.2	*15'*: 0.72 *45'*: 1.00	0.47	*15'*: 6.2 *45'*: 22.4	*15'*: 5.0 *45'*: 12.0	*15'*: 3.9 *45'*: 7.2
FA 25[3]	*15'*: 17.4 *45'*: 21.2	*15'*: 0.41 *45'*: 0.76	0.13	*15'*: - *45'*: 23.6	*15'*: - *45'*: 7.1	*15'*: - *45'*: 4.7

[3]*The fly ash mixture showed severe shear-thinning behavior, and the viscosity was approximated as the differential viscosity at 50 s^{-1}. Due to irregularity in static yield stress measurement at 15 min, the results are not shown in table.*

Table 2.5 Rheological properties of cement pastes with binary composition (cement + SCM or filler) cont.

LF 10	*15'*: 1.9 *45'*: 8.6	*15'*: 0.40 *45'*: 0.58	0.22	*15'*: 0.9 *45'*: 4.7	*15'*: 0.9 *45'*: 3.6	*15'*: 1.2 *45'*: 3.5
SL 25	*15'*: 6.2 *45'*: 22.4	*15'*: 0.46 *45'*: 0.78	0.54	*15'*: 4.8 *45'*: 24.6	*15'*: 5.3 *45'*: 13.5	*15'*: - *45'*: 9.2
SF 5	*15'*: 1.7 *45'*: 5.5	*15'*: 0.43 *45'*: 0.57	0.13	*15'*: 5.0 *45'*: 10.8	*15'*: 4.5 *45'*: 8.4	*15'*: 4.8 *45'*: 7.8
MK 25	*15'*: 2.2 *45'*: 3.8	*15'*: 0.59[4] *45'*: 0.77[3]	0.07	*15'*: 2.5 *45'*: 6.3	*15'*: - *45'*: 6.2	*15'*: 3.0 *45'*: 12.4
K 1	*15'*: 3.9 *45'*: 11.8	*15'*: 0.32 *45'*: 0.46	0.26	*15'*: 3.3 *45'*: 12.0	*15'*: - *45'*: 6.7	*15'*: 1.7 *45'*: 5.9
NS 1	*15'*: 1.3 *45'*: 7.0	*15'*: 0.39 *45'*: 0.61	0.19	*15'*: 3.9 *45'*: 12.9	*15'*: 2.6 *45'*: 8.9	*15'*: 3.2 *45'*: 8.1
AC 0.5	*15'*: 1.5 *45'*: 1.6	*15'*: 0.27 *45'*: 0.38	0.00	*15'*: 5.3 *45'*: 6.2	*15'*: 2.2 *45'*: 2.4	*15'*: 1.5 *45'*: 2.4

slag. It is also noteworthy to state that the mixture with 0.5% attapulgite clay showed no increase in dynamic yield stress and a slight increase in plastic viscosity. Comparing the increase in static yield stress during the 1st minute for the 15 min test, the reference mixture with plain OPC showed the largest increase, while the mixtures with attapulgite

[4] *The metakaolin mixture showed severe shear-thickening behavior, and the viscosity was approximated as the differential viscosity at 50 s^{-1}.*

clay, silica fume and slag showed similar behavior (Figure 2.16). Limestone filler and metakaolin, at the used dosages, significantly reduce the thixotropic build-up.

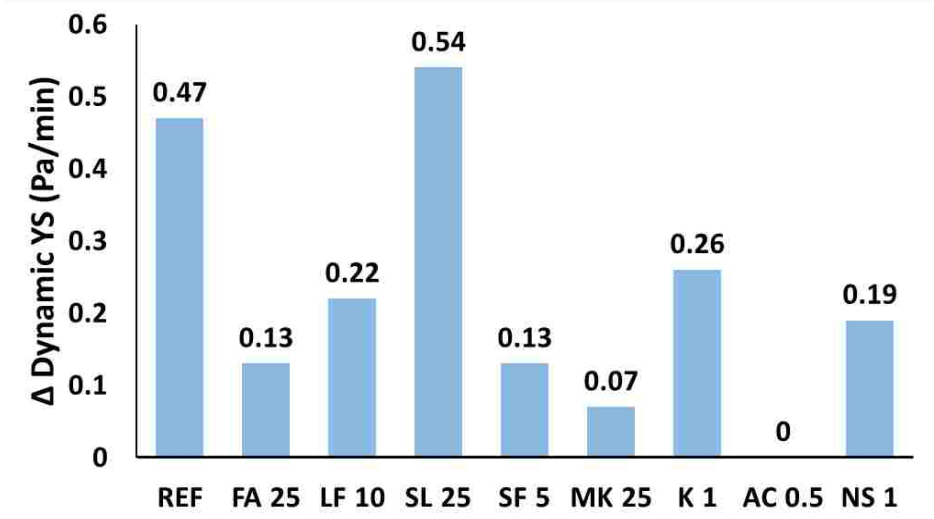

Figure 2.15 Increase in dynamic yield stress of binary systems.

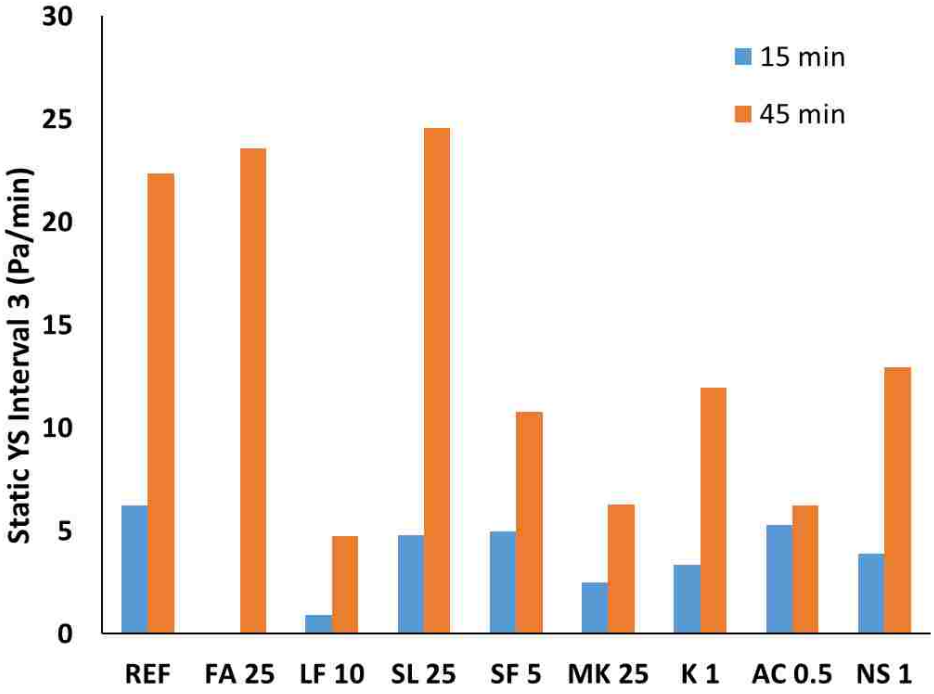

Figure 2.16 Static yield stress in interval 3 for binary systems.

However, the difference between the static yield stress at 15 min and the one at 45 min is largely influenced by the workability loss, as for the highly restructuring mixtures (REF, SL 25, SF 5 and AC 0.5), a direct relationship between the increase in dynamic yields stress from 15 to 45 min, and the static yield stress at 45 min can be found. From the average increase in static yield stress (Figure 2.15), for the test started at 15 min, the silica fume mixture shows the most important increase in static yield stress (considering that the results on the slag mixture were deemed erroneous). The mixtures with metakaolin and nanosilica also show a substantial increase in static yield stress, but the speed of development in the first minute was lower than the other mixtures. The attapulgite clay mixture shows a large increase in static yield stress in the first minute, but the increase in yield stress slows down over time.

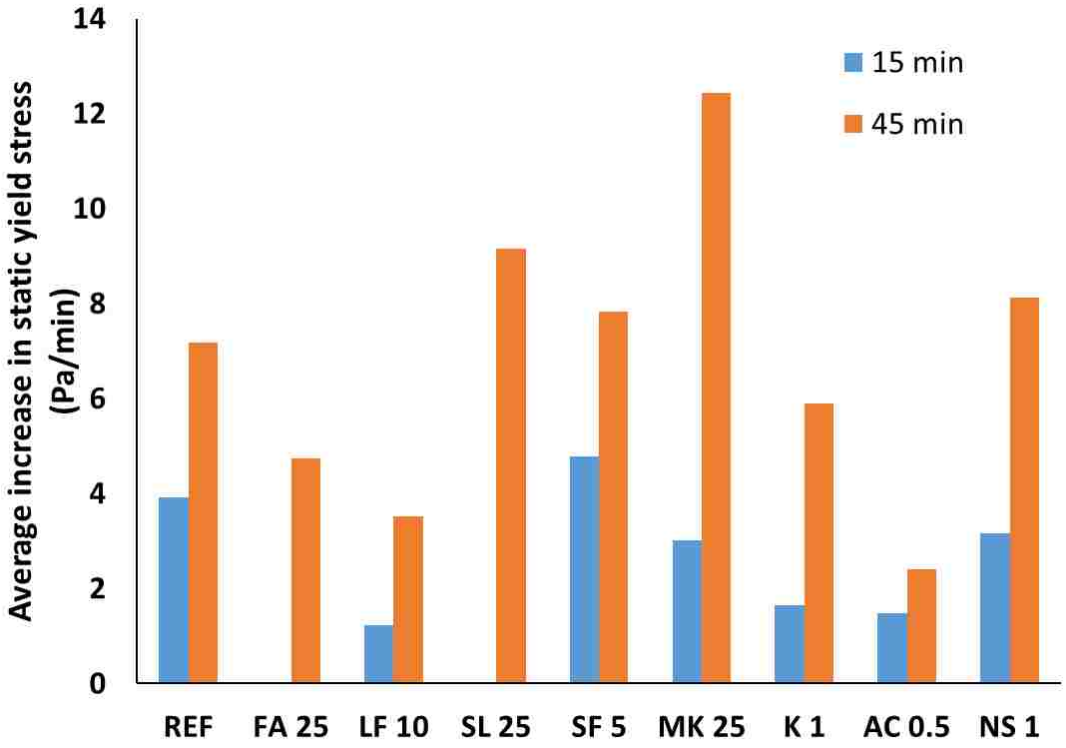

Figure 2.17 Average increase in static yield stress for binary systems.

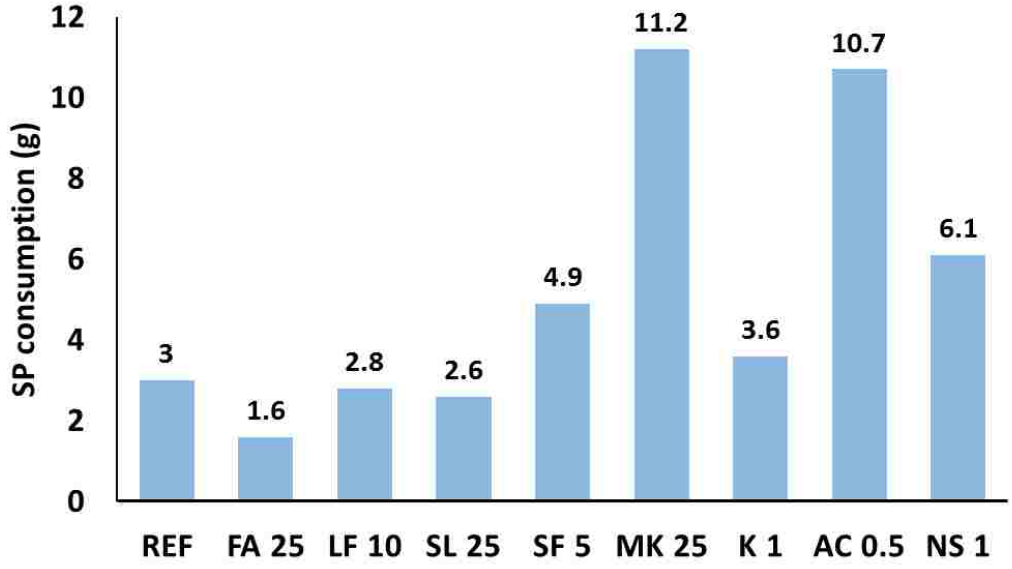

Figure 2.18 SP consumption of binary mixtures

Based on the above observations, silica fume, slag, and attapulgite clay are retained for further analysis. Silica fume is a performance-enhancing SCM, it can reduce viscosity at a low dose, it increases the thixotropic response of the mixture and reduces the workability loss, potentially due to the larger SP amount. The attapulgite clay is mostly beneficial for the immediate development of yield stress, but it requires a significant addition of dispersant, potentially causing the negligible workability loss. Slag shows a quick increase in static yield stress, potentially due to a large workability loss, rendering the cement-slag combination on its own less favorable for potential extended transportation of the mixture.

2.5.2.2 Ternary and quaternary binder systems. When starting the subtask on ternary binder systems, a new delivery of cement was made to the laboratory. Although the cement is the same type, produced by the same producer as the previous delivery, some changes in physical properties and chemical composition may affect the

rheological response of the mixtures. Therefore, the reference mixture with no SCMs or fillers, a w/b = 0.35 and the PCE dispersing admixture, was reproduced and the new values of the rheological properties are reported in Table 2.6. It should also be noted that the SP quantity necessary to achieve a mini-slump flow of 300 ± 20 mm was slightly lower: 2.9 g (for the entire produced volume of the mixture) for the new cement relative to 3.0 g for the old delivery.

The results for the ternary and quaternary mixtures are summarized in Table 2.6. In Figure 2.19 to Figure 2.21, the rheological properties of the ternary and quaternary mixtures are shown.

Table 2.6 Rheological properties of ternary and quaternary system

Paste	Dynamic YS (Pa)	Viscosity (Pa s)	ΔYS (Pa/min)	Static YS Interval 3 (Pa/min)	Static YS Interval 5 (Pa/min)	Average Static YS (Pa/min)
REF-new	*15'*: 11.0 *45'*: 27.9	*15'*: 0.34 *45'*: 0.53	0.56	*15'*: 5.3 *45'*: 23.3	*15'*: 0.6 *45'*: 7.8	*15'*: 3.9 *45'*: 7.2
SL 25 – AC 0.5	*15'*: 6.7 *45'*: 7.7	*15'*: 0.33 *45'*: 0.44	0.03	*15'*: 18.9 *45'*: 22.4	*15'*: 8.3 *45'*: 8.6	*15'*: 7.8 *45'*: 7.7
SF 5 – AC 0.5	*15'*: 10.5 *45'*: 10.7	*15'*: 0.47 *45'*: 0.53	0.01	*15'*: 6.9 *45'*: 7.7	*15'*: 1.8 *45'*: 1.8	*15'*: 1.2 *45'*: 1.3
SL 25 – SF 5 – AC 0.5	*15'*: 3.6 *45'*: 4.0	*15'*: 0.29 *45'*: 0.36	0.02	*15'*: 6.7 *45'*: 7.4	*15'*: 3.5 *45'*: 3.4	*15'*: 2.7 *45'*: 2.8
SL 25 – SF 5	*15'*: 7.8 *45'*: 16.8	*15'*: 0.37 *45'*: 0.50	0.30	*15'*: 12.5 *45'*: 23.3	*15'*: 4.2 *45'*: 10.9	*15'*: 4.1 *45'*: 8.6

The new reference cement mixture and the binary systems with slag, silica fume, and attapulgite clay are also included in the figures to enhance visual assessment. Figure 2.22 shows the SP demand of the studied binder systems. The increase in dynamic yield stress from 15 to 45 min is substantially lower for all mixtures containing attapulgite clay, despite the inclusion of slag in some of the mixtures. This can most likely be attributed to the increased SP dosage, as the dosage is at least of the same magnitude as the binary mixture with attapulgite clay.

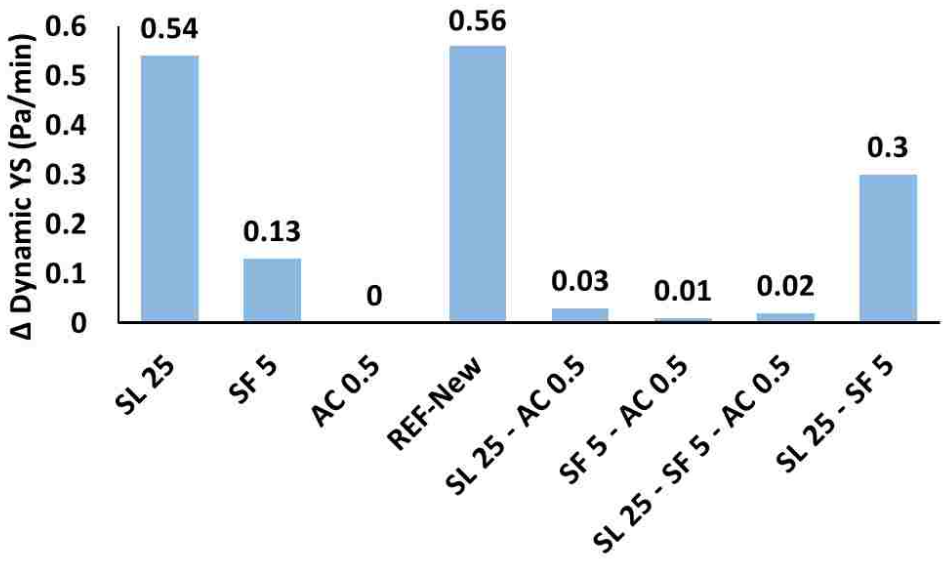

Figure 2.19 Increase in dynamic yield stress for ternary and quaternary systems.

The ternary mixture with slag and silica fume shows a workability loss in between that of the binary mixtures with slag and silica fume separately. The increase in static yield stress within the first minute (interval 3), is for all ternary and quaternary mixtures higher than for the reference and binary mixtures. However, the benefit of combining attapulgite clay and silica fume is only minor and a significant increase in SP consumption is noted, making these mixtures less favorable. The mixture with slag

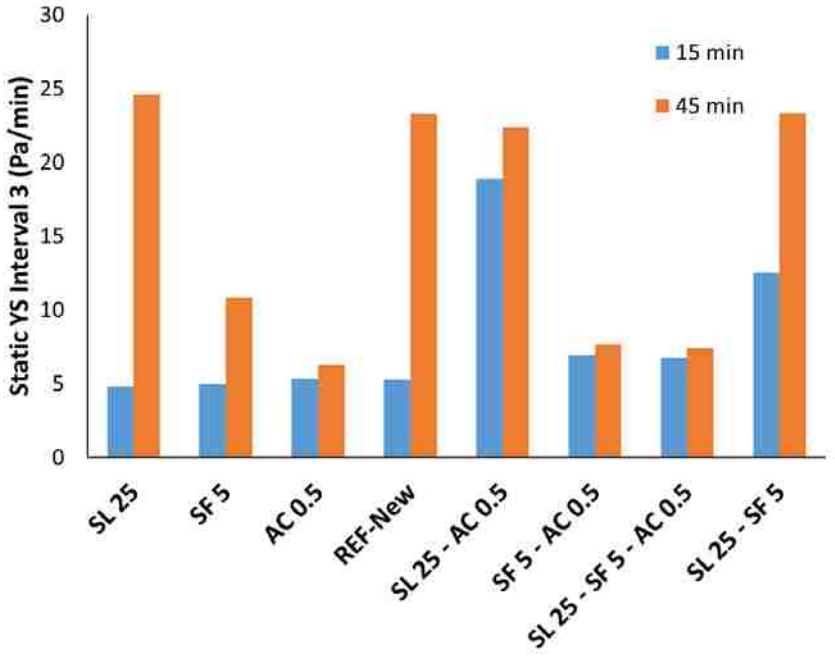

Figure 2.20 Static yield stress at the end of the 3rd measurement interval for ternary and quaternary systems.

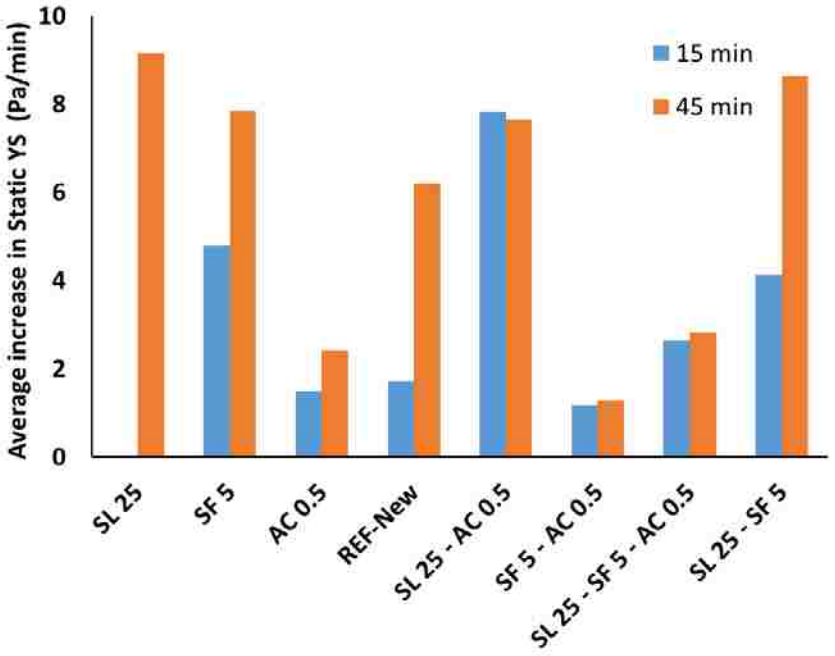

Figure 2.21 Average increase in static yield stress for ternary and quaternary systems.

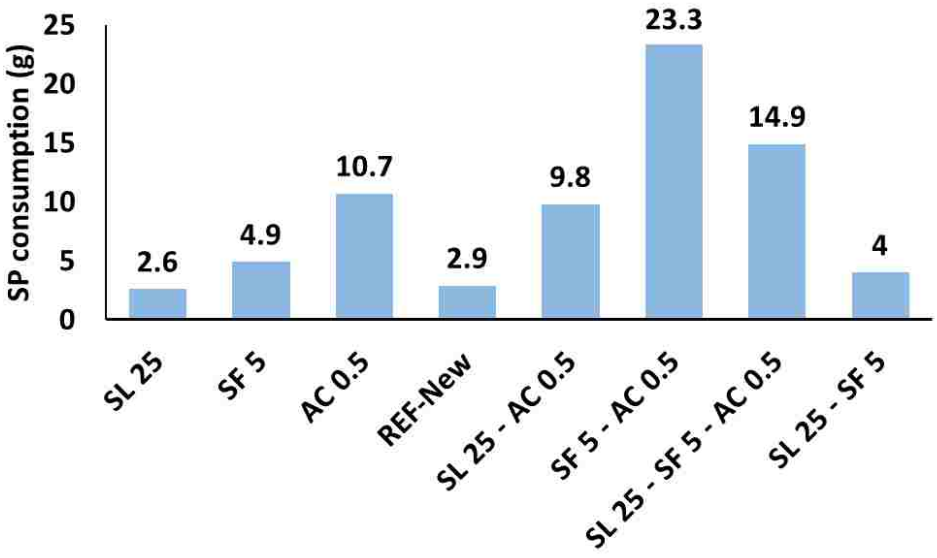

Figure 2.22 SP demand for ternary and quaternary systems.

and attapulgite clay shows a significant increase in thixotropic capacity, without showing a significant loss in workability. Combining slag and silica fume also delivers a significant increase in static yield stress development, but the workability loss may affect the results. The average increase in static yield stress shows similar behavior: combining silica fume and attapulgite clay, with or without slag, results in inferior rheological response compared to only employing silica fume.

2.6 SUMMARY

Based on all data shown, the results on cement paste incorporating different superplasticizer types, SCMs, and mineral filler can be summarized in following points:

- Irrespective of w/b ratio, the selected PNS based SP required a higher amount than the evaluated PCE based SP to achieve flow spread of 300±20 mm.
- The workability loss is larger for the selected PNS based SP than for the selected PCE based SP.

- The rate of thixotropy development and workability loss decreases significantly with an increase in w/b ratio.
- The workability loss is deemed to be the main mechanism for the static yield stress development in a binary mixture with only 25% slag.
- The amount of SP controls the workability loss but also affects the structural build up rate in cement paste incorporating SCMs and mineral fillers.
- Overall, the evaluated silica fume, slag and attapulgite clay are considered effective binder materials for further ternary and quaternary system analysis.
- A ternary mixture combining the evaluated 25% slag and 0.5% attapulgite clay could be intended for extended transportation times, as the thixotropic build-up is significant and the workability loss is minor.
- A ternary mixture containing the evaluated 25% slag and 5% silica fume can be considered as an alternative if attapulgite clay is not available. This mixture also shows substantial thixotropic build-up, but the workability loss can be significant. Hence, this mixture could be suitable for on-site or nearby concrete production and placement. A mixture with only 5% silica fume could work as second alternative. Non-reversible build-up of yield stress could limit self-consolidation if the waiting time is too elevated.

3. FRESH PROPERTIES OF SFSCC/VFC

This section discusses the testing methods from previous research on the development and characterization of fresh properties of SFSCC, influence of constituent materials on fluidity and shape stability of SFSCC, and mixture design procedure. In addition, based on the results obtained from the cement paste study, materials, mixing procedure and standard test methods employed in this project are discussed. A new test setup to study the evolution of green strength is developed.

The excess paste layer concept was adopted to evaluate the mixture design of VFC based on the aggregate packing density study. The influence of the excess paste layer and superplasticizer (SP) on thixotropy, workability loss, fluidity and green strength development was investigated in detail. Furthermore, different binary and ternary mixtures using silica fume, slag and attapulgite clay were investigated. A correlation between green strength and static yield stress was established to evaluate the suitability of mixtures for different pavement thicknesses.

3.1 SFSCC TESTING METHODS

To develop suitable concrete mixtures for slip form paving, it is important to identify, study and evaluate the test methods useful for the application. In order to evaluate the fresh properties such as shape stability, green strength, thixotropy, flowability and consolidation of designed mixtures, various test methods have been developed to evaluate the performance of the mixtures as well as to establish acceptance criteria for slip form pavement construction.

3.1.1 Slump Flow Test and Flow Table Test. The slump flow test method used for conventional SCC was used to evaluate the flowability of SFSCC mixtures according to ASTM C1611 [8], [10]. The flowability of paste or concrete mixtures was

evaluated by the flow ratio using the flow table test, according to EN-206 and ASTM 1437, by Voigt et al. [63] and Pekmezci et al. [9], respectively. The flow ratio is defined as the ratio of the diameter of the concrete cone at the base before and after the material was subjected to desired number of drops. The Pekmezci et al. [9] studied flowability by applying 25 drops of the drop table, while Voigt et al. [63] conducted the flowability test on a two plate drop table, in which the plate was dropped 15 times from a 40 mm height. Wang et al.[8] evaluated the flowability of paste or mortar according to the flow table test described in ASTM C230 and final flow was obtained after 18 drops.

3.1.2 Shape Stability or Green Strength Test. Breitenbucher et al. [64] determined the shape stability of paste and mortar by means of the mini slump cone test. A slump cone with an upper diameter of 70 mm, a height of 60 mm, and a base diameter of 100 mm was filled with fresh paste. The shape stability was evaluated 5 minutes after the initial mixing and after re-mixing of the mixture at 10 minutes.

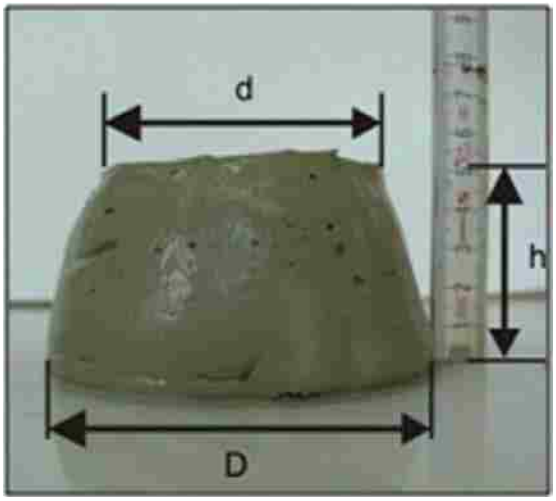

$$Kp(m) = \frac{11}{(D + d - h)} \qquad Kc = \frac{15}{(w + l - h)}$$

Figure 3.1 Left: Shape stability of paste/mortar test specimen with equation[64]
Right: Shape stability of fresh concrete test specimen with equation[64]

The height (h), the top diameter (d) and bottom diameter (D) of the paste or mortar after removal of the cone were measured. The shape stability of concrete was also determined using a standard cubical formwork (150 x 150 x 150 mm^3). The shape stability coefficient of fresh paste or mortar, K_p (m), and concrete, K_c, was measured from the equations shown in the left and right parts of 3.1, respectively.

Figure 3.2 R. Breitenbucher et al. [64] test setup for the green strength.

Similarly, Hoornahad et al. [65] evaluated the shape stability by determining the shape preservation factor (SPF). SPF is the ratio of the vertical cross-sectional area of the sample before and after demolding i.e. A_f/A_o. Therefore, a higher shape stability coefficient or factor indicates a high shape stability of the mixture. Breitenbucher et al. [64] evaluated the green strength of a concrete cube which consist of a lever beam centered on the demolded concrete as shown in Figure 3.2. A bucket at the other end of the lever beam was filled continuously with sand until a deformation of 10 mm in the concrete was reached. The mass of the sand in the form of load was measured to determine green strength of concrete.

However, Voigt et al. [63] and Pekmezci et al. [9] evaluated the shape stability using a modified flow table method. A 100 mm x 200 mm loosely filled concrete cylinder was consolidated with 15 [63] or 25 [9] drops on the flow table. Then, the

cylinder was demolded and loaded slowly but continuously with a small amount of sand until the sample collapsed as shown in Figure 3.3. Wang et al. [8] evaluated the green strength using a simple sand method, as shown in Figure 3.4.

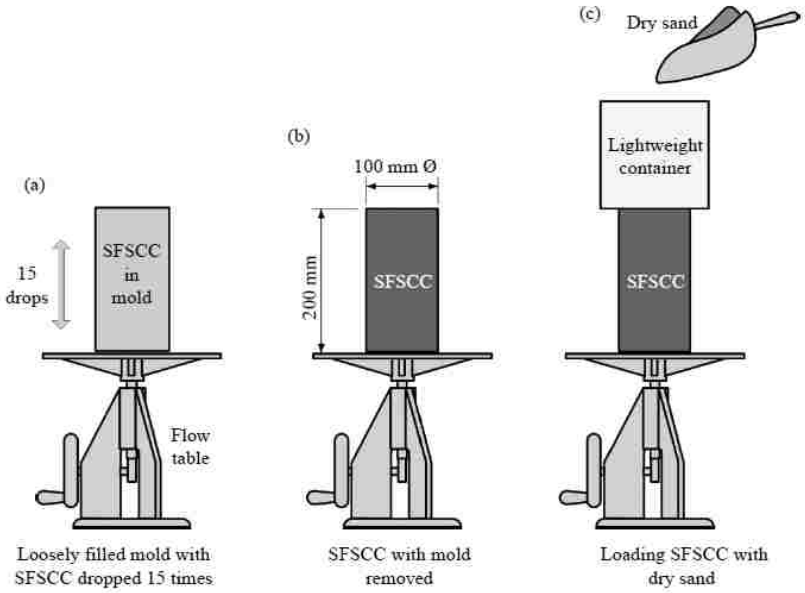

Figure 3.3 Voigt et al. [63] and Pekmezci et al. [9] green strength test setup.

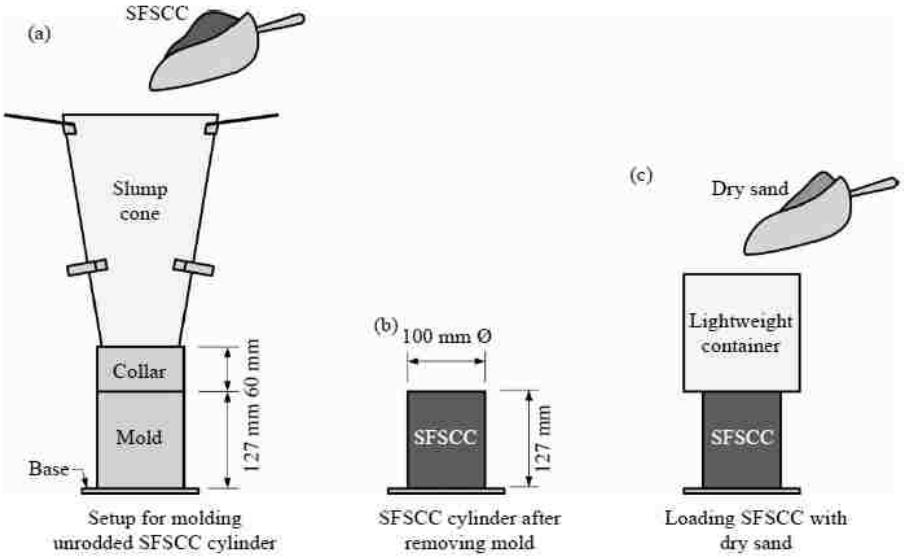

Figure 3.4 Wang et al. [8] green strength test setup.

In this method, the SFSCC mixture was poured into the small cylinder mold (100 mm x 127 mm) at a height of 300 mm. After the casting, the formwork was removed immediately and a cylinder showing small or no deformation was considered further for the green strength evaluation. A plastic cylinder (150 mm x 150 mm) was placed on top of the cylinder and gradually filled with sand until the specimen collapsed. The total quantity of sand used (load) during the test divided by the loading area of the sample is defined as the green strength of the concrete.

3.1.3 Mini-paver Test. To simulate the field slip form paving method in the lab, a mini-paver test [8], [9], [63], [66] system was developed. It comprised of three parts: (1) L-shaped box with a platform on top; (2) a towing system; and (3) a working table as shown in Figure 3.5. Initially, concrete was placed on the platform as shown in Figure 3.5 (left) and pushed up to a certain height through the vertical leg of the L-box to consolidate the mixture. Then, the mini-paver was pulled forward with crank system at a designed speed of 1.5-2.5 cm/s. Lastly, as the mini-paver moved forward, the concrete slab was extruded out of the horizontal leg of the L-box as shown in

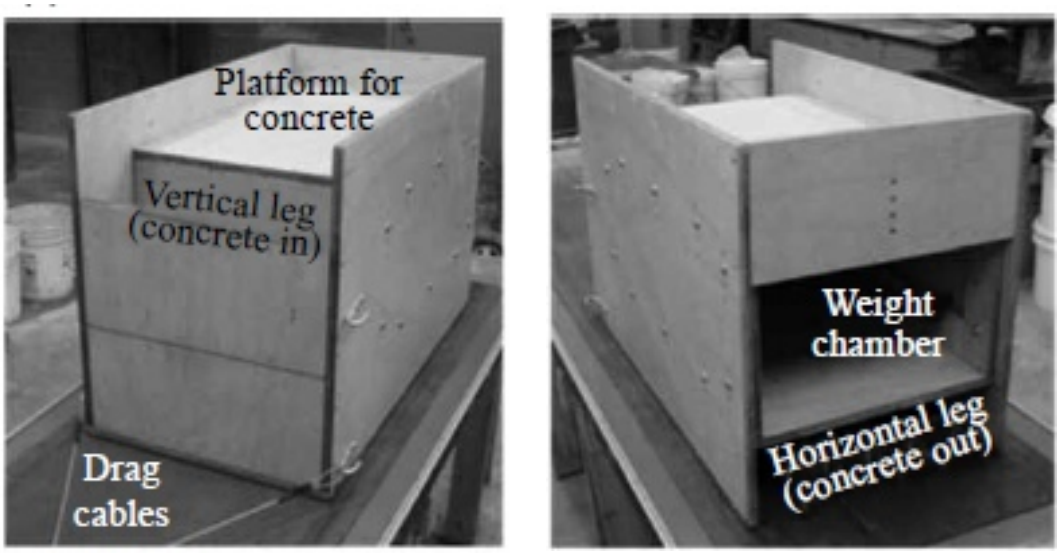

Figure 3.5 Mini-paver system [8]–[10], [63], [67]

Figure 3.5 (right). The surface quality and the edge slump of the concrete slab resulting from the mini paver indicated the consolidation, shape holding ability and ultimately the feasibility of the SFSCC mixture for slip form pavement construction [8].

3.1.4 Compaction Factor Test. The self-consolidating ability of the SFSCC mixture was evaluated by the modified compaction factor test method [10] as shown in Figure 3.6. In this method, a cylinder (100 mm x 200 mm) was filled with freshly mixed concrete through an inverse slump cone under its own weight. The unit weight of the concrete specimen was then determined and compared with unit weight of the concrete specimen obtained with three layers and rodded 25 times for each layer. The ratio of the unit weight of loosely filled concrete to the unit weight of compacted concrete is defined as the compaction factor. A compaction factor closes to, or equal to 1 represents a good self-consolidating concrete [10].

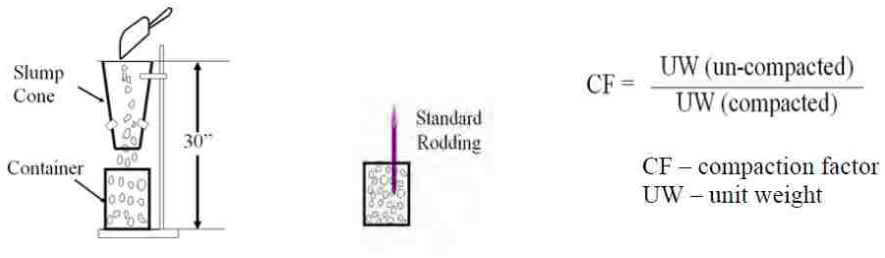

Figure 3.6 Compaction factor test setup [10]

3.2 INFLUENCE OF CONSTITUENT ELEMENTS ON FLUIDITY AND SHAPE STABILITY OF SFSCC

The evaluation of fluidity and stability of SCC are important concerns for slip forming. Few researchers have investigated the factors affecting the balance between flowability and shape stability (green strength) of mixtures requiring low compaction energy. Shape stability, i.e. green strength can be defined as the ability of the mixture

to support its own weight in its given shape. It is the crucial parameter in slip form paving where no formwork is used. Breitenbucher et al. [64] investigated the effect of SCMs, clays and thixotropic agents on the slump flow and shape stability of paste, mortar and concrete mixtures for slip form pavement applications. The authors investigated two different approaches to develop concrete mixtures with good flowability and high shape stability.

One approach was to add thixotropic agents in the original mixture to develop a thixotropic concrete. This concrete shows consistent flowability during transport and placement, while viscosity increases with time after casting. In this approach, mineral admixtures (consisting of kaolinite, illite, and quartz powder), metakaolin, bentonite, modified starch, tetrasaccharides and other modified polymers were employed as thixotropy-enhancing agents. Their investigation showed that paste with metakaolin and a polycarboxylate ether (PCE) superplasticizer reached the targeted values (Shape stability coefficient (K_p) > 0.9 and mini slump flow > 200 mm). After re-mixing, to check the behavior of the mixture during delivery and casting, none of the pastes mixed with the polymeric thixotropic agent (tetrasaccharides and other modified polymers) and mineral additions (e.g. bentonite, metakaolin, modified starch) achieved the targeted values. Also, re-mixing led to a 97% reduction in green strength of concrete with thixotropic agents (modified polymer, modified starch and metakaolin).

In the another approach, Breitenbucher et al. [64] used viscosity-increasing agents to achieve sufficient shape stability and stiffening behavior. In this approach, an SCC mixture with slump flow of 700 ± 20 mm was obtained using PCE superplasticizer and when the viscosity-increasing additive was added 15 min after the initial mixing. They reported that the addition of the viscosity-increasing additive, superabsorbent polymer (SAP), with PCE superplasticizer led to a significant decrease

in slump flow and a shape stability coefficient (K_c) of 0.76 to 0.79 was determined. A higher shape stability coefficient was achieved when naphthalene sulfonate (NaS) was combined with PCE superplasticizer. In a concrete mixture with 3% PCE and 1% NaS of cement weight, slump flow was reduced from 690 to 490 mm and a shape stability coefficient of 0.85 was achieved [64]. In a concrete mixture containing 3% PCE and 1.5 % NaS, slump flow was reduced from 690 to 440 mm and shape stability coefficient of 0.95 was achieved [64]. Therefore, the targeted shape stability and high flowability could not be achieved simultaneously using this approach [64].

Pekmezci et al. [9] determined the flowability and shape stability under the effect external compaction energy, i.e., using the drop table test as explained in sections 3.1.1 and 3.1.2. They discovered that more flowability was achieved in concrete mixtures with naphthalene-based (PNS) plasticizers compared to polycarboxylate-based (PCE) plasticizers, while still showing sufficient green strength. Their results also showed that the addition of an air-entraining agent (AEA) to attain enhanced air-void structure does not affect the flowability and green strength of the mixture. Moreover, adding clay minerals up to 1% of attapulgite clay and 1.5% of metakaolin of cement weight proved beneficial in modifying flowability with effective green strength development. However, concrete mixtures containing VMA or kaolinite provided higher green strength with a small loss in flowability. The work of Pekmezci et al. [9] and Voigt et al. [63] also indicated that the incorporation of fly ash and a naphthalene-based superplasticizer (PNS) led to an increase in flowability but showed negative impact on the green strength. Pekmezci et al. [9] attributed this higher flowability behavior of concrete due to the spherical shape, finer size and lower specific gravity of fly ash. Also, for a given water/binder (w/b), fly ash decreased the water demand causing an increase in flowability [68].

Voigt et al. [63] investigated the effect of clay minerals and fibers in fly ash-modified SCC (replaced 30% of cement weight) (SCCF) mixtures to achieve the required balance between flowability and green strength. They reported that attapulgite clay displayed a maximum green strength (2.4 kPa) with minimal negative impact on flowability. SCCF with other clay minerals, MgO and fibers showed similar green strength (1.3-1.8 kPa). SCCF with polypropylene fibers showed maximum flow ratio among all SCCF mixtures. The relationship between the green strength and flowability is shown in Figure 3.7 [9]. From these results, a general trend can be observed: As the flow ratio increased, the green strength value decreased. However, some concrete mixtures followed a different trend i.e. for a given flow ratio, a plain mixture with naphthalene-based plasticizer (Plain (naphth) in the figure), the mixtures with fly ash (FA) and clay minerals and mixtures containing VMA and AEA, displayed higher green strength values.

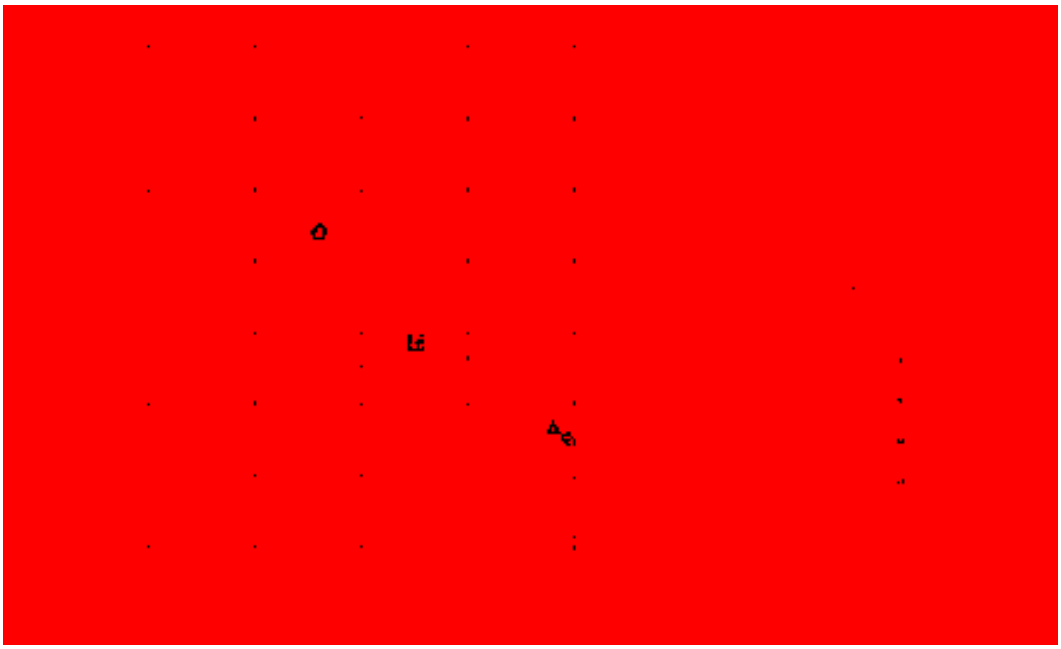

Figure 3.7 Relationship between green strength and flowability (flow diameter after 25 drops on drop table) [9]

These mixtures may be considered as potential candidates for concrete requiring reduced or no consolidation energy. From the mini paver tests, it has been observed that all concrete mixtures with clay minerals and fibers improved the edge stability, while good surface quality without any internal or external vibration was observed [9], [63]. In an accelerated slab replacement study, Armaghani et al. [69] reported that SCC mixtures with four admixtures i.e., HRWR, slump retaining admixture, regular water reducing admixture and set retarder (Type D according to ASTM C494), and accelerator, displayed high workability retention without segregation. They stated that workability was retained for one hour after adding the accelerator. Their results also showed an effective early age strength of 54 MPa (1 day) for a given SCC mixture, which is more than what is required for accelerated slab replacement application. From the feasibility study [8] and the field investigation [10] of SCC for slip form pavement application, it has been determined that a new slip form SCC (SFSCC) might have a symmetric cone shape (indicates well compacted) as shown in Figure 3.8, along with slump value of around 200 mm and a flow value range of 330-380 mm. Wang et al. [70] reported that SFSCC mixtures with higher replacement of cementitious materials (40%FA+15%MK), with and without nano-limestone resulted in good flowability and shape stability satisfying SFSCC design criteria.

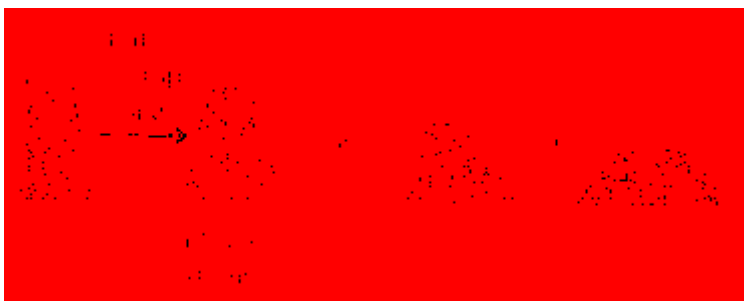

Figure 3.8 A well compacted slump cone shape [10]

Garg and Wang [71] studied the performance of mortars containing a combination of three clays and fly ash. They concluded that all three clays decreased the flowability of the mortars and an optimum amount of attapulgite clay can be helpful in improving shape stability of concrete for slip form pavement application. Attapulgite clay led to a significant reduction in flowability due to its high water adsorption capacity [61], [72] and thixotropic behavior [53]. Tregger et al. [45] also concluded that an increase in stiffness resulted in concrete mixtures containing attapulgite clay having the highest green strength compared to other clay additives.

Garg and Wang [71] reported that a higher content of metakaolin led to a significant decrease in flowability [73], caused by the imbalance between the extra fine particles and a lack of water. Ge et al. [74] found that the incorporation of nano-limestone resulted in a decrease in slump flow while an increase in particle size of nano-limestone led to increase in slump flow. The fly ash-cement mortar study conducted by Kawashima et al. [48], concluded that flowability increased with the addition of fly ash, while it decreased with addition of CNS (colloidal nanosilicate). Modification in particle shape, size and paste volume of SCMs and clay minerals causes variations in the dosage of superplasticizer required to reach a target slump flow value. Han et al. [75] found that in high-strength SCC mixtures, the addition of SRA (shrinkage reducing admixtures) and SAP (super-absorbent polymers) lowered the flowability requiring an adjustment of the HRWR dosage.

3.3 MIXTURE OPTIMIZATION OF SFSCC

In this section, previous studies focusing on aggregate optimization and excess paste layer thickness concept are discussed in detail.

3.3.1 Aggregate Optimization. The aggregate gradation, shape, and angularity significantly influence SCC characteristics [76]. SCC made with coarser aggregates may lead to lower HRWR demand and lower plastic viscosity. The optimization of the aggregate proportioning and grain size distribution is a common practice in developing an economical mix design of SCC, as it allows for a reduction of the paste volume. A higher maximum packing density of aggregate reduces the voids which need to be filled with paste and helps in reducing shrinkage in the mixture.

The modified Andreasen and Andersen model (A&A model) is commonly employed to optimize the aggregate proportion and to reduce the paste volume in SCC mixtures (equation(3.1)) [72–75].

$$P\,(D) = \frac{D^q - D_{min}^q}{D_{max}^q - D_{min}^q} \tag{3.1}$$

where, q = distribution modulus

D = sieve size

D_{min}= minimum particle size

D_{max} = maximum sieve size in which 100% passing takes place

The modified A&A model with q values between 0.25 and 0.30 produces a particle size distribution (PSD) suitable to design SCC mixtures [79], [80]. Maximum packing density or compactibility of granular materials can be measured by means of the Gyratory compactor testing equipment, also known as the intensive compaction tester (ICT), shown in Figure 3.9. It is a popular equipment to investigate the compactibility and stability of zero-slump concrete or conventional pavement concrete [81]. The ICT consists of a test cylinder, a piston, and an electronic pressure device. It calculates the density of the specimen by continuously measuring the height during the compaction of the cylinder subjected to shear movement and constant pressure (commonly known

as compaction cycles) [82]. Mueller et al. [77] and Khayat and Mehdipour [78] recently proposed that the ICT is a simple and effective tool to determine the maximum packing density of solid particles of SCC mixtures, including aggregates [78] or aggregates and cementitious materials [77]. Their results showed that a good PSD of the aggregates for ecological and economical SCC can be obtained by using the modified A&A model with a q-value of approximately 0.27 [77] or 0.29 [78]. Esmaeilkhanian et al. [83] also showed that a q value between 0.28 to 0.30 provided maximum packing density when the coarse aggregate volume was between 32% - 35% of the total concrete volume.

Figure 3.9 Left: Intensive compaction tester (ICT),
Right: ICT compaction principal [81]

For the development of a SFSCC mix design, the loose and bulk density of coarse aggregate were tested according to ASTM C 29 (2003) by Wang et al. [8] to study the influence of different aggregate gradations on compactibility and green strength of concrete. The difference between the loose and bulk density indicated the external energy required to achieve the maximum packing density of the aggregates [8]. Therefore, a small difference between the loose and bulk density of coarse aggregate represents a more compacted and dense granular system. This relationship was further

verified by the compaction factor test of fresh concrete as explained in section 3.1.4, and aggregate proportions with higher compaction factor were selected to continue the research on SFSCC [8].

3.3.2 Excess Paste Layer Concept. The excess paste layer theory was developed by Kennedy [84] in 1940 to explain the driving factor influencing the workability of concrete. According to this theory, the total paste volume is divided into a paste volume to fill the voids between the aggregates, and an excess paste volume to cover the surface area of the aggregates to achieve desired workability. This excess paste thickness reduces the inter-particle friction

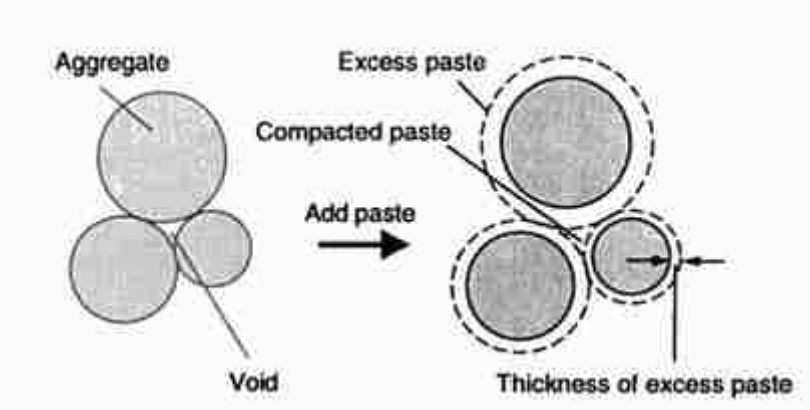

Figure 3.10 Excess paste layer theory concept [85]

between the aggregates and improves the workability of the mixture. As can be seen in Figure 3.10, concrete with an aggregate system without excess paste layer moves when overcoming the friction between the particles, while aggregate voids filled with paste and an excess paste layer modifies the interaction between the aggregate from inter-particle friction to a lubricating effect. In this case the mobility of aggregate particles is enhanced. Hoornahad et al. [65] and Oh et al. [85] systematically explained the excess paste layer system in two parts, i.e. the void paste and the excess paste. Figure 3.11(a)

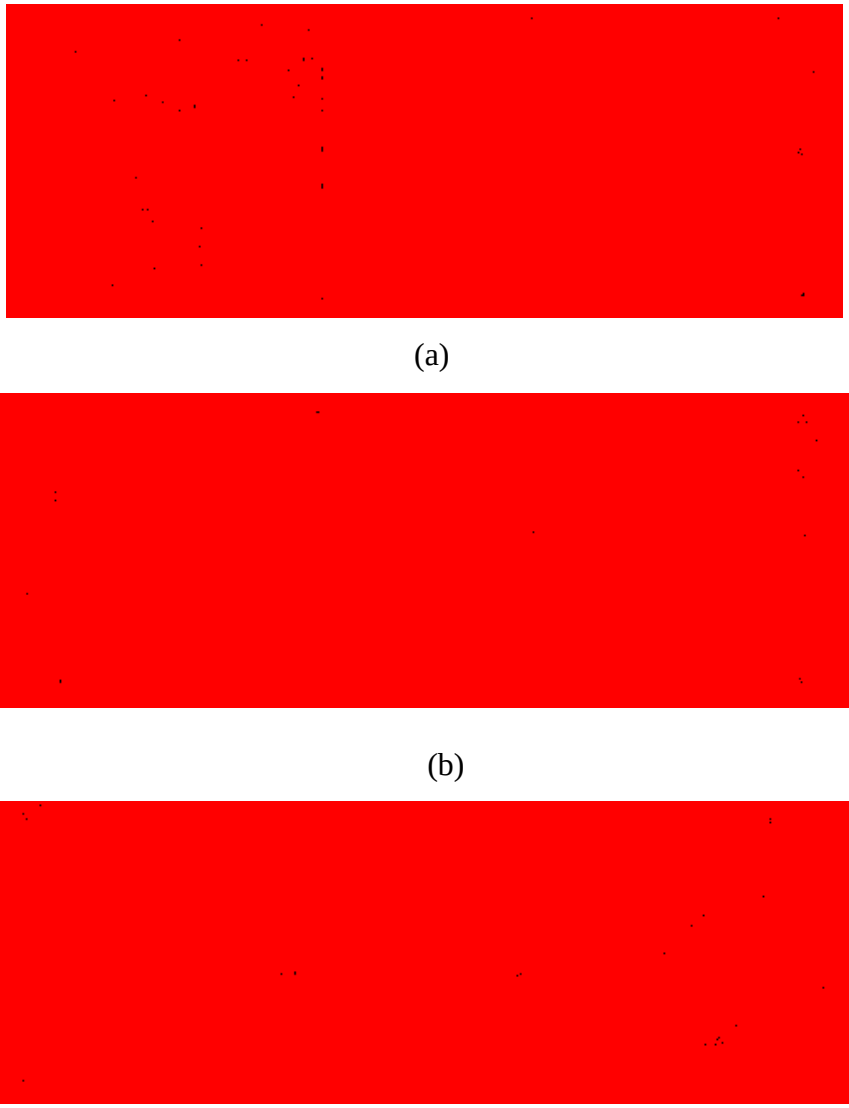

(a)

(b)

(c)

Figure 3.11 Two phase aggregate-paste system in the excess paste layer where, V_t, V_a, V_b, V_p, V_{pv} and V_{pex} are volume of the sample, specific volume of the aggregate, bulk volume of the aggregate in compacted state, total paste volume, void paste volume and excess paste volume, respectively [65]

shows a total volume of a sample equivalent to the volume of aggregate and total paste volume in loose state. Figure 3.11(b) shows a system with bulk volume of the aggregates, consisting of the volume of aggregate and paste volume in compacted state, and excess paste volume. Lastly, Figure 3.11(c) shows a total volume of sample

containing the aggregate volume, paste volume to fill the voids between the aggregate, and the excess paste volume.

$$V_{pv} = \left(\frac{1}{\zeta} - 1\right) V_a \tag{3.2}$$

$$V_{pex} = V_p - V_{pv} \tag{3.3}$$

where,

V_{pv} = void paste volume,

ζ = maximum packing density of aggregate,

V_a= volume of aggregate

V_{pex}= excess paste volume

V_p= total paste volume

It can also be said that for a given paste volume, a higher packing density of the granular system provides a higher excess paste amount than what is required to fill the voids between the aggregates, and as such, a thicker paste layer coats the aggregates. Thus, a granular system with a high packing density with a sufficient excess paste layer is beneficial for better flowability due to lower inter-particle interaction. The correlation of excess paste layer thickness to flowability of fresh concrete is also confirmed by Denis et al. [86] and Kwan and Li [87]. Kwan and Li [87] reported that the fines in the aggregate (particles finer than 75 μm) are considered a part of the paste volume. To develop concrete mixtures with good shape stability and flowability, without compromising its self-consolidating characteristics, a sufficiently large paste volume is required, which will not only fill the voids between aggregates but also provide a sufficiently thick paste layer to ensure adequate flowability [10], [65]. Hoornahad et al.

[65] stated that paste consistency (ability to flow) is significantly controlled by the amount of superplasticizer and an increase in excess paste volume causes the yield stress and shape preservation factor (shape stability) to decrease.

Geiker et al. [88] investigated the effect of coarse aggregate volume fraction and shape on the rheology of SCC. Their results showed that not only volume fraction but also the aspect ratio, angularity, shape, and surface texture of coarse aggregate influence the yield stress and viscosity. Kohler [76] reported that natural aggregates, well-shaped crushed coarse aggregates, and well-shaped manufactured sands showed low interparticle friction, causing low HRWRA demand, and low plastic viscosity. Jovein and Shen [89] reported that for SCC mixtures at w/c = 0.35 and slump flow ranging between 580 mm to 740 mm, increasing aggregate volume resulted in higher static and dynamic yield stress. Their results also confirmed the Coussot [90] model relating the mixture yield stress to the yield stress of suspending fluid as shown in equation (3.4), which implies increasing aggregate volume increases yield stress of the mixture.

$$\tau_m = \tau_f \left(1 - \frac{\emptyset}{\emptyset^m}\right)^{-m} \tag{3.4}$$

where,

τ_m = yield stress of mixture,

τ_f = yield stress of suspending fluid,

ϕ = the volume fraction of particles,

$\emptyset_m$ = the maximum packing density of particles, and

m = a coefficient representing factors such as shape, angularity, roughness, etc.

Jovein and Shen [89] also confirmed the applicability of the Krieger-Dougherty equation [91] relating viscosity and volume fraction in concrete as shown below:

$$\eta_c = \eta_p \left(1 - \frac{\phi}{\phi_m}\right)^{-[\eta]\phi_m} \tag{3.5}$$

where:

η_c = the apparent viscosity of the suspension,

η_p = the apparent viscosity of the solution,

ϕ = the volume fraction of particles,

ϕ_m = the maximum packing density of particles,

$[\eta]$ = the intrinsic viscosity of the particles.

The Krieger-Dougherty (K-D) equation implies that higher aggregate volumes corresponds to higher plastic viscosity. Jovein and Shen [89] mentioned that the K-D equation is valid at t = 0 and plastic viscosity changes with time (t > 0). Their study further concluded that yield stress increases with an increase in FA/CA ratio and decreases with an increase in coarse aggregate (19 mm) due to greater surface area to volume ratio of the fine aggregate and lower aggregate surface area/mass ratio, respectively. Mahaut et al. [92] investigated the influence of coarse particle volume fraction on the yield stress and thixotropy of cementitious materials. Their results followed the Chateau-Ovarlez-Trung model [93] with $\varphi_m = 0.56$ for monodispersed spherical particles as shown below in equation (3.6):

$$\tau_c^{hom} / \tau_c = (1 - \varphi)^{1/2} (1 - \varphi / \varphi_m)^{-1.25\varphi_m} \tag{3.6}$$

Their study also reported that measurement of yield stress evolution of cement pastes in time and measurement of increase of the yield stress with the volume fraction of coarse particles for a single resting time is adequate to predict the value of the structuration rate of fresh concrete.

3.4 EXPERIMENTAL PROGRAM

3.4.1 Materials. In this section, properties of binder materials and aggregate employed in the development of VFC for slip-form paving are discussed in detail.

3.4.1.1 Cement, SCMs, and mineral fillers. Based on the paste component results, described in section 2.5, cement, silica fume, slag, and attapulgite clay have been selected maintaining the replacement proportion for the concrete scale. Although, new slag from three different sources (SL-A, SL-B, and SL-C) was tested. The chemical composition and physical properties of the slags are listed below in Table 3.1. SL-B has a higher aluminum and calcium oxide content compared to SL-A and SL-C. SL-C has the highest SiO_2 content (35.99%). For the chemical composition of cement, silica fume, and attapulgite clay, the reader is referred to Table 2.1.

3.4.1.2 Fine aggregate. Missouri river sand was employed. The density and absorption test were conducted according to ASTM C128-15 [112]. The gradation was carried out according to ASTM C136-14 [113]. Table 3.2 shows the physical properties of the fine aggregate.

3.4.1.3 Coarse aggregate. Two nominal maximum size (NMS) of 19 mm and 9.5 mm crushed limestone were used. Table 3.2 shows the physical properties of coarse aggregates. The density and absorption test were conducted according to ASTM C127-15 [114]. The gradation was carried out according to ASTM C136-14 [113].

Table 3.1 Chemical and physical properties of different slag deliveries

Basic compounds (%)	SL - A	SL - B	SL - C
MgO	8.65	4.77	8.30
Al_2O_3	8.57	10.90	7.13
SiO_2	32.80	29.58	35.99
SO_3	1.88	3.10	2.30
K_2O	0.37	0.32	0.39
CaO	45.93	49.41	44.09
TiO_2	0.52	0.64	0.43
Mn_2O_3	0.33	0.28	0.70
Fe_2O_3	0.70	0.25	0.45
Specific gravity	2.85	2.73	2.72
Mean Particle size (μm)	13.6	13.6	11.6

Table 3.2 Physical properties of aggregates

Aggregate	Specific gravity (g/cm^3)	Absorption (%)
19 mm	2.74	0.70
9.5 mm	2.78	0.46
Sand	2.61	0.37

3.4.1.4 Dispersing admixture. Based on the results obtained from the cement paste study with different w/b and different types of dispersing admixtures, the selected polycarboxylate-based dispersing admixture was employed. The dosage of the admixture was varied to assure slump flow of 500 ± 50 mm.

3.4.2 Mix Design and Mixing Procedure. The investigation on VFC mixtures was divided in two subtasks. A binary system: cement with 5% silica fume replacement (CEM - SF 5), was first employed to study the influence of modifications in excess paste layer thickness on thixotropy, fluidity, and green strength of VFC. Then, the best performing paste layer thickness was tested in systems with two different slags at 25% replacement and attapulgite clay at 0.5% replacement. Lastly, a ternary system with slag and attapulgite clay was tested.

3.4.2.1 Mix design. Table 3.3 represents the mix designs of different excess paste layer thicknesses evaluated. Table 3.4 represents the mix designs of the other binary and ternary mixtures evaluated. Detailed information on the mix design development and excess paste layer calculation can be found in Appendix. The reported dosage of SP is for the amount of commercial product added. The w/b has been kept constant at 0.35. The SL-C-AC has w/b ratio of 0.33.

3.4.2.2 Mixing procedure. All VFC mixtures were prepared in 75 L batches in a drum mixer with capacity of 150 L. Similar to the paste mixing procedure, the contact between water and binder is taken as the reference time. The elapsed times when executing green strength measurements and rheological measurements are relative to this reference time. The dispersing admixture (SP) is added in delayed If necessary, the SP dosage was increased. The testing procedure was started at 15 min and it was repeated on all VFC mixtures at 70 ± 5 min, in the same manner. The speed of the drum mixer was lowered between the 1st and 2nd testing procedure to mimic a

Table 3.3 Concrete mix proportion of different excess paste layer mixture

Material (kg/m3)	C-SF-40	C-SF-30	C-SF-25	C-SF-20	C-SF-25.1	C-SF-30.1
Cement	455	416.4	396	374.8	396.1	416.5
Silica fume	23.9	21.9	20.8	19.7	20.9	21.9
19 mm agg.	517.8	538.9	550.2	562	551	539.6
9.5 mm agg	369.9	384.3	392.6	401	392.7	384.6
Sand	884.2	917.1	936.5	956.7	939.5	920.1
Water	166.5	156.9	149.4	141.9	145.6	153
SP	1.66	1.74	2.15	2.15	1.45	1.52
w/b	0.35	0.35	0.35	0.35	0.35	0.35

Table 3.4 Concrete mix proportion of binary and ternary mixtures

Material (kg/m3)	SL-A	SL-B	SL-B-1	AC	SL-B-AC	SL-C-AC
Cement	357.5	355.6	355.6	478.3	352.2	350.8
Slag	119.2	118.5	118.6	-	118.2	117.7
Attapul-gite clay	-	-		2.4	2.4	2.4
19 mm agg.	518.7	518.7	517.5	517.5	517.1	519
9.5 mm agg	369	369	369.1	369.1	369.2	369.8
Sand	885.9	885.9	890.7	890.7	898.1	906.3
Water	164.1	163.2	159.7	159.8	150.4	138.8
SP	1.11	1.11	1	2.7	3	3.83
w/b	0.35	0.35	0.35	0.35	0.35	0.33

Table 3.5 Concrete mixing procedure

Time	Duration	Action and Addition
-1.00	1 min	Mix Aggregates + 1/2 water
0.00	30 sec	Add binders then add rest of water
0.50	1 min 30 sec	Mixing
2.00	1 min	Add SP
3.00	1 min	Rest and scraping
4.00	2 min	Mixing
6.00		Stop mixer
6.00	6 min	If slump flow 500 ± 50 mm achieved - Mixer agitated on slow speed and start testing at 15 min
		Else addition of SP and remixing

truck mixer in agitation mode. The mouth of the mixer was also covered with a plastic sheet to prevent evaporation of mixture water.

3.4.3 Test Method for Aggregate Maximum Packing Density. The. maximum packing density of the sand and coarse aggregates was determined using the gyratory intensive compaction tester (ICT). A dry homogenous mixture of coarse and fine aggregates was placed in the cylinder mold, rotating at a gyratory angle of 40 mrad for 124 cycles under a constant vertical pressure of 1.5 bar. Due to the gyratory inclination, shear movement under vertical pressure permits to attain a higher packing

density. The packing density of granular materials or aggregates (φ) is calculated as shown in the following equations (3.7) and (3.8):

$$\varphi = \frac{\rho_d}{\rho_{dmax}} \tag{3.7}$$

$$\rho_{dmax} = \frac{1}{\frac{P_1}{\rho_1} + \frac{P_2}{\rho_2} + \frac{P_3}{\rho_3} + \cdots} \tag{3.8}$$

where, P_1, P_2, and P_3 are weight percentages of the aggregates used in the mixture, and ρ_1, ρ_2, and ρ_3 represent the specific gravity values of the different aggregates. After a few trials, the selected vertical pressure was below a critical value which led to grinding or crushing of the particles. The critical pressure for the tested granular material was determined by observing the top surface of the cylinder mold after each trial. It can also be determined using the difference between its particle size distribution (PSD) before and after applying various pressures. Also, the number of cycles selected was based on when density reaches to its peak value and there is no considerable change on further increase in cycles [94]. The applied testing parameters to ICT are also shown in Table 3.6.

Table 3.6 Testing parameters imposed to ICT

Parameter	Unit	Available range	Selected
Cycles		2 - 512	124
Gyratory angle	mrad	0 - 50	40
Velocity	rpm	0 - 60	60
Vertical pressure	bar	0.5 - 10	1.5

3.4.4 Test Method for VFC Mixture Characterization. The flowability, workability loss, and green strength are related to the rheological properties such as yield stress, viscosity, and thixotropy. So, workability and rheological measurements were conducted simultaneously. Table 3.7 shows the different tests conducted for the characterization of VFC mixtures. Table 3.8 shows the testing procedure in detail. The testing procedure was repeated after 60 min for C-SF-40 mixture, at 80 min for C-SF-30, and at 70 ± 5 min for the other mixtures.

Table 3.7 Test methods used to evaluate properties of VFC

Property	**Test**
Yield stress and viscosity	Slump flow, T_{50}, ICAR – flow curve
Thixotropy	Green strength, Static yield stress

Table 3.8 Testing procedure protocol

Time	Duration	Action and Addition	Criteria
13.00	1 min	Mixing	
14.00	1 min	Get sample and filling up slump cone	
		Get sample and filling up ICAR container	
15.00	2 min	Slump flow measurement	Slump flow 500 ± 50 mm
		Dynamic flow measurement	ICAR Dynamic flow measurement
			Preshear - 20 sec at 0.5 rps
			Flow curve - 0.5 to 0.03 rps in 10 steps (each step = 5 sec)
			Total = 70 sec

Table 3.8 Testing procedure protocol cont.

17.00	4-5 min	Filling up all four molds for green strength test	
		Remix sample in ICAR	
22.00	2 min	Remove 1st mold + loading	Green strength measurement
		Start measurement for static yield stress - ICAR	apply 0.003 rps
27.00	2 min	Remove 2nd mold + loading	Green strength measurement
		Start measurement for static yield stress - ICAR	apply 0.003 rps
35.00	2 min	Remove 3rd mold + loading	Green strength measurement
		Start measurement for static yield stress - ICAR	apply 0.003 rps
50.00	2 min	Remove 4th mold + loading	Green strength measurement
		Start measurement for static yield stress - ICAR	apply 0.003 rps

3.4.4.1 Slump flow test and T50. The slump test was carried out according to ASTM-C1611-14 [115]. This test is specified for SCC mixtures in which a sample of freshly mixed concrete is placed in the Abram's cone in one layer on a flat, level, and nonabsorbent surface without any tamping or vibration. The cone was then raised in 3 ± 1 s and the average of two orthogonal diameters of the concrete spread was measured. After removal of the mold, the time required to reach 50 cm circle was measured to determine the T_{50} of VFC mixture. A longer T_{50} time represents higher viscosity. The slump flow test, including T_{50}, was repeated around 75 min from the water-binder contact. The change in slump flow indicates the workability loss of the VFC mixture.

Figure 3.12 Typical slump flow

3.4.4.2 Green strength test. In this test, removable cylindrical metal molds of 100 mm in diameter and 200 mm in height were used for concrete casting (Figure 3.13 (a)). On a flat surface, the two semi-cylinder molds were clamped together, standing on a nonabsorbent metal plate (Figure 3.13 (b)). During casting, freshly mixed concrete was placed in the cylinder in two layers without any vibration or rodding. After each layer, the mold was gently tapped to remove entrapped air. The cylinders were cast in a sequence of the testing protocol and remained undisturbed during the resting time. Each cylinder mold was removed at a given time and a cylinder with good shape stability i.e. with slightly or no deformation, was further tested for green strength as shown in Figure 3.13 (c). A square shaped plate was placed on top of the cylinder, guided by two vertical rods, and the cylinder was loaded with standard load blocks until collapse as shown in Figure 3.13 (d). The total weight of load applied during the test divided by the loading area provides the green strength of concrete mixture.

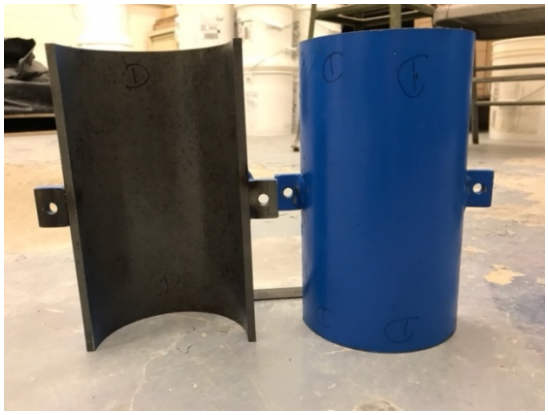

(a) a removable 100 mm x 200 mm mold

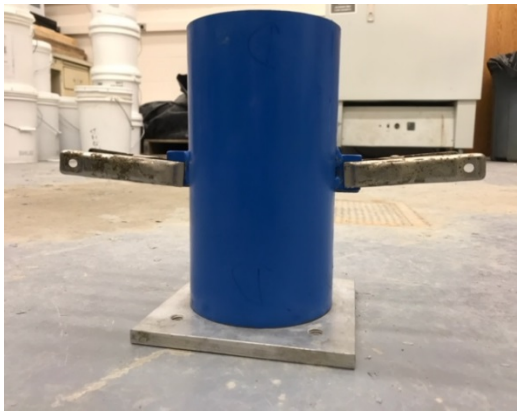

(b) molds clamp together for casting of fresh concrete on a square plate

(c) Typical shape stable concrete mixture

(d) Loading of sample using square plate on top and loading blocks

Figure 3.13 Green strength test setup

During casting, freshly mixed concrete was filled in four molds and the same sequence was followed for the green strength measurement to study the development of shape stability with time. The first cylinder was demolded after a resting time (sample remains undisturbed) of 5 min, and similarly, the 2nd, 3rd, and 4th cylinder was demolded after a resting period of 9 min, 16 min, and 30 min, respectively. Before the repeat measurement at 70 min, the speed of the mixer is increased to simulate the re-mixing process of a truck mixer before discharging on site. The entire procedure was repeated and green strength tests were conducted on four molds at identical resting times.

3.4.4.3 Density and air content test. The density of freshly mixed concrete was determined according to ASTM C 138-08 [116]. A sample of freshly mixed concrete was placed without any rodding or vibration in a measuring bowl conforming ASTM C 231. A strike-off bar was used to remove top surface of concrete and finished it smoothly. The same mixture was also used to determine the air content by pressure method, using type B-meter, according to ASTM 231-14 [117].

3.4.4.4 Rheology. The ICAR rheometer consists of a four-bladed vane, container, frame, laptop, and rheometer with torque and velocity sensors as shown in Figure 3.14. The four-bladed vane has a radius (R_i) of 62.5 mm and a height (h) of 127 mm. The container in which freshly mixed concrete is placed has vertical ribs and has an outer radius (R_o) of 143 mm.

Figure 3.14 ICAR rheometer parts [95]

3.4.4.4.1 <u>Testing procedure.</u> Immediately after mixing, freshly mixed concrete was placed in the rheometer container and the impeller is inserted in the concrete. The required parameters such as rotational velocity and time were provided

for the preshear, flow curve, static yield stress or thixotropy measurements. Firstly, like when determining the cement paste rheology, a pre-shear period was imposed for 20 seconds at a rotational velocity of 0.50 rps to eliminate the shear history from the sample prior to measuring. During this process, the torque gradually declines till it reaches equilibrium. This represents the amount of energy required to break down the internal structure of concrete mixture. After the pre-shear, the flow curve was measured by decreasing the rotational velocity stepwise from 0.5 to 0.03 rps in 10 steps of 5 s each. The rotational velocity profile is shown in Figure 3.15. The flow curve was used to determine the dynamic yield stress and plastic viscosity using the Bingham model.

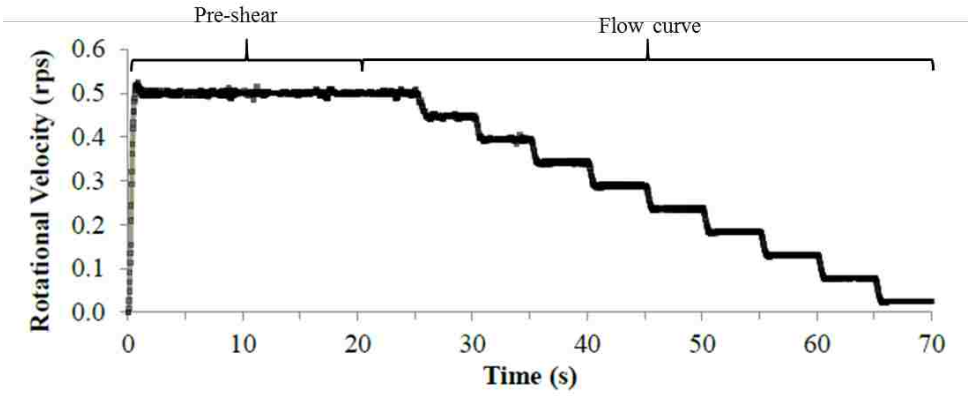

Figure 3.15 The rotational velocity profile imposed in ICAR rheometer

After the flow curve, the top of the rheometer was removed from the container and sample was mixed with a shovel to regain homogeneity prior to the thixotropic measurements. To measure the thixotropic properties, a rotational velocity of 0.003 rps was imposed on the sample at rest and a steady increase in torque was monitored. The test was terminated after the peak in torque was achieved. The maximum torque value can be related to the stress required to initiate the flow after rest.

The stress growth or thixotropy test was measured four times, i.e., the measurements ware conducted at resting periods of 3 min (i.e. 22nd min from water-binder contact), 5 min, 8 min, and 15 min, respectively. For example, sample is at rest for 5 min between the 1st and 2nd measurement. The sample is then returned to the mixer and agitated (slow speed). Before the second measurement, the speed of mixer is increased to simulate the re-mixing process of a truck mixer before the placement process on site. The entire procedure was repeated and thixotropy measurements were conducted in a similar fashion. The flow curve and stress growth results obtained after 1st and 2nd measurements were compared to determine the workability loss in concrete and its influence on the thixotropic properties.

3.4.4.4.2 <u>Determination of rheological properties.</u> Before mixing, the stress growth and flow curve measurements were conducted with an empty container to obtain "empty measurement". The raw torque and rotational velocity data obtained on concrete were plotted and corrected using the empty measurement data to avoid the effect of a residual torque. From the data collected in each step of the rotational velocity, the data of the first second of each step were discarded to eliminate the transition time between the velocity steps. For each step, torque data are monitored for equilibrium. On the remaining data during the last four seconds of each step, the average torque and rotational velocity were calculated. The torque measurements were eliminated in case of excessive scattering of data points, or non-equilibrium for each rotational velocity. Lastly, the torque-rotational velocity (T-N) was plotted using Bingham model as shown in Figure 3.16. The rheological properties are calculated by means of Reiner-Riwlin type of equation as shown below in equation (3.9), (3.10), and (3.11). The Reiner-Riwlin equation transforms the parameters G and H into (dynamic) yield stress (τ_o) and plastic viscosity (μ_p).

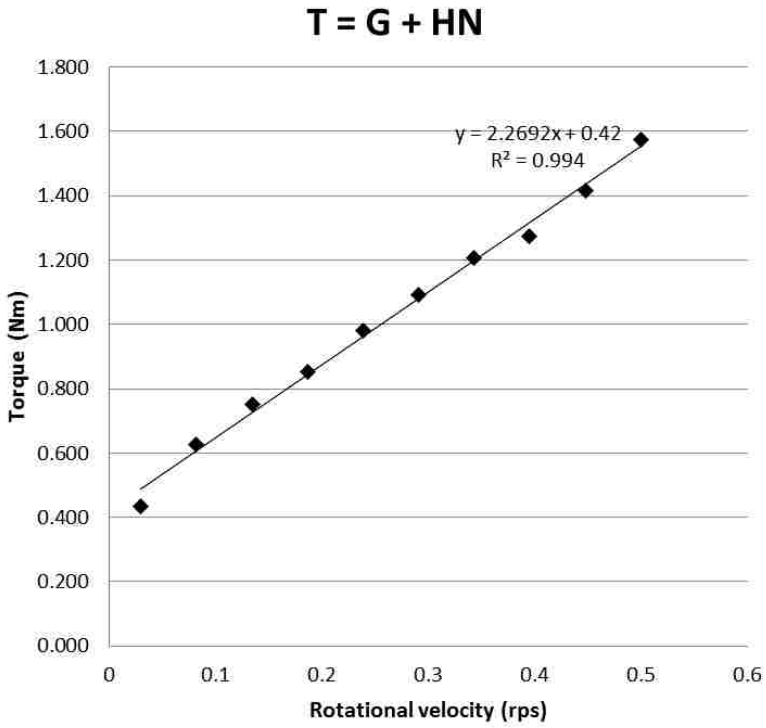

Figure 3.16 A typical flow curve at 15 min for the CEM-SF-30 mixture

$$\tau_0 = \frac{\left(\frac{1}{R_i^2} - \frac{1}{R_o^2}\right)}{4\pi \mathrm{h}\, ln\left(\frac{R_o}{R_i}\right)} G \tag{3.9}$$

$$\mu_p = \frac{\left(\frac{1}{R_i^2} - \frac{1}{R_o^2}\right)}{8\pi^2 \mathrm{h}} H \tag{3.10}$$

$$T = G + H\mathrm{N} \tag{3.11}$$

where: τ_o= yield stress (Pa)

G= intercept of T-N curve (Nm)

R_i= radius of inner cylinder (m)

R_o= radius of outer cylinder (m)

h= height of inner cylinder submerged into the material (m)

μ_p= plastic viscosity (Pa s)

H= the slope of T-N curve (Nm s)

The stress growth measurements were conducted at four different intervals. The corrected maximum torque value as explained in section 3.4.4.4.3 is then transformed to measure the static yield stress by following equation (3.12):

$$\tau_{o,s} = \frac{T_{max}}{2\pi R_i^2 h} \tag{3.12}$$

where, $\tau_{o,s}$ = static yield stress

T_{max} = maximum Torque (N-m)

R_i = radius of inner cylinder (m)

h= height of inner cylinder submerged into the material (m)

Figure 3.17 shows the typical stress response where intervals 1, 2, 3, and 4 represent the stress measurements at resting periods of 3 min, 5 min, 8 min, and 15 min; i.e. 22nd, 27th, 35th, and 50th min from the water-binder contact.

Similar to the cement paste study, the thixotropy is further evaluated by the average increase in static yield stress with time ($\Delta\tau_{0,s}$: static yield stress minus shear stress at end of interval 1 / elapsed time between two yield stress measurements), as well as the individual value of the 2nd interval, corresponding to a 5 min rest (depends time taken by 1st interval to achieve maximum stress) as shown in equation (3.13).

$$\Delta\tau_{0,s} = \frac{\tau_{0,s,x} - \tau_{0,s,1}}{t_x - t_1} \tag{3.13}$$

Where: $\Delta\tau_{0,s}$ = the increase of static yield stress (Pa/min)

$\tau_{0,s,x}$ = the static yield stress measured in interval x (Pa) (x = 2, 3, or 4)

t_x = time at which $\tau_{0,s,x}$ is measured

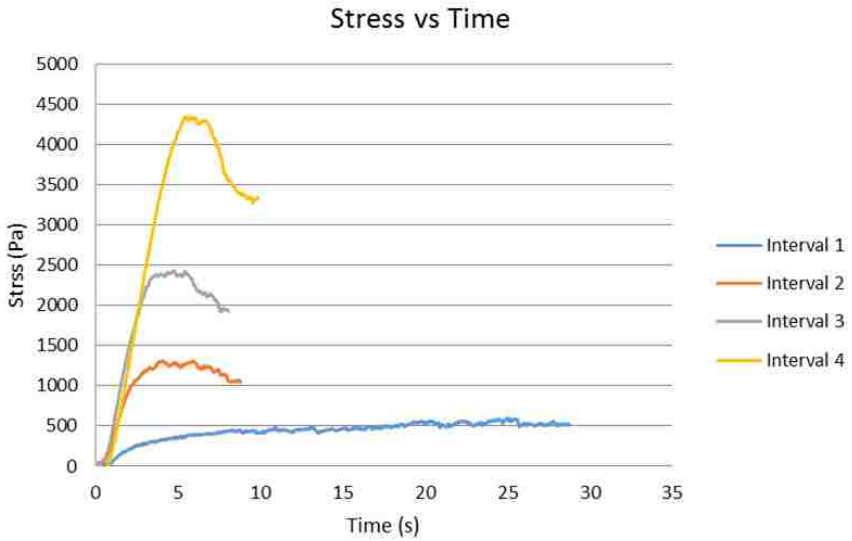

Figure 3.17 Typical result of increase in shear stress at a constant rotational velocity 0.003 rps. Results shown is for the 20 micrometers paste layer thickness

3.4.4.4.3 <u>Plug flow correction.</u> After determining the yield stress and viscosity using the Bingham model, the flow curve measurements were checked for plug flow, as the transformation equations assume that all material in the rheometer is sheared. Therefore, the shear stress at the outer cylinder is compared to the calculated yield stress value. If this value is smaller than the yield stress, there is plug flow as shown in detail in Figure 3.18. The plug flow correction was calculated using an iterative procedure in which an original estimation of yield stress and plastic viscosity obtained from the direct transformation is introduced. These values are compared to the yield stress and plastic viscosity obtained from the shear stress-shear rate data using the plug radius (partially sheared) instead of the outer cylinder radius (fully sheared) for the points that

have plug flow. The sums of differences between the rheological values at each iteration are minimized to a value smaller than 0.001. The resulting final values are considered as rheological properties of the mixtures.

Static yield stress measurements were also corrected by measuring an average empty torque value. An average torque value is subtracted from each maximum torque value obtained during the static yield stress measurement. Then, the corrected maximum torque value is transformed to determine the static yield stress value.

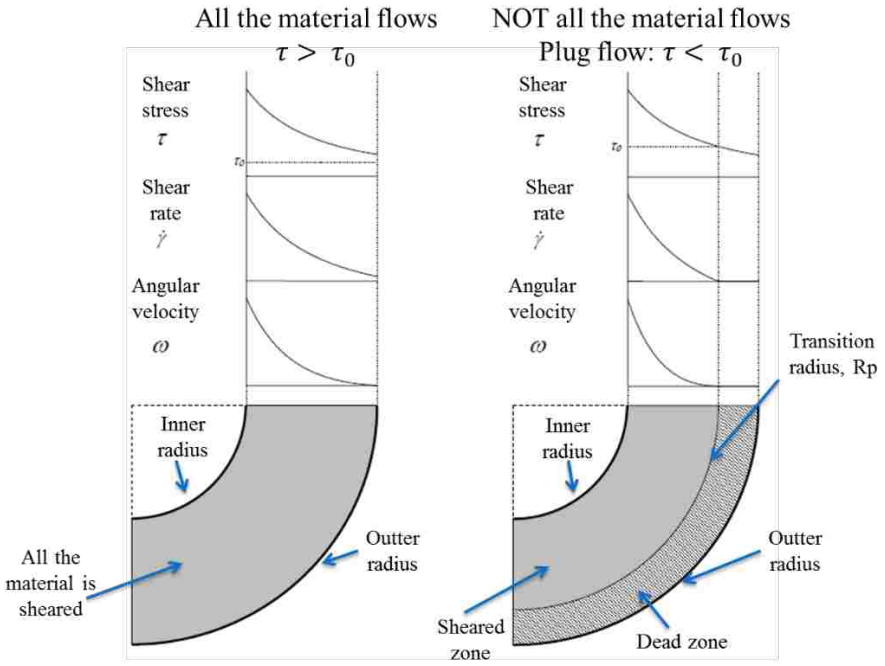

Figure 3.18 Plug flow correction

3.5 RESULTS AND DISCUSSION

The experimental task is divided in three different parts. Firstly, the aggregate proportions were optimized using the gyratory intensive compaction testing (ICT) machine. By means of the excess paste layer concept, concrete mixtures were developed and evaluated. Different paste layer thicknesses were considered for the evolution of thixotropy, flowability, workability loss, and green strength. The best

performing paste layer thickness was selected to investigate different SCMs and filler materials, as selected in the part studying the cement paste performance.

3.5.1 Optimization of Aggregate Proportions. Two different sizes of coarse aggregate with nominal maximum aggregate sizes of 9.5 mm and 19 mm, were used in the following tasks:

- Task 1 – Obtain two aggregate proportions using the Modified A&A model with a q-value of 0.29
- Task 2 – Evaluate maximum packing density of selected mix proportions using ICT

The modified Andreasen and Andersen (A&A model) was applied to obtain a maximum packing density using an equation (3.1) The distribution modulus (q) in the A&A model is a significant parameter controlling maximum packing density of aggregates and ultimately, the fresh and hardened properties of SCC. The least square difference method was applied to obtain a PSD of a mixture of three aggregates similar to the modified A&A model (Figure 3.19) by means of two different approaches:

- Approach 1 – At q = 0.29, selection of aggregate proportion with least square difference
- Approach 2 – At q = 0.29, selection of coarse aggregate proportions (9.5 mm and 19 mm), keeping the fine aggregate proportion constant at 50% (by weight) to ensure proper self-consolidating properties of the resulting SCC.

The aggregate proportions obtained by means of these approaches are shown in Table 3.9. Brouwers [96] reported that a q-value between 0.25 and 0.35 is favorable when targeting a large maximum packing density to reduce the quantity of cementitious materials or paste volume needed to ensure appropriate flow. The aggregate proportions

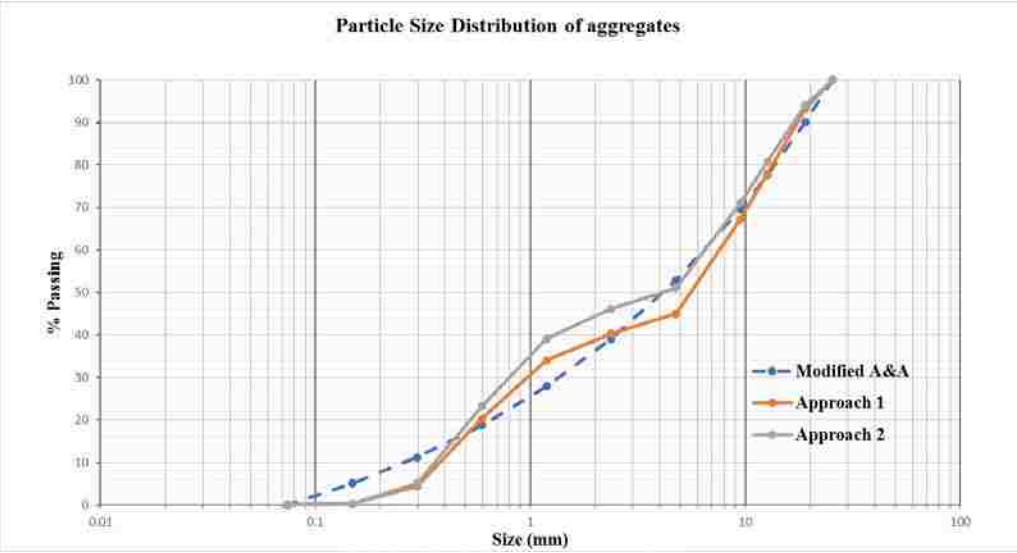

Figure 3.19 Particle size distribution of combined aggregates with two different approaches and Modified A&A model (dashed)

as shown in Table 3.9 were further tested by means of the ICT and the aggregate proportion with a maximum packing density is selected for the concrete mix design. For both aggregate proportions, the ICT test was conducted three times and the average of the maximum packing density was determined. A theoretical maximum density was determined using equations (3.7) and (3.8). The theoretical maximum density (ρ_{dmax}) for the aggregate proportions in approach 1 and approach 2 was 2689.5 and 2681.4 kg/m^3, respectively. A typical curve between density-cycles obtained from the ICT test is shown in Figure 3.20.

Table 3.9 Selected aggregate proportion

	q	19 mm (%)	9.5 mm (%)	Fine aggregate (%)
Approach 1	0.29	33	23	44
Approach 2	0.29	29	21	50

An increase in fine aggregate proportion from 0.44 (approach 1) to 0.5 (approach 2) increased the maximum packing density from 0.77 to 0.79 as shown in Table 3.10. The sand-to-total aggregate ratio was 0.44 and 0.5 in approach 1 and 2 respectively. Therefore, in this case, an increase in fine aggregate quantity plays an important role in achieving maximum packing density and reducing the paste volume to attain a required workability. The aggregate proportion from approach 2 i.e., 29% crushed limestone with NMS of 19 mm, 21% crushed limestone with NMS of 9.5 mm, 50% sand was used.

Table 3.10 Maximum packing density results from ICT

	Theoretical max. density (ρ_{dmax}) (kg/m^3)	Aggregate density (ρ_d) (kg/m^3)	Average max. packing density $\varphi = \frac{\rho_d}{\rho_{dmax}}$
Approach 1	2689.5	2077.5	0.77
Approach 2	2681.4	2109.0	0.79

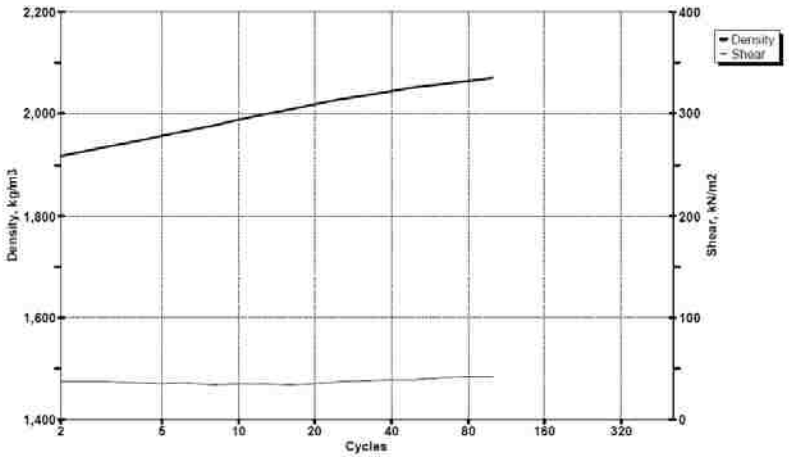

Figure 3.20 A typical density-cycles curve obtained from ICT. Result shown is for approach 1

The optimization of the aggregate proportions varies with the shape, size, and surface texture of the aggregates. More angular aggregates will require a larger portion of finer particles to fill the voids. Therefore, depending on the availability of aggregates, the aggregate proportions to achieve maximum packing density will change.

3.5.2 Influence of Excess Paste Layer and SP Dosage on Fresh Properties of VFC. The influence of four different paste layer thicknesses (40 μm, 30 μm, 25 μm, and 20μm) on the rheological properties of SFSCC, including dynamic properties, workability loss and thixotropy is shown in Table 3.11.

Table 3.11 Rheological results for the concrete with different paste layer and SP dosage.

Note that YS stands for the yield stress, ΔYS is the change in dynamic yield stress between the given time (in minute) flow curve measurements. The average static yield stress increase stands for the evolution of static yield stress over interval 1, 2, 3, and 4 (i.e. average static yield stress increase over 30 min).

Mixture	Dynamic YS (Pa)	Viscosity (Pa s)	ΔYS (Pa/min)	Average Static YS (Pa/min)	SP dosage (gm/kg)
C-SF-40	*15'*: 119.8 *60'*: 142.9	*15'*: 28.1 *60'*: 24.3	0.51	*15'*: 144.0 *60'*: 92.6	3.47
C-SF-30	*18'*: 77.2 *80'*: 205.2	*18'*: 40.8 *80'*: 34.8	2.06	*18'*: 70.9 *80'*: 173.2	3.97
C-SF-25	*17'*: 39.6 *72'*: 91.0	*17'*: 50.1 *72'*: 58.3	0.93	*17'*: 49.1 *72'*: 134.0	5.15
C-SF-20	*19'*: 92.0 *70'*: 209.7	*19'*: 89.0 *70'*: 69.8	2.31	*19'*: 139.3 *70'*: 174.5	5.44
C-SF-30.1	*16'*: 91.1 *70'*: 429.3	*16'*: 55.5 *70'*: 21.3	6.26	*16'*: 113.9 *70'*: 229.4	3.47
C-SF-25.1	*15'*: 155.5 *70'*: 624.2*	*15'*: 57.3 *70'*: 16.8	8.52	*15'*: 189.7 *70'*: 250.9	3.47

A binary system of cement with 5% silica fume has been selected for the evaluation of the excess paste layer concept. Initially, for all mixtures, the SP-content was adjusted to achieve a slump flow of 500 ± 50 mm. The fresh properties of all mixtures are shown in Table 3.12.

The first four rows in Table 3.11 show all results of different paste layer thicknesses and last two rows are mixtures (C-SF-30.1 and C-SF-25.1) with a constant SP dosage of 3.47 g/kg of binder. The results of the flow curve measurements i.e. dynamic yield stress, plastic viscosity, and change in dynamic yield stress (workability loss) were conducted at 15 min (1^{st}) and at 70 ± 5 min (2^{nd}), except for the C-SF-40 (at 60 min) and the C-SF-30 mixture (at 80 min). The thixotropic build-up was evaluated by the average increase in static yield stress as shown in the fifth column of Table 3.11.

From the results shown in Table 3.11 and Table 3.12 and Figure 3.21 to Figure 3.24, it can be seen that a change in excess paste layer thickness significantly affects the rheological properties. Thixotropy decreases substantially with a decrease in excess paste layer. A similar trend has also been seen in the change in dynamic yield stress. The average increase in static yield stress and dynamic yield stress of the concrete mixture with 25 μm excess paste thickness (C-SF-25) is 66% less than the concrete mixture with 40 μm excess paste thickness (C-SF-40).However, the plastic viscosity increases with a decrease in paste layer thickness. This substantial change in dynamic flow properties and thixotropy can be explained by the amount of dispersant (SP) dosage.

To achieve the desired flowability (slump flow of 500 mm), the SP dosage is increased from 3.47 to 5.15 g/kg of binder when decreasing the paste layer thickness from 40 to 25 μm. However, even with a large amount of SP, it was difficult to achieve the desired flowability in the 20 μm excess paste thickness mixture (C-SF-20). Thus,

Table 3.12 Fresh properties of all concrete mixtures

Mixture	Slump flow (mm)	Slump (mm)	T_{50} (sec)	Air content (%)	Density (Kg/m^3)
C-SF-40	*15'*: 525 *60'*: 390	*15'*: 280 *60'*: 235	*15'*: 1.36 *60'*: -	3.5	2428.4
C-SF-30	*18'*: 515 *80'*: 340	*18'*: 265 *80'*: 235	*18'*: 5.8 *80'*: -	Error	2430.0
C-SF-25	*17'*: 525 *72'*: 405	*17'*: 260 *72'*: 230	*17'*: 5.44 *72'*: -	4.1	2418.8
C-SF-20	*19'*: 330 *70'*: 315	*19'*: 220 *70'*: 215	*19'*: - *70'*: -	7.8	2375.5
C-SF-30.1	*16'*: 450 *70'*: 300	*16'*: 255 *70'*: 215	*16'*: - *70'*: -	4.3	2399.6
C-SF-25.1	*15'*: 360 *70'*: discard	*15'*: 220 *70'*: discard	*15'*: - *70'*: -	5.2	2385.1
SL-A	*16'*: 450 *77'*: 295	*16'*: 260 *77'*: 150	*16'*: - *77'*: -	4.1	2391.5
SL-B	*16'*: 570 *72'*: 370	*16'*: 280 *72'*: 240	*16'*: 0.66 *72'*: -	2.8	2425.2
SL-B-1	*16'*: 500 *75'*: -	*16'*: - *75'*: 175	*16'*: 4.6 *75'*: -	3.7	2393.2
AC	*16'*: 520 *73'*: 430	*16'*: - *73'*: -	*16'*: 0.52 *73'*: -	2.9	2436.4
SL-B-AC	*16'*: 500 *71'*: 420	*16'*: - *71'*: 250	*16'*: 3.2 *71'*: -	3.3	2438.0
SL-C-AC	*16'*: 575 *73'*: 600	*16'*: 280 *73'*: 270	*16'*: 1.92 *73'*: 1.82	3.6	2410.7

due to lower flowability, it is obvious that all static yield stress values are higher compared to other mixtures. However, in the 1st measurement, it is notable that the average increase in static yield stress value in the 20 μm mixture is lower than the 40

μm mixture. It can be stated that an increase in SP dosage leads to a more flowable paste and can reduce the workability loss due to delays in the hydration reaction [89]. Figure 3.22 also gives a clear indication of the lower structure build up with a decrease in paste layer thickness. The effect of the SP seems very clear in the first measurement period (from 15 to 45 min), leading to a significant decrease in static yield stress or build up in structure.

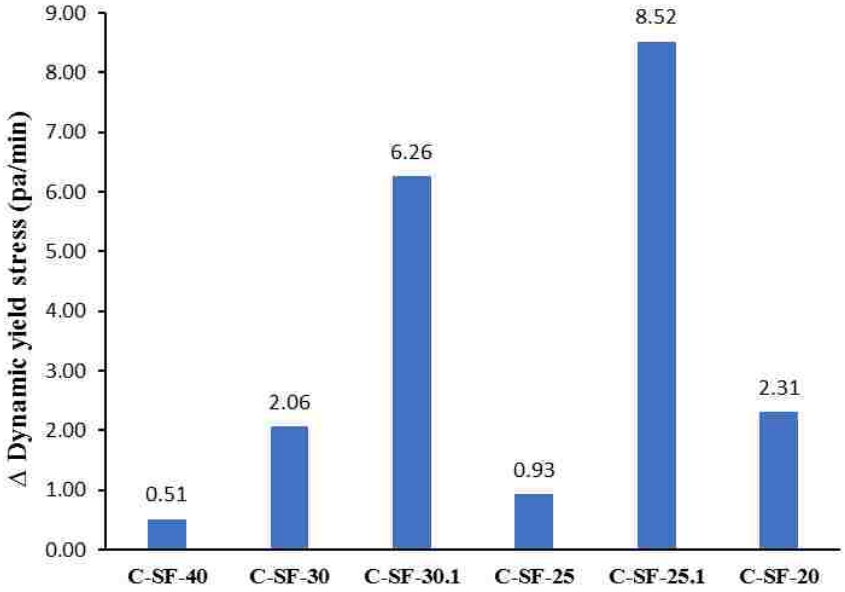

Figure 3.21 Increase in dynamic yield stress

However, in the 40 μm excess paste thickness mixture, the static yield stress growth declines in the 2nd measurement compared (started at 60 min) to the 1st measurement. However, for the 30 μm excess paste thickness (C-SF-30) mixture, the second measurement was started at 80 min and significant workability loss has been observed compared to C-SF-40 and C-SF-25. The average increase in static yield stress accelerates in the C-SF-30, C-SF-25, and C-SF-20 mixtures, compared to the C-SF-40 mixture, during the second measurement period.

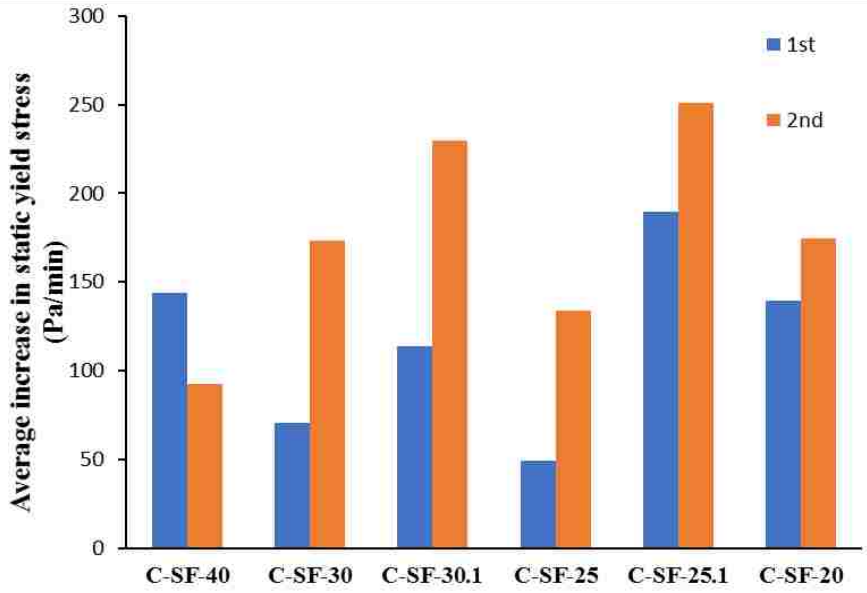

Figure 3.22 Average increase in static yield stress in 1st and 2nd measurement

Theoretically [89], [92], [93], with a decrease in excess paste layer thickness or increase in aggregate volume, an increase in dynamic yield stress, viscosity and thixotropy should be obtained. However, by increasing the SP content when decreasing the excess paste layer thickness, the rheological properties of the paste are modified (especially static and dynamic yield stress), countering the expected effect of increasing the aggregate contents. The 40 μm excess paste layer mixture delivers higher structural build up and lower workability loss. In order to understand influence of the SP quantity, the 30 μm and 25 μm excess paste layer thickness mixtures were repeated with a constant 3.47 g/kg of binder - SP dosage, which is the quantity of SP in the CF-S-40 mixture.

As expected, the flowability of the C-SF-30.1 and C-SF-25.1 mixtures decreases significantly and the rheological properties such as dynamic yield stress and average increase in static yield stress increase in both the mixtures. The dynamic yield stress increment is related to the change in slump flow. However, the average increase

in static yield stress of the C-SF-30.1 mixture is still less than that of the C-SF-40 mixture. A significant workability loss is observed in both lower excess paste layer mixtures i.e. 6.26 and 8.52 Pa/min respectively, rendering both mixtures less favorable for prolonged transportation time. Moreover, the workability loss can also explain the static yield stress growth in 2nd measurement (after remixing) as shown in Figure 3.24. In both mixtures, C-SF-30.1 and C-SF-25.1, during the last static yield stress measurement i.e. at 105 min, the torque limit was reached in the ICAR rheometer and the test was terminated. Therefore, the last measurement data provided is based on the maximum torque value achieved by the rheometer. During the second measurement, a slump flow of 300 mm and a slump of 215 mm was recorded for the C-SF-30.1 mixture. For the C-SF-25.1 mixture, the slump test was discarded due to shear failure. This also signifies the failing in self-consolidating properties of both mixtures. Due to low consistency or slump flow, the second measurement data for flow curve was also difficult to analyze. Thus, data was discarded.

In summary, the SP dosage has a significant role in maintaining the consistency of the mixture. With a decrease in paste layer thickness, the SP dosage to maintain a fluidity level increases. But, this increase in SP dosage has a contra productive effect on the thixotropy. Also, the loss of workability is higher and the self-consolidating properties of the mixtures are at risk. Thus, a mixture with an excellent stability and a proper balance between rheological properties and relatively low amount of SP is required. The mixture with 40 μm excess paste layer thickness shows the highest thixotropy, low viscosity, low workability loss and low SP dosage compared to other mixtures. Therefore, the 40 μm paste layer is selected for the next series of experiments on binary and ternary binder systems.

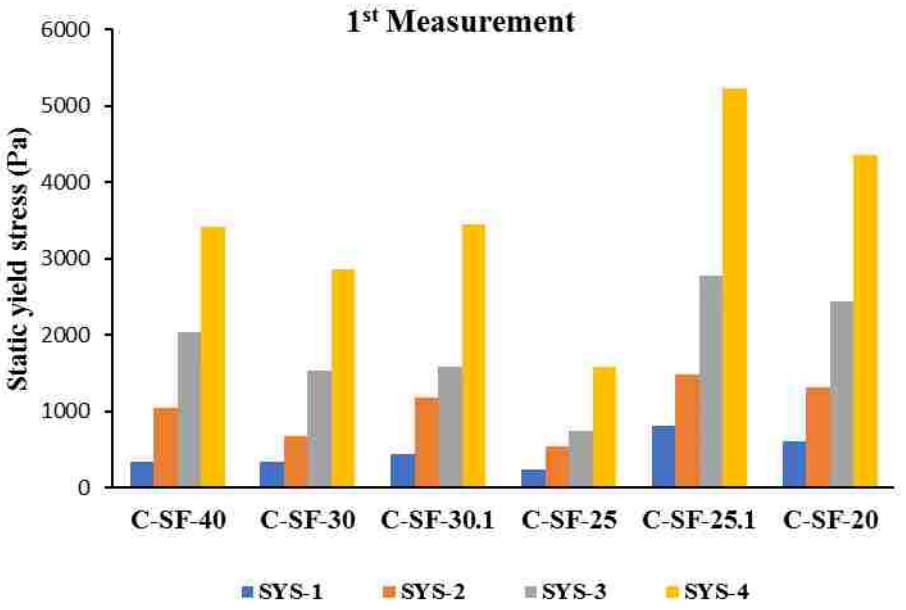

Figure 3.23 Static yield stress (SYS) growth for 1st measurement in interval 1, 2, 3, and 4 represented as SYS-1. SYS-2, SYS-3, and SYS-4 respectively.

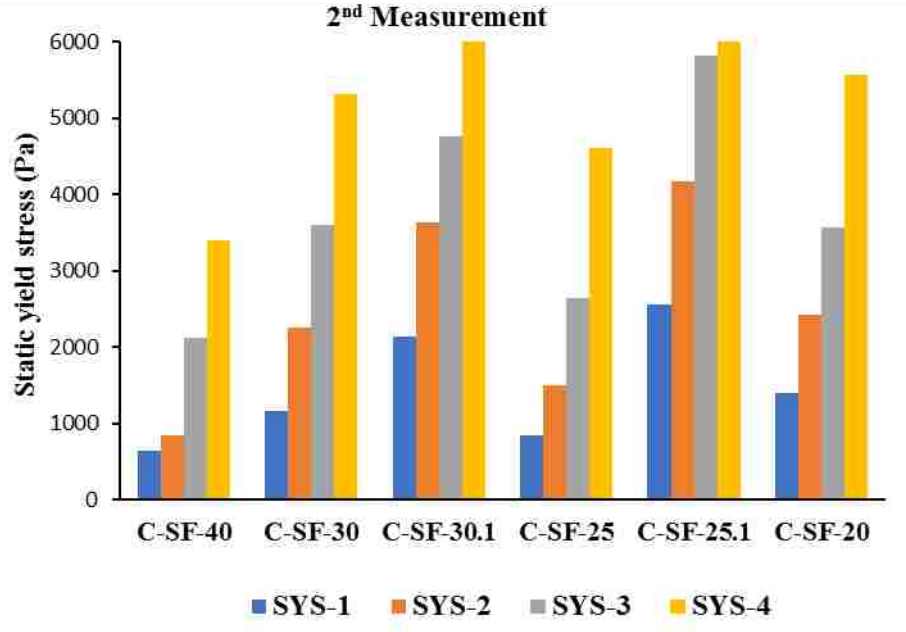

Figure 3.24 Static yield stress (SYS) growth for 2nd measurement in interval 1, 2, 3, and 4 represented as SYS-1. SYS-2, SYS-3, and SYS-4 respectively.

3.5.3 Influence of Binary and Ternary Binder Composition on Fresh Properties of VFC. Based on the results from the cement paste study, binary mixtures with slag and attapulgite clay and a ternary mixture combining the slag and attapulgite clay were selected for the evaluation of flowability and rheological parameters. In this task, slag from two different sources and attapulgite clay were tested separately in binary systems i.e., SL-A, SL-B, and AC. SL-A and SL-B were tested at identical SP dosage used in the paste study to investigate the influence of the SP dosage on concrete scale. Due to excess flowability in the SL-B mixture, the SP dosage was reduced and a new mixture (SL-B-1) was prepared to achieve the desired flowability. The best performing slag was then further combined with the attapulgite clay (SL-B-AC). Moreover, slag obtained from the third source was only tested on a ternary system (SL-C-AC).

All rheological properties are shown in Table 3.13 and in Figure 3.25 and Figure 3.26 The mixture with silica fume and with a 40 μm excess paste layer thickness (C-SF-40) is included as reference for comparison. In all binary and ternary systems, the change in dynamic yield stress is substantially higher and the thixotropic growth is lower compared to the C-SF-40 reference mixture. The binary mixture with attapulgite clay shows the lowest workability loss and higher average increase in static yield stress, compared to the mixtures with slag. However, attapulgite clay consumes more than double the amount of SP compared to slag mixtures. Comparing the slag mixtures with an equal SP dosage, SL-A performs better in terms of static yield stress development, but shows higher workability loss compared to SL-B. However, with a reduction of the SP dosage for slag B, rheological parameters such as plastic viscosity, thixotropy, and workability loss are increased in SL-B-1 by more than 100% compared to SL-B.

In all, SL-B-1 shows significant workability loss but a moderate thixotropy build-up compared to SL-A, whereas attapulgite clay shows a significant increase in static yield stress growth development and low workability loss. Therefore, a binary system with attapulgite clay could be suitable for slip forming for extended transportation time. Slag mixtures consume less SP than mixtures with attapulgite clay. Thus, a combination of SL-B with attapulgite clay is further evaluated to investigate the rheological properties.

Table 3.13 Rheological properties of binary and ternary systems.

Mixtures	Dynamic YS (Pa)	Viscosity (Pa s)	ΔYS (Pa/min)	Average Static YS (Pa/min)	SP dosage (gm/kg)
C-SF-40	*15'*: 119.8 *60'*: 142.9	*15'*: 28.1 *60'*: 24.3	0.51	*15'*: 144.0 *60'*: 92.6	3.47
SL-A	*15'*: 99.3 *80'*: 460.6	*15'*: 32.1 *80'*: 19.2	5.92	*15'*: 82.5 *80'*: 106.0	2.31
SL-B	*15'*: 75 *70'*: 277.8	*15'*: 20.6 *70'*: 13.9	3.62	*15'*: 52.5 *70'*: 84.2	2.31
SL-B-1	*15'*: 124.8 *70'*: 558.0	*15'*: 43.7 *70'*: 20.7	7.34	*15'*: 114.3 *70'*: 106.9	2.11
AC	*15'*: 124.4 *70'*: 209.9	*15'*: 11.8 *70'*: 13.7	1.50	*15'*: 125.3 *70'*: 134.4	5.55
SL-B-AC	*15'*: 78.9 *70'*: 284.9	*15'*: 30.1 *70'*: 20.9	3.75	*15'*: 136.9 *70'*: 226.7	6.39
SL-C-AC	*15'*: 67.6 *70'*: 22.9	*15'*: 20.9 *70'*: 24.6	-0.78	*15'*: 54.0 *70'*: 44.8	8.10

As mentioned earlier, slag from a third source is also tested by means of a ternary system (SL-C-AC). From the results, a change in chemical compositions and

physical properties of different slag sources significantly affects the rheological properties.

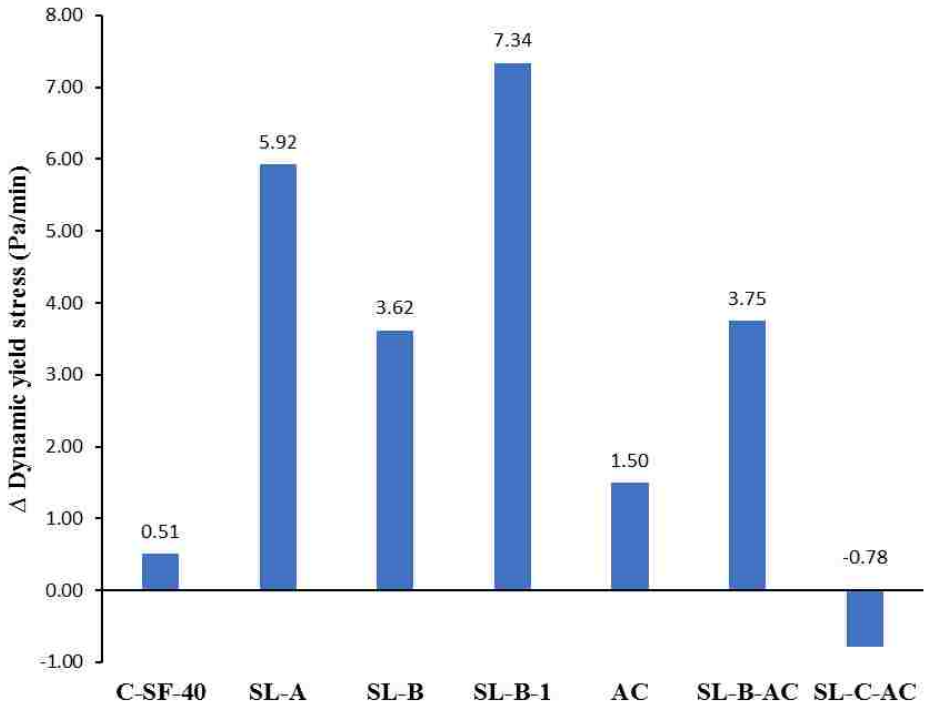

Figure 3.25 Increase in dynamic yield stress of binary and ternary systems.

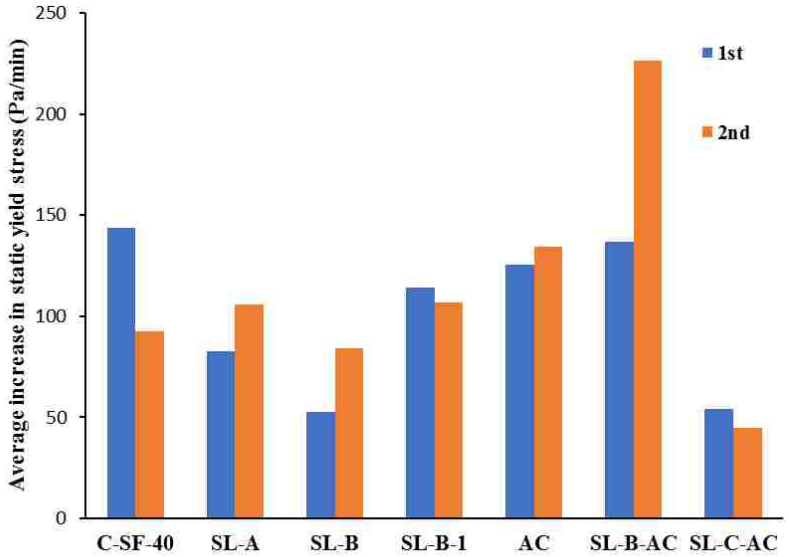

Figure 3.26 Average increase in static yield stress for binary and ternary systems.

The slump flow in SL-C- AC increases from 575 mm to 600 mm between1st and 2nd measurement. This also leads to a reduction in dynamic yield stress with time and low thixotropic build-up. This behavior can most likely be attributed to the large SP dosage. However, SL-B-AC mixture shows substantial growth in static yield stress, close to the reference mixture. Combining slag with attapulgite clay, in SL-B-AC, yields positive outcomes in both thixotropy build-up and workability loss compared to their binary slag mixtures. Therefore, SL-B-AC mixture could be a more economical and favorable option for extended transportation time.

3.5.4 Green Strength Evolution and Static Yield Stress Growth. Table 3.14 and Figure 3.27 show the green strength results and the static yield stress values for a given time (from water-binder contact). SL-B-1 and C-SF-25.1 shows the earliest shape stability around 50 min. Other mixtures gain sufficient green strength after remixing of the sample and evaluating after 70 min. Mixtures such as C-SF-30.1, C-SF-25.1, and C-SF-20 achieve significant green strength in the 2nd measurement. This can be attributed to higher workability loss and less flowability, potentially reducing the self-consolidating characteristics of the mixtures. Mixtures such as SL-A and SL-B-1 achieve good shape stability at low static yield stress compared to other mixtures.

Roussel and Coussot [97] proposed a yield stress analysis based on the slump test for different flow regimes, based on dimensional criteria i.e., H>>R and H<<R. Using this principle on the green strength test method, H and R are final height and radius of the standing concrete. The following equation (3.14) was derived to measure the yield stress of a standing concrete pile: (H>>R):

$$\tau_c = \frac{\rho g(H - z_c)}{\sqrt{3}} \tag{3.14}$$

where, τ_c= yield stress

ρ = density of material

g = gravitational constant

H = initial height

z_c = slumped height

Based on the above equation, the minimum yield stress required to achieve good shape stability or sufficient green strength can be estimated.

In this case, $z_c = 0$ as no deformation is permitted

H = 200 mm or H can vary depending on thickness of the pavement.

ρ = 2438 kg/m^3 - the maximum density obtained from all mixtures

Therefore, yield stress should be around

τ_c = 2761.7 Pa.

However, this is an estimation of the yield stress and is only valid when H>>R. In this case, the height to radius ratio (H/R) is 4. Therefore, based on this estimation, the static yield stress measurement can be related with flow regime yield stress analysis proposed by Roussel and Cousssot [97]. This estimation can be used to evaluate the suitable mixtures for different pavement thickness.

The relationship between static yield stress and green strength shows some irregularity to form a conclusion (Figure 3.27). In above Figure 3.27 shows relationship between static yield stress obtained from ICAR (Y- axis) and addition of yield stress calculated using Roussel and Coussot [97] equation for a standing concrete pile and from green strength measurement (X- axis). This can be explained by the errors in the green strength test.

Table 3.14 Green strength and static yield stress data

Mixture	Static yield stress (Pa)	τ_c + Green strength (Pa)	Time (min)
C-SF-30.1	4760.3	4774.3	90
	7335.6	7226.6	105
C-SF-25.1	5223.2	7300.1	52
	4173.2	9164.3	82
	5824.0	9256.7	90
	7544.8	10957.3	105
C-SF-20	5563.9	5636.0	107
SL-A	2640.1	9423.7	98
SL-B-1	3989.8	3432.3	50
	4346.1	6965.9	105

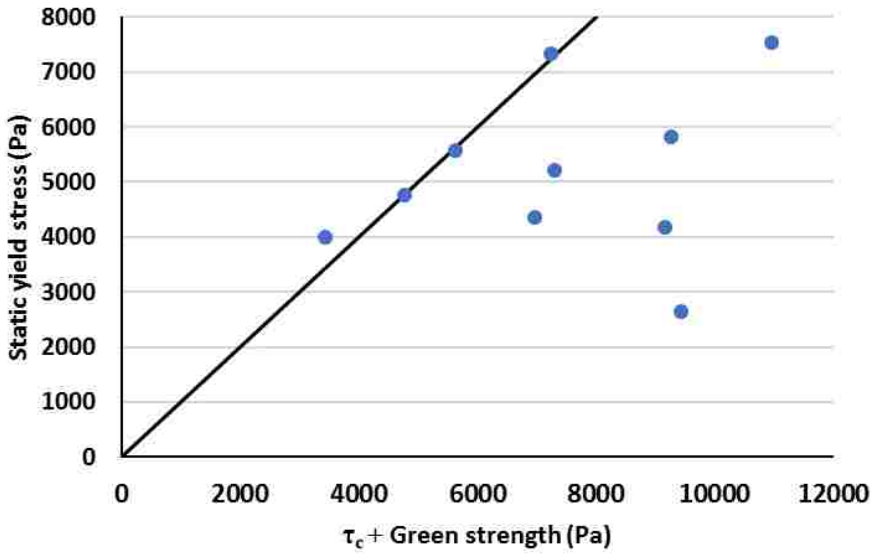

Figure 3.27 Green strength and static yield stress relationship

Firstly, concrete is filled in two-layers and tapped from outside to remove entrapped air. But, the variation in height or quantity in filling of concrete mixture in

two layers may have created discontinuity between two layers, causing shear failure in the mixture. Also, tapping the mold might have led to instability of the test setup. Secondly, sticky mixtures or insufficient smoothness of the mold's surface lead to difficult demolding of the samples, causing movement of the shape stable fresh concrete and failure of sample. Therefore, a test procedure providing a better casting and demolding process is required to ease the measurement of the green strength of concrete. It can be seen that either data points follow the relationship or static yield stress measurement from ICAR is lower than the green strength measurement result. So, error could also be happened due to static yield stress measured by ICAR.

4. KEY HARDENED PROPERTIES OF VIBRATION-FREE CONCRETE

It is important to study the effect of SCMs, mineral and chemical admixtures on the hardened properties to evaluate the feasibility of the SFCC mixtures concerning durability and sustainability of slip form paving construction.

4.1 INFLUENCE OF CONSTITUENT ELEMENTS ON THE HARDENED PROPERTIES OF SLIP-FORMING SCC (SFSCC)

The following sub-sections discuss how SCMs, mineral and chemical admixtures affect the hardened properties of the slip form self-consolidating concrete.

4.1.1 Effect of Supplementary Cementitious Materials (SCMs). The effect of high replacement rates of cement by fly ash and silica fume on mechanical properties has been studied by several researchers [68], [98], [99]. Results illustrate that the application of high amounts of FA combined with 10% SF replacement improve the mechanical properties, freeze-thaw and chloride penetration resistance [98]. Higher amounts of fly ash also resulted in a reduction of shrinkage [68]. The total shrinkage of the specimen can be reduced by using fly ash and slag whereas drying shrinkage increased when using silica fume in binary blended mixtures [100]. Celik et al. [101] investigated the mechanical properties and durability of SCC containing higher proportions of fly ash (up to 50%) and limestone powder (up to 25%). The study stated that the incorporation of fly ash or fly ash with limestone powder resulted in an increase in resistance to chloride penetration compared to mixtures with pure cement and other control mixtures i.e., mixtures blended with 15% and 25% limestone powder. Their results also indicated that the presence of the limestone powder reduces void and pore formation and the hydration of fly ash, resulting in a pore size reduction explaining the increased chloride penetration resistance. Binary mixtures blended with 30% and 50% fly ash showed lower water absorption compared to control mixtures and ternary

mixtures blended with limestone powder and fly ash. However, for ternary mixtures, increasing the limestone and fly ash content resulted in higher water absorption in mixtures [101].

4.1.2 Effect of Clay Minerals. Metakaolin (MK) replacement can enhance the compressive strength [70], [102], freeze-thaw resistance value [70], [102] and reduced chloride penetration [70] and drying shrinkage [70]. Bumanis et al. [73] indicated that concrete with 15 % MK replacement resisted more than 500 freeze-thaw cycles, chloride penetration was decreased more than 3.7 times compared to the reference mixture and compressive strength of 70 MPa (28 days) was achieved. Garg and Wang [71] investigated the performance of different clay minerals on fly ash-modified mortars. Their results indicated that replacement of up to 15% MK led to an increase in compressive strength. However, other clay minerals such as Kaolin enhanced the compressive strength only by 5-10% and attapulgite clay showed minimal effect on strength [71]. It has also been found that all clay minerals led to higher rate of heat generation i.e. acceleration of hydration process and reduction in setting time due to its finer size and filler effect [71]. The field investigation conducted by Iowa state University and Northwestern University also stated that SFSCC with attapulgite clay resulted in similar compressive strength compared to conventional concrete mixtures for pavements [10]. Also, SFSCC with attapulgite clay displayed less deterioration in freeze-thaw durability and scaling compared to other concrete mixtures. The results presented that all SFSCC mixtures were more freeze-thaw durable compared to conventional concrete pavement mixtures. Furthermore, an addition of up to 1% of nano-limestone increased the compressive strength but this decreased with further increasing dosage [70]. A compressive strength of more than 40 MPa was achieved in [70].

Wang et al. [70] reported that the incorporation of nano-limestone (1%) in SFSCC mixtures led to an increase in compressive strength and freezing-thawing resistance while drying shrinkage and chloride penetration decreased. Clay minerals used in fly ash-modified concrete mixtures for slip form paving [103] indicated that low dosages (up to 2%) of clay showed similar shrinkage and cracking behavior as conventional slip form concrete. The addition of attapulgite clay and kaolin led to an increase in drying shrinkage, whereas metakaolin reduced it. Also, the incorporation of attapulgite clay and metakaolin displayed cracking at earlier age in SCC with fly ash. However, for other hardened properties, such as compressive strength and splitting tensile strength all SFSCC exhibited comparable performance to conventional concrete [104]. The small difference was found between the compressive strength values of loosely filled (non-vibrated) and vibrated cylinders cast from the same mixture as evaluated by Pekmezci et al. [9] and Armaghani et al. [69].

4.1.3 Effect of Chemical Admixtures. The addition of shrinkage reducing admixture (SRA) or super-adsorbent polymers (SAP) can result in a decrease in compressive strength [75], [105]. Han et al. [75] also concluded that SAP is beneficial for the reduction of autogenous shrinkage at later ages while SRA performed better than SAP for drying shrinkage reduction. Wang et al. [105] stated that to control the loss in compressive strength, it is necessary to control the dosage of SAP and its entrained water content. The use of SRA can result in a significant decrease of drying shrinkage of SCC by reducing surface tension [106], [107], [108]. As both SRA and VMA increase the viscosity of the pore fluid [109], they may help reducing evaporation and change the rate of drying shrinkage. However, no impact was found in drying shrinkage of high strength SCC containing VMA [110].

The effect of SRA was investigated in the field study of SFSCC for slip form pavement [10]. The results indicated that low dosages (2.5 $1/m^3$) of SRA decreased the shrinkage property effectively whereas a higher dosage (7.5 $1/m^3$) not only decreased the amount of drying shrinkage but also diminished the cracking phenomena in the pavement. Heikal et al. [111] investigated the influence of PCE superplasticizer on compressive strength of cement paste containing silica fume. The authors indicated that compressive strength of ordinary Portland cement (OPC) paste was higher than OPC containing silica fume in absence of superplasticizer, however between 0.75-1.5 wt % PCE the compressive strength of OPC with silica fume was higher than OPC.

4.2 TESTING METHODS

In this section testing method of key hardened properties of VFC such as compressive strength and split tensile strength are discussed.

4.2.1 Compressive Strength Test. For each mixture, nine specimens were produced to test compressive strength according to ASTM C31-15 [118]. The specimens were cast in two layers and rodded 5 times each layer. After casting, the cylinders were covered with a plastic sheet to avoid moisture loss and demolded after 24 hours. All specimens were cured under water for 1, 7, and 28 days. The testing of cylinders was conducted according to ASTM C39-C39M-11a [119] on a Tinius-forney machine.

4.2.2 Split Tensile Strength Test. Three specimens were produced and cured similar to the compressive strength specimens. All specimens were tested at 28 days according to ASTM C496-11 [120] on a Tinius-forney machine.

4.3 RESULTS AND DISCUSSION

Table 4.1 represents compressive strength of all concrete mixtures. Severe surface defects were observed in the C-SF-40 mixture and only three specimens were tested for the compressive strength at 28 days. It can be seen that compressive strength decreases on increasing the paste layer thickness from 25 μm to 40 μm. Slag – B shows higher compressive strength compared to slag – A.

Table 4.1 Compressive strength results of all mixtures

Mixture	1 day (MPa)	7 days (MPa)	28 days (MPa)
C-SF-40	-	-	55.1
C-SF-30	38.0	52.3	57.5
C-SF-25	34.8	49.5	62.7
C-SF-20	-	43.5	55.4
C-SF-25.1	35.5	46.6	55.8
C-SF-30.1	38.4	47.3	58.0
SL-A	26.2	40.5	44.1
SL-B	28.0	38.4	44.9
SL-B-1	27.2	39.9	47.4
AC	37.0	44.6	48.1
SL-B-AC	31.7	53.2	54.4
SL-C-AC	Samples were discarded due to poor workability		

Addition of attapulgite clay leads to an increase in compressive strength (AC and SL-B-AC) compared to mixtures with slag (SL-A, SL-B, SL-B-1). The incorporation of attapulgite clay also shows higher one-day strength. However, all binary and ternary mixtures incorporating slag and attapulgite clay shows lower compressive strength than C-SF-40 mixture. Table 4.2 represents split tensile strength of all mixtures at 28 days.

Table 4.2 Split tensile strength results of all mixtures

Mixture	28 days (MPa)
C-SF-40	-
C-SF-30	4.0
C-SF-25	3.9
C-SF-20	4.0
C-SF-25.1	3.1
C-SF-30.1	3.6
SL-A	4.0
SL-B	-
SL-B-1	4.2
AC	2.3
SL-B-AC	3.8
SL-C-AC	-

Due to severe surface defects in the C-SF-40 and SL-B mixtures, the specimens were discarded. The split tensile strength shows negligible change on increasing paste layer thickness from 20 μm to 30 μm. It can be seen that the incorporation of attapulgite clay shows a reduction in split tensile strength in mixtures AC and SL-B-AC.

4.4 FUTURE TESTING RECOMMENDATION

To investigate the suitability of VFC mixtures for slip form paving, it is also important to test mixtures for mechanical and durability tests. Due to the low air content in the mixture the concrete may susceptible to freeze-thaw or scaling issues, although the low w/b ratio is beneficial to resist freezing and thawing. The application of air-entrainment should be investigated in future. Other important mechanical properties, such as drying and autogenous shrinkage, can also be improved with the application of shrinkage reducing admixtures. The shrinkage increases with increasing paste volume (and thus excess paste layer thickness), making the requirement of fresh properties challenges for the hardened properties. Thus, application of shrinkage reducing admixture should be studied to control drying and autogenous shrinkage. Durability tests such as sorptivity and air void analysis should be carried out on best performing mixtures. Cores should be taken from a field implementation study to perform non-destructive tests for the investigation of the air void system and the aggregate distribution through the depth of the pavement. Lastly, samples should be tested at early age (1 and 7 day) and long-term age (28, 56 day) for compressive and split tensile strength.

5. CONCLUSION AND FUTURE RECOMMENDATIONS

In this research, flowability, workability loss, thixotropic development and green strength of vibration-free concrete (VFC) was evaluated for the application of slip-form paving construction. The research task was mainly divided into two parts. Firstly, the paste component of VFC was determined by evaluating different types of superplasticizer, supplementary-cementitious materials (SCM), and mineral fillers. In this task, the dynamic rheological properties and thixotropic development of pastes was investigated. Secondly, the excess paste layer concept was implemented and different paste layer thicknesses were examined. Further in the concrete task, the best performing paste layer thickness was evaluated on binary and ternary systems with slags and attapulgite clay.

5.1 CONCLUSION

Based on the results obtained, the following conclusions can be drawn:

1. The structural build-up method provides a good understanding to assess the thixotropy development of paste. A static yield stress measurement directly after the flow curve (Instant build-up) is an effective measurement to assess the immediate build-up of internal structure in paste.

2. Parameters such as instant build-up, increase in static yield stress in each interval and average increase in static yield stress with time are important in the assessment of thixotropy.

3. The selected polycarboxylate ether (PCE) based superplasticizer (SP) shows higher thixotropic development and lower workability loss compared to the evaluated polynaftalene sulfonate (PNS) based superplasticizer.

4. It has been found that the demand of SP increased in pastes incorporating nanoparticles compared to micro-sized additive materials.

5. A ternary mixture with silica fume 5% and attapulgite clay 0.5% and a quaternary mixture with the selected slag 25%, silica fume 5% and attapulgite clay 0.5% significantly increases the demand of SP which causes a reduction in thixotropy development.

6. From the paste study, a ternary mixture with the evaluated cement, 25% slag and 5% silica fume yield high thixotropy development but also high workability loss, potentially suitable for onsite production of SCC for slip form paving application.

7. The gyratory intensive compaction testing machine is an effective tool for measuring the maximum packing density of aggregates.

8. When decreasing the paste layer thickness, the initial yield stress and thixotropy development decrease significantly due to increase in SP demand, when keeping the initial slump flow constant.

9. When keeping the SP quantity constant relative to the amount of cement, the viscosity, initial yield stress and thixotropic build-up generally increase with decreasing excess paste layer thickness.

10. An excess paste layer of 40 μm is selected due to its higher structural build-up rate and lower workability loss compared to mixtures with lower excess paste layer thickness. However, when keeping the SP dosage per kg of binder constant, the self-consolidating characteristics are compromised due to the low flowability.

11. A mixture with attapulgite clay (AC) shows consistent thixotropy development in the early and the extended time due to low workability loss.

12. A significant workability loss in binary mixtures with slag-B can be controlled by the application of attapulgite clay. A ternary mixture with slag-B and attapulgite shows high structural build up rate in the early and the more extended time period.

13. A binary mixture with attapulgite clay and a ternary mixture with slag-B and attapulgite clay could be good options for slip form paving application to investigate in future.

14. A better casting and demolding process is required to improve the green strength test, as results do not correlate well with the static yield stress development.

5.2 FUTURE RECOMMENDATIONS

1. Low-range and mid-range water reducers may be investigated on mixtures with different excess paste layer thickness to prevent loss in thixotropic buildup.

2. For VFC mixtures suitable for slip form pavement construction, SCMs and mineral admixtures should be re-investigated by reducing slump flow criteria to 450 mm.

3. More fine-inert material should be implemented in mixtures to reduce workability loss and to achieve better flowability and thixotropy.

4. Evaluation of correlation between static yield stress value and green strength is needed.

5. Green strength measurement need to be conducted on different molds with height varying from 75 mm to 200 mm. This can give better understanding of suitability of a particular mixture for a different pavement thickness. The correlation between the static yield stress and green strength measurement on different height molds can be evaluated.

APPENDIX

In this section, the mix design of the 40 μm excess paste layer mixture (C-SF-40) is explained.

1. Calculation of coarse and fine aggregate content

Based on the results obtained from ICT, following coarse and fine aggregate volume fractions and masses, ensuring high maximum packing density were selected.

Table III. Aggregate volume fraction data

Aggregates	Density kg/m^3 (ρ)	Vol. fraction	Mass/m^3 (W_{agg})	Vol./m^3
CA1 (19.0 mm)	2740	28.38%	598.5	0.22
CA2 (9.5 mm)	2780	20.25%	427.1	0.15
Fine Aggregate (FA)	2610	51.37%	1083.4	0.42

Therefore, total volume fraction of aggregate = 0.22 + 0.15 + 0.42

= 0.79

Paste volume fraction to fill voids between the aggregates (V_v) = 1 – 0.79

= 0.21

2. Calculation of total paste volume

From the aggregate gradation data, the surface area of aggregate was calculated for 19.0 mm, 9.5 mm, and fine aggregate. Particles finer than 75 μm are excluded from the gradation data and added into paste volume calculation. Aggregates are assumed to be spherical in shape.

Here, a sample calculation of 19.0 mm is shown below in Figure I:

Sieve size	Sieve size (m)	% Passing	% Passing between two subsequent sieves	Mass passing between two subsequent sieves, (kg)	Vol. passing between two subsequent sieves (V), (m^3)	Avg. diam (D) (m)	Particle volume (m^3)	Number of particles (N)	Surface area,(A) (m^2)
0	0	0.00	0	0.00	0.00	0.00	0.00	0.00E+00	0.00
No. 200	7.40E-05	0	0.00	0.00	0.00	3.70E-05	2.65E-14	0.00E+00	0.00
No. 100	1.49E-04	0.29	0.29	1.74	6.33E-04	1.12E-04	7.26E-13	8.73E+08	34.09
No. 30	5.95E-04	0.49	0.20	1.20	4.37E-04	3.72E-04	2.70E-11	1.62E+07	7.05
No. 8	2.38E-03	0.81	0.32	1.92	6.99E-04	1.49E-03	1.72E-09	4.06E+05	2.82
No. 4	4.76E-03	3.27	2.46	14.72	5.37E-03	3.57E-03	2.38E-08	2.26E+05	9.03
3/8	9.51E-03	18.07	14.80	88.58	3.23E-02	7.14E-03	1.90E-07	1.70E+05	27.19
1/2	1.27E-02	33.53	15.46	92.53	3.38E-02	1.11E-02	7.17E-07	4.71E+04	18.25
3/4	1.90E-02	79.26	45.73	273.71	9.99E-02	1.59E-02	2.08E-06	4.79E+04	37.81
1	2.54E-02	100	20.74	124.14	4.53E-02	2.22E-02	5.73E-06	7.91E+03	12.24

Figure I. Sample calculation of 19.0 mm aggregate surface area

Sample calculation for No. 100 sieve is as follows:

1) Mass passing between two subsequent sieves, (kg)

= (% Passing between two subsequent sieves $*$ $W_{agg}/100$)

= (0.29*598.5)/100 = 1.74 kg

2) Vol. passing between two subsequent sieves

= (Mass passing between two subsequent sieves / ρ_{agg})

= (1.74 / 2740) = 6.33E-04 m^3

3) Avg. diameter (D)

= Avg. of two subsequent sieve size

= (No. 200 + No. 100)/2

= (7.40E-05 + 1.49E-04)/2

= 1.12E-04 m

4) Particle volume

= $4*\pi*(0.5*D)^3/3$

= $4*\pi*(0.5*1.12E\text{-}04)^3/3$

= 7.26E-13 m^3

5) Number of particles (N)

= (Vol. passing between two subsequent sieves)/ particle volume

= (6.33E-04)/(7.26E-13)

= 8.73E+08

6) Surface area (A)

= $4 * \pi * (0.5*D)^2 * N$

= $4 * \pi * (0.5*1.12E-04)^2 * 8.73E+08$

= 34.09 m^2

Therefore, total surface area of 19.0 mm aggregate = 148.80 m^2

Similarly, total surface area of 9.5 mm aggregate = 138.71 m^2

total surface area of fine aggregate = 4313.31 m^2

For a 40 μm paste layer thickness,

$V_{pt} = ((SA_{CA1}+SA_{CA2}+SA_{FA}) * t) + V_v + V_{fa}$

Where,

V_{pt} = total paste volume

SA_{CA1} = 19.0 mm coarse aggregate surface area

SA_{CA2} = 9.5 mm coarse aggregate surface area

SA_{FA} = fine aggregate surface area

t = paste layer thickness

V_v = paste volume to fill voids between the aggregate

V_{fa} = aggregate particles finer than 75 μm in 19.0 mm, 9.5 mm, and fine aggregate

Therefore,

V_{pt} = ((148.8 + 138.71 + 4313.31) * 4.00E-05)) + 0.21 + 2.88E-04 + 2.98E-04 + 8.58E-04

= 0.184 + 0.21 + 2.88E-04 + 2.98E-04 + 8.58E-04

= 0.398 m^3

3. Calculation of paste component

Density of materials and specific gravity of aggregates are shown in Table below

Table IV Density of materials

Material	Density (γ) (g/cm^3)
Water (21 °C) (γ_w)	0.99802
Cement (γ_c)	3.1635
Silica fume (γ_{sf})	2.3878
Superplasticizer (γ_{sp})	1.032
CA1(19.0 mm) (γ_{CA1})	2.74
CA2 (9.5 mm) (γ_{CA2})	2.78
Fine aggregate (γ_{FA})	2.61

Table V. Paste component of C-SF-40 mixture

Material	Mass (kg)	Volume (m^3)	Volume (m^3)	Mass (kg)
Water	194.62	0.19500	0.193305	192.92
Cement	531.68	0.16806	0.166602	527.04
Silica fume	27.98	0.01171	0.011617	27.74
19.0 mm	0.79	0.00028	0.000286	0.78
9.5 mm	0.83	0.00029	0.000295	0.82
Fine agg.	2.24	0.00085	0.000851	2.22
SP Water (W_{spw})	1.26	0.00126	0.001255	1.25
SP Solid ($W_{sps)}$	0.69	0.00062	0.000620	0.68
Air		0.02368	0.023474	
TOTAL		0.402	0.398	

- w/b ratio = 0.35
- Air (%)/m^3 = 2%

  To proportionate air % with excess paste volume

  = (1+ paste volume to coat aggregate) * 2 % = (1+ 0.184) * 2 = 2.37%
- Superplasticizer with 35.2% solid content and dosage of 3.47 g/kg of binder materials is employed.

Results of paste component are shown in Table below. First two columns show obtained mass and volume of constituent materials. Then obtained volume and mass are proportioned back to the total volume of 0.398 m^3.

- Calculation of cement quantity

$$W_c = \left(\frac{V_{pt}-V_{air}-V_{af}}{\left(\frac{1}{\gamma_c}\right)+\left(\frac{w/b}{\gamma_w}\right)}\right) * \left(1 - \frac{\%\ binder\ replacement}{100}\right)$$

$$V_{af} = \text{Vol. fraction of aggregate} * \text{weight of finer particle in aggregates}$$

Vol. fraction of aggregate is obtained from Table I and weight of finer particles (< 75 μm) in aggregate is obtained from gradation data.

similarly, silica fume quantity

$$W_{sf} = \left(\frac{V_{pt}-V_{air}-V_{af}}{\left(\frac{1}{\gamma_c*1000}\right)+\left(\frac{w/b}{\gamma_w*1000}\right)}\right) * \left(\frac{\%\ binder\ replacement}{100}\right)$$

- Calculation of water content in SP

$$(W_{spw}) = \left[\left(\frac{V_{pt}-V_{air}}{\left(\frac{1}{\gamma_c*1000}\right)+\left(\frac{w/b}{\gamma_w*1000}\right)}\right) * \left(\frac{SP\ dosage}{1000}\right)\right] \left(\frac{100 - \%\ solid\ in\ SP}{100}\right)$$

similarly, solid content in SP,

$$(W_{sps}) = \left[\left(\frac{V_{pt} - V_{air}}{\left(\frac{1}{\gamma_c * 1000}\right) + \left(\frac{w/b}{\gamma_w * 1000}\right)} \right) * \left(\frac{SP\ dosage}{1000}\right) \right] \left(\frac{\%\ solid\ in\ SP}{100}\right)$$

- Calculation of water content = $\left(\text{Mass of binder materials} * \frac{w}{b}\right) - W_{spw}$

- Calculation of finer particles in all aggregate:

For example, in CA1 aggregate (W_{FCA1}) = V_{af} of CA1 * $\gamma_{CA1} * 1000$

Due to finer particles in aggregate and SP quantity total volume of paste is 0.402 m^3 which is slightly higher than calculated total paste volume (V_{pt}) = 0.398 m^3. So, volume of all materials is proportioned back to 0.398 m^3 as shown in column 3 of Table by multiplying the calculated total paste volume and divided by obtained total paste volume i.e., (0.398/0.402). Then, the mass of all materials is calculated by multiplying density of materials or specific gravity of aggregates as given in Table II.

4. Adjustment of total volume of concrete including excess paste layer to 1 m^3

Table IV below represents mix proportion of C-SF-40 mixture. First column shows obtained mass of paste component and aggregate from Table III and Table I. Second column shows volume of constituent materials and total volume of concrete including excess paste volume. The volume of constituent materials is calculated by multiplying density of materials or specific gravity of aggregates. Third and fourth column shows obtained volume and mass of constituent materials respectively proportioned back to 1 m^3 as explained in step 3.

Table III Mix proportion of C-SF-40 mixture

Material	Mass (kg)	Vol. (m3)	Vol. (m3)	Mass (kg)
Water	192.92	0.19	0.17	166.506
Cement	527.04	0.17	0.14	454.880
Silica fume	27.74	0.01	0.01	23.941
SP	1.93	0.00	0.00	1.668
Air		0.02	0.02	
3/4 agg	598.53	0.22	0.19	516.580
3/8 Agg	427.07	0.15	0.13	368.596
Fine Agg	1083.39	0.39	0.34	877.871
Total		1.16	1.00	

5. Adjustment of moisture content in mix design

Finally, according to absorption and total moisture content in aggregates the actual amount of water for mixing and aggregate is adjusted.

REFERENCES

[1] Pavementinteractive.org, "Slipform Paving," *Pavement Interactive*, 2012. [Online]. Available: http://www.pavementinteractive.org/slipform-paving/.

[2] ACP, "Construction of Portland Cement Concrete Pavements.," *Natl. Highw. Inst. Course No. 13133. AASHTO/FHWA/Industry Jt. training.*, p. VI23-26, 1995.

[3] R. Rodden, "Roadway paving operations," *Construction and rehabilitation of concrete pavements*, 2015.

[4] Texas Department of Transportation, "Pavement Manual," *Texas Departmetn Transp.*, 2017.

[5] S. Tymkowicz and R. Steffes, "Vibration study for consolidation of Portland cement concrete.," *Transp. Res. Rec. J. Transp. Res. Board*, no. 1574, pp. 109–115, 1997.

[6] A. Ardani, S. Hussain, and R. Laforce, "Evaluation of Premature PCC Pavement Longitudinal Cracking in Colorado," in *Proceedings of the 2003 Mid-Continent Transportation Research Symposium*, 2003, pp. 1–9.

[7] USACE, *Engineering and Design – Evaluation and Repair of Concrete Structures*, EM 1110-2-. Washinton, D.C.: U.S. Army Corps of Engineers, 1995.

[8] K. Wang, S. P. Shah, D. J. White, T. Voigt, J. Gray, L. Gang, J. Hu, C. Halverson, and B. Y. Pekmezci, "Self-Consolidating Concrete — Applications for Slip-Form Paving : Phase I (Feasibility Study)," 2005.

[9] B. Y. Pekmezci, T. Voigt, K. Wang, and S. P. Shah, "Low compaction energy concrete for improved slipform casting of concrete pavements," *ACI Mater. J.*, vol. 104, no. 3, pp. 251–258, 2007.

[10] K. Wang, S. P. Shah, J. Grove, P. Taylor, P. Wiegand, B. Steffes, G. Lomboy, Z. Quanji, L. Gang, and N. Tregger, "Self-Consolidating Concrete—Applications for Slip-Form Paving: Phase II," Ames, IA, 2011.

[11] C. W. Macosko, *Rheology: principles, measurements, and applications*. Wiley-vch, 1994.

[12] E. P. Koehler, "Use Rheology to specify, Design and manage self-consolidating concrete," in *9th ACI International Conference on Superplasticizers & 10th International Conference on Recent*, 2009, pp. 609–623.

[13] H. A. Barnes, "Thixotropy," *J. Nonnewton. Fluid Mech.*, vol. 257, no. 97, pp. 4–9, 1997.

[14] P. Coussot, Q. D. Nguyen, H. T. Huynh, and D. Bonn, "Avalanche behavior in yield stress fluids," *Phys. Rev. Lett.*, vol. 88, no. 17, pp. 1755011–1755014, 2002.

[15] D. Feys, "Interacties tussen de reologische eigenschappen en het verpompen van zelfverdichtend beton Interactions between Rheological Properties and Pumping of Self-Compacting Concrete," 2009.

[16] R. Ferron, A. Gregori, Z. Sun, and S. P. Shah, "Rheologic& Method to Evaluate Structura Buildup in Self-Consolidating Concrete Cement Pastes," *ACI Mater. J.*, vol. 104, no. 3, pp. 242–250, 2007.

[17] J. Assaad and K. H. Khayat, "Assessment of Thixotropy of Self-Consolidating Concrete and Concrete-Equivalent-Mortar - Effect of Binder Composition and Content," *ACI Mater. J.*, vol. 101, no. 5, pp. 400–408, 2004.

[18] N. Roussel, "A thixotropy model for fresh fluid concretes: Theory, validation and applications," *Cem. Concr. Res.*, vol. 36, no. 10, pp. 1797–1806, 2006.

[19] N. Roussel, G. Ovarlez, S. Garrault, and C. Brumaud, "The origins of thixotropy of fresh cement pastes," *Cem. Concr. Res.*, vol. 42, no. 1, pp. 148–157, 2012.

[20] J. E. Wallevick, "Rheology of particle suspension: fresh concrete, mortar and cement paste with various types of lignosulfates," The Norwegian University of Science and Technology, 2003.

[21] J. Mewis and N. J. Wagner, "Thixotropy," *Adv. Colloid Interface Sci.*, vol. 147–148, no. C, pp. 214–227, 2009.

[22] P. Billberg, *Form Pressure Generated by Self-Compacting Concrete — Influence of Thixotropy and Structural Behaviour at Rest Peter Billberg School of Architecture and the Built Environment Division of Concrete Structures Royal Institute of Technology*, no. May. 2006.

[23] P. Jarvis, B. Jefferson, J. Gregory, and S. A. Parsons, "A review of floc strength and breakage," *Water Res.*, vol. 39, no. 14, pp. 3121–3137, 2005.

[24] J. E. Wallevik, "Rheological properties of cement paste: Thixotropic behavior and structural breakdown," *Cem. Concr. Res.*, vol. 39, no. 1, pp. 14–29, 2009.

[25] A. M. Neville and J. J. Brooks, *Concrete technology*. 1987.

[26] R. J. Flatt and Y. F. Houst, "A simplified view on chemical effects perturbing the action of superplasticizers," *Cem. Concr. Res.*, vol. 31, no. 8, pp. 1169–1176, 2001.

[27] P. Coussot, *Rheometry of Pastes, Suspensions, and Granular Materials*. New Jersey: John Wiley & sons, 2005.

[28] K. H. Khayat, M. Saric-Coric, and F. Liotta, "Influence of thixotropy on stability characteristics of cement grout and concrete," *ACI Mater. J.*, vol. 99, no. 3, pp. 234–241, 2002.

[29] K. H. Khayat and J. Assaad, “Use of thixotropy-enhancing agent to reduce formwork pressure exerted by self-consolidating concrete,” *ACI Mater. J.*, vol. 105, no. 1, pp. 88–96, 2008.

[30] J. Assaad and K. H. Khayat, “Formwork pressure of self-consolidating concrete made with various binder types and contents,” *ACI Mater. J.*, vol. 102, no. 4, pp. 215–223, 2005.

[31] J. Assad and K. H. Khayat, “Effect of Viscosity-Enhancing Admixtures on Formwork Pressure and Thixotropy of Self-Consolidating Concrete,” *ACI Mater. J.*, vol. 103, no. 4, pp. 280–287, 2006.

[32] R. Lapasin, A. Papo, and S. Rajgelj, “Flow behavior of fresh cement pastes. A comparison of different rheological instruments and techniques,” *Cem. Concr. Res.*, vol. 13, no. 3, pp. 349–356, 1983.

[33] R. S. Ahari, T. K. Erdem, and K. Ramyar, “Thixotropy and structural breakdown properties of self consolidating concrete containing various supplementary cementitious materials,” *Cem. Concr. Compos.*, vol. 59, pp. 26–37, 2015.

[34] P. F. G. Banfill and D. C. Saunders, “On the viscometric examination of cement pastes,” *Cem. Concr. Res.*, vol. 11, no. 3, pp. 363–370, 1981.

[35] G. Ovarlez and N. Roussel, “A Physical Model for the Prediction of Lateral Stress Exerted by Self-Compacting Concrete on Formwork,” *Mater. Struct.*, vol. 39, no. 2, pp. 269–279, 2007.

[36] N. Roussel and F. Cussigh, “Distinct-layer casting of SCC: The mechanical consequences of thixotropy,” *Cem. Concr. Res.*, vol. 38, no. 5, pp. 624–632, 2008.

[37] M. K. Rahman, M. H. Baluch, and M. A. Malik, “Thixotropic behavior of self compacting concrete with different mineral admixtures,” *Constr. Build. Mater.*, vol. 50, pp. 710–717, 2014.

[38] B. Topçu and T. Uygunoğlu, “Influence of mineral additive type on slump-flow and yield stress of self-consolidating mortar,” *Sci. Res. Essays*, vol. 5, no. 12, pp. 1492–1500, 2010.

[39] K. H. Khayat and J. Assaad, “Effect of w/cm and high-range water-reducing admixture on formwork pressure and thixotropy of self-consolidating concrete,” *ACI Mater. J.*, vol. 103, no. 3, pp. 186–193, 2006.

[40] J. Assaad and K. H. Khayat, “Effect of coarse aggregate characteristics on lateral pressure excerted by Self-Consolidating Concrete,” *ACI Mater. J.*, vol. 102, no. 3, pp. 145–153, 2005.

[41] A. Ghezal, K. H. Khayat, and D. Beaupré, “Effect of High-Range Water-Reducer—Viscosity-Modifying Admixture Combination on Rheological Properties of Concrete Equivalent Mortar,” in *In Proceedings of the First North American Conference on the Design and Use of Self-Consolidating Concrete*, 2002, pp. 159–165.

[42] A. Leemann and F. Winnefeld, “The effect of viscosity modifying agents on mortar and concrete,” *Cem. Concr. Compos.*, vol. 29, no. 5, pp. 341–349, 2007.

[43] G. Tattersall and P. Banfill, “The rheology of fresh concrete,” *London: Pitman*, vol. 759, 1983.

[44] E. Güneyisi and M. Gesoğlu, “Properties of self-compacting mortars with binary and ternary cementitious blends of fly ash and metakaolin,” *Mater. Struct.*, vol. 41, no. 9, pp. 1519–1531, 2008.

[45] N. A. Tregger, M. E. Pakula, and S. P. Shah, “Influence of clays on the rheology of cement pastes,” *Cem. Concr. Res.*, vol. 40, no. 3, pp. 384–391, 2010.

[46] S. Kawashima, J. H. Kim, D. J. Corr, and S. P. Shah, “Study of the mechanisms underlying the fresh-state response of cementitious materials modified with nanoclays,” *Constr. Build. Mater.*, vol. 36, pp. 749–757, 2012.

[47] Z. Quanji, G. R. Lomboy, and K. Wang, “Influence of nano-sized highly purified magnesium alumino silicate clay on thixotropic behavior of fresh cement pastes,” *Constr. Build. Mater.*, vol. 69, pp. 295–300, 2014.

[48] S. Kawashima, P. Hou, D. J. Corr, and S. P. Shah, “Modification of cement-based materials with nanoparticles,” *Cem. Concr. Compos.*, vol. 36, no. 1, pp. 8–15, 2013.

[49] H. G. Roby, “Pressure of Concrete on Forms,” *Civ. Eng.*, vol. 5.

[50] J. Assaad and K. H. Khayat, “Variations of Lateral and Pore Water Pressure of Self-Consolidating Concrete at Early Age,” *ACI Mater. J.*, vol. 101, no. 4, pp. 310–317, 2004.

[51] S. Nunes, P. M. Oliveira, J. S. Coutinho, and J. Figueiras, “Rheological characterization of SCC mortars and pastes with changes induced by cement delivery,” *Cem. Concr. Compos.*, vol. 33, no. 1, pp. 103–115, 2011.

[52] K. Juvas, A. Kappi, K. Salo, and E. Nordenswan, “The Effects of Cement Variations on Concrete Workability,” *Nord. Concr. Res.*, vol. 26, pp. 39–46, 2001.

[53] Z. Quanji, “Thixotropic behavior of cement-based materials : effect of clay and cement types,” Iowa State University, 2010.

[54] N. Yildiz, M. Erol, B. Baran, Y. Sarikaya, and A. Calimli, “Modification of rheology and permeability of Turkish ceramic clays using sodium silicate,” *Appl. Clay Sci.*, vol. 13, no. 1, pp. 65–77, 1998.

[55] A. A. A. Hassan, M. Lachemi, and K. M. A. Hossain, “Effect of Metakaolin on the Rheology of Self-Consolidating Concrete,” in *Design, Production and Placement of Self-Consolidating Concrete*, no. 9, K.H. Khayat and D. Feys, Ed. Dordrecht: Springer Netherlands, 2010, pp. 103–112.

[56] E. L. Ore and J. J. Straughan, “Effect of cement hydration on concrete form pressure,” *ACI J.*, vol. Title No., pp. 111–120, 1968.

[57] N. J. Gardner, “Formwork Pressures and Cement Replacement by Fly Ash,” *Concr. Int.*, vol. 6, no. 10, pp. 50–55, 1984.

[58] N. J. Gardner, “The Effect of Superplasticizers and Fly Ash on Formwork Pressures,” *Form. Econ. Concr. Build. Portl. Cem. Assoc.*, p. 21.1-21.12., 1982.

[59] K. H. Khayat, “Viscosity-Enhancing Admixtures for Cement-Based Materials - An Overview,” *Cement*, vol. 20, pp. 171–188, 1998.

[60] B. Helnan-Moussa, Y. Vanhove, and E. Wirguin, “Thixotropic behaviour and structural breakdown of fresh cement paste: comparison between two types of VMA,” *Adv. Cem. Res.*, vol. 25, no. 4, pp. 235–244, 2013.

[61] F. Van Der Vurst, S. Grünewald, and G. De Schutter, “The Impact of VMA on the Rheology, Thixotropy and Robustness of Self-compacting Mortars,” *Calcined Clays Sustain. Concr.*, vol. 10, pp. 159–167, 2015.

[62] Q. Yuan, D. Zhou, K. H. Khayat, D. Feys, and C. Shi, “On the measurement of evolution of structural build-up of cement paste with time by static yield stress test vs. small amplitude oscillatory shear test,” *Cem. Concr. Res.*, vol. 99, no. September 2016, pp. 183–189, 2017.

[63] T. Voigt, J.-J. Mbele, K. Wang, and S. P. Shah, “Using Fly Ash, Clay, and Fibers for Simultaneous Improvement of Concrete Green Strength and Consolidatability for Slip-Form Pavement,” *J. Mater. Civ. Eng.*, vol. 22, no. 2, pp. 196–206, 2010.

[64] R. Breitenbücher, D. Sarmiento, and F. Holzmann, “Development of Self-compacting Concrete with Good Shape Stability for Slipform Construction,” *Adv. Civ. Eng. Mater.*, vol. 3, no. 2, p. 20130106, 2015.

[65] H. Hoornahad, E. A. B. Koenders, and K. Van Breugel, “Towards the development of self-compacting no-slump concrete mixtures,” *J. Sillicate Based Compos. Mater.*, vol. 67, no. 4, pp. 135–139, 2015.

[66] K. Wang, S. P. Shah, and T. Voigt, “A novel self-consolidating concrete for slip-form application,” *Transp. Res. Board*, pp. 1–11, 2006.

[67] G. Lomboy, K. Wang, P. Taylor, and S. P. Shah, “Guidelines for design, testing, production and construction of semi-flowable SCC for slip-form paving,” *Int. J. Pavement Eng.*, vol. 13, no. 3, pp. 216–225, 2011.

[68] J. M. Khatib, “Performance of self-compacting concrete containing fly ash,” *Constr. Build. Mater.*, vol. 22, no. 9, pp. 1963–1971, 2008.

[69] J. Armaghani, K. Tawfiq, S. Squillacote, and M. Bergin, “Accelerated Slab Replacement Using Self-Consolidating Concrete,” *Transp. Res. Rec. J. Transp. Res. Board*, vol. 2508, pp. 93–101, 2015.

[70] X. Wang, K. Wang, J. Li, N. Garg, and S. P. Shah, “Properties of self-consolidating concrete containig high-volume supplementary cementitious materials and nano-limestone,” *J. Sustain. Cem. Mater.*, vol. 13, pp. 245–255, 2014.

[71] N. Garg and K. Wang, “Comparing the performance of different commercial clays in fly ash-modified mortars,” *J. Sustain. Cem. Mater.*, vol. 1, no. 3, pp. 111–125, 2012.

[72] H. Lindgreen, M. Geiker, H. Krøyer, N. Springer, and J. Skibsted, “Microstructure engineering of Portland cement pastes and mortars through addition of ultrafine layer silicates,” *Cem. Concr. Compos.*, vol. 30, no. 8, pp. 686–699, 2008.

[73] G. Bumanis, D. Bajare, and A. Korjakins, “Durability of High Strength Self Compacting Concrete with Metakaolin Containing Waste,” *Key Eng. Mater.*, vol. 674, pp. 65–70, 2016.

[74] Z. Ge, K. Wang, R. Sun, D. Huang, and Y. Hu, “Properties of self-consolidating concrete containing nano-CaCO $_3$,” *J. Sustain. Cem. Mater.*, vol. 3, no. 3–4, pp. 191–200, 2014.

[75] J. Han, H. Fang, and K. Wang, “Design and control shrinkage behavior of high-strength self-consolidating concrete using shrinkage-reducing admixture and super-absorbent polymer,” *J. Sustain. Cem. Mater.*, vol. 3, no. 3–4, pp. 182–190, 2014.

[76] E. P. Koehler, “Aggregates in self-consolidating concrete.,” The University of Texas at Austin, 2007.

[77] F. V. Mueller, O. H. Wallevik, and K. H. Khayat, “Linking solid particle packing of Eco-SCC to material performance,” *Cem. Concr. Compos.*, vol. 54, pp. 117–125, 2014.

[78] K. H. Khayat and I. Mehdipour, “Design and Performance of Crack-Free Environmentally Friendly Concrete Design and Performance of Crack-Free Environmentally Friendly Concrete ‘ Crack-Free Eco-Crete ,’” 2014.

[79] J. Brouwers and H. J. Radix, “Self-compacting concrete: the role of the particle size distribution,” *First Int. Symp. Des. Perform. Use Self-Consolidating Concr.*, vol. 0, no. May, pp. 109–118, 2005.

[80] M. Hunger and J. Brouwers, “Natural Stone Waste Powders Applied to SCC Mix Design,” *Restor. Build. Monum.*, vol. 14, no. 2, pp. 131–140, 2008.

[81] P. Ferrari, “Testing of no-slump concrete with gyratory compactor,” October, 2006.

[82] F. Concrete, “Compactibility With IC–Tester–Method NT BUILD 427.,” *Nord. Scand. Institution.*, 1994.

[83] B. Esmaeilkhanian, K. H. Khayat, and O. H. Wallevik, “Mix design approach for low-powder self-consolidating concrete: Eco-SCC—content optimization and performance,” *Mater. Struct.*, vol. 50, no. 2, p. 124, 2017.

[84] C. T. Kennedy, “The design of concrete mixesNo Title,” *J. Proc.*, vol. 36, no. 2, pp. 373–400, 1940.

[85] S. G. Oh, T. Noguchi, and F. Tomosawa, “Toward mix design for rheology of self-compacting concrete,” in *In proc. of First International RILEM Symposium on Self-Compacting Concrete*, 1999, pp. 361–372.

[86] A. Denis, A. Attar, D. Breysse, and J. J. Chauvin, “Effect of coarse aggregate on the workability of sandcrete,” *Cem. Concr. Res.*, vol. 32, no. 5, pp. 701–706, 2002.

[87] A. K. H. Kwan and L. G. Li, “Combined effects of water film, paste film and mortar film thicknesses on fresh properties of concrete,” *Constr. Build. Mater.*, vol. 50, pp. 598–608, 2014.

[88] M. Geiker, M. Brandl, L. Thrane, and L. Nielsen, “On the Effect of Coarse Aggregate Fraction and Shape on the Rheological Properties of Self-Compacting Concrete,” *Cem. Concr. Aggregates*, vol. 24, no. 1, p. 3, 2002.

[89] H. B. Jovein and L. Shen, “Effects of Aggregate Properties on Rheology of Self-Consolidating Concrete,” *Adv. Civ. Eng. Mater.*, vol. 5, no. 1, pp. 235–255, 2016.

[90] B. Ildefonse, C. Allain, and C. Coussot, *Des grands écoulements naturels à la dynamique du tas de sable: introduction aux suspensions en géologie et en physique*. Editions Quae, 1997.

[91] I. M. Krieger and T. J. Dougherty, “A mechanism for non-Newtonian flow in suspensions of rigid spheres,” *Trans. Soc. Rheol.*, vol. 3, no. 1, pp. 137–152, 1959.

[92] F. Mahaut, S. Mokéddem, X. Chateau, N. Roussel, and G. Ovarlez, “Effect of coarse particle volume fraction on the yield stress and thixotropy of cementitious materials,” *Cem. Concr. Res.*, vol. 38, no. 11, pp. 1276–1285, 2008.

[93] X. Chateau, G. Ovarlez, and K. L. Trung, “Homogenization approach to the behavior of suspensions of noncolloidal particles in yield stress fluids,” pp. 1–17, 2010.

[94] I. Mehdipour, “Characterization and performance of eco and crack-free high-performance concrete for sustainable infrastructure,” Missouri university of science and technology, 2017.

[95] Avantech Engineering Consortium Pvt. Ltd., “ICAR Rheometer,” 2017. .

[96] H. Brouwers, “The Role of Nanotechnology for the Development of Sustainable Concrete (Michigan),” in *Proceedings of ACI Session Nanotechnology of concrete: recent developments and future perspectives*, 2006, vol. 7, no. November, pp. 69–90.

[97] N. Roussel and P. Coussot, "'Fifty-cent rheometer' for yield stress measurements: from slump to spreading flow," *J. Rheol. (N. Y. N. Y).*, vol. 49, no. 3, pp. 705–718, 2005.

[98] H. Yazici, "The effect of silica fume and high-volume Class C fly ash on mechanical properties, chloride penetration and freeze-thaw resistance of self-compacting concrete," *Constr. Build. Mater.*, vol. 22, no. 4, pp. 456–462, 2008.

[99] H. A. Mohamed, "Effect of fly ash and silica fume on compressive strength of self-compacting concrete under different curing conditions," *Ain Shams Eng. J.*, vol. 2, no. 2, pp. 79–86, 2011.

[100] M. Gesoğlu, E. Güneyisi, and E. Özbay, "Properties of self-compacting concretes made with binary, ternary, and quaternary cementitious blends of fly ash, blast furnace slag, and silica fume," *Constr. Build. Mater.*, vol. 23, no. 5, pp. 1847–1854, 2009.

[101] K. Celik, C. Meral, A. Petek Gursel, P. K. Mehta, A. Horvath, and P. J. M. Monteiro, "Mechanical properties, durability, and life-cycle assessment of self-consolidating concrete mixtures made with blended portland cements containing fly ash and limestone powder," *Cem. Concr. Compos.*, vol. 56, pp. 59–72, 2015.

[102] D. Ouyang, W. Xu, T. Y. Lo, and J. F. C. Sham, "Increasing mortar strength with the use of activated kaolin by-products from paper industry," *Constr. Build. Mater.*, vol. 25, no. 4, pp. 1537–1545, 2011.

[103] X. Gao, S. Kawashima, X. Liu, and S. P. Shah, "Influence of clays on the shrinkage and cracking tendency of SCC," *Cem. Concr. Compos.*, vol. 34, no. 4, pp. 478–485, 2012.

[104] G. Lomboy, K. Wang, M. Asce, and C. Ouyang, "Shrinkage and Fracture Properties of Semiflowable Self-Consolidating Concrete," *J. Mater. Civ. Eng.*, vol. 23, no. 11, pp. 1514–1524, 2011.

[105] F. Wang, Y. Zhou, B. Peng, Z. Liu, and S. Hu, "Autogenous shrinkage of concrete with super-absorbent polymer," *ACI Mater. J.*, vol. 106, no. 2, pp. 123–127, 2009.

[106] R. Loser and a. Leemann, "Shrinkage and restrained shrinkage cracking of self-compacting concrete compared to conventionally vibrated concrete," *Mater. Struct.*, vol. 42, pp. 71–82, 2009.

[107] S. D. Hwang and K. H. Khayat, "Effect of mixture composition on restrained shrinkage cracking of self-consolidating concrete used in repair," *ACI Mater. J.*, vol. 105, no. 5, pp. 499–509, 2008.

[108] K. Saito, M. Kinoshita, H. Umehara, and R. . Yoshida, "Properties of low-shrinkage, high-strength SCC using shrinkage-reducing admixture, blast furnace slag and limestone aggregates.," in *Design, Production and Placement of Self-Consolidating Concrete*, 2010, pp. 283–293.

[109] D. Bentz, M. Peltz, K. Snyder, and J. Davis, "VERDiCT: viscosity enhancers reducing diffusion in concrete technology," *Concr. Int.*, vol. 31, no. 1, pp. 31–36, 2009.

[110] K. H. Khayat and W. J. Long, "Shrinkage of precast, prestressed self-consolidating concrete," *ACI Mater. J.*, vol. 107, no. 3, 2010.

[111] M. Heikal, M. S. Morsy, and I. Aiad, "Effect of polycarboxylate superplasticizer on hydration characteristics of cement pastes containing silica fume," *Ceram. - Silikaty*, vol. 50, no. 1, pp. 5–14, 2006.

[112] ASTM C128-15, 2015, "Standard Test Method for Relative Density (Specific Gravity) and Absorption of Fine Aggregate," ASTM international, West Conshohocken, PA, 2015

[113] ASTM C136-14, 2014, "Standard Test Method for Sieve Analysis of Fine and Coarse Aggregates," ASTM international, West Conshohocken, PA, 2014

[114] ASTM C127-15, 2015, "Standard Test Method for Relative Density (Specific Gravity) and Absorption of Coarse Aggregate," ASTM international, West Conshohocken, PA, 2015

[115] ASTM C1611/C1611M-14, 2014, "Standard Test Method for Slump Flow of Self-Consolidating Concrete," ASTM international, West Conshohocken, PA, 2014

[116] ASTM C138/C138M-08, 2008, "Standard Test Method for Density (Unit Weight), Yield, and Air Content (Gravimetric) of Concrete," ASTM international, West Conshohocken, PA, 2008

[117] ASTM C231/C231M-14, 2014, "Standard Test Method for Air Content of Freshly Mixed Concrete by the Pressure Method," ASTM international, West Conshohocken, PA, 2014

[118] ASTM C31/C31-15,2015, "Standard Practice for Making and Curing Concrete Test Specimens in the Field," ASTM international, West Conshohocken, PA, 2015

[119] ASTM C39/C39M – 11a, "Standard Test Method for Compressive Strength of Cylindrical Concrete Specimens," ASTM international, West Conshohocken, PA, 2011

[120] ASTM C496-11, "Splitting Tensile Strength of Cylindrical Concrete Specimens," ASTM international, West Conshohocken, PA, 2011

VITA

Piyush Rajendra Lunkad was born in Jalgaon, Maharashtra, India. In the fall of 2009, he started his undergraduate studies at G.H. Raisoni College of Engineering and graduated in fall 2013. During his undergraduate study, Piyush had the opportunity to work as a site engineer intern at Angira Buildcon Pvt. Ltd. After his undergraduate studies, he worked as a trainee design engineer at Structures - a structural design consultancy firm for a year. In fall 2015, he started the Civil Engineering Master's program at the Missouri University of Science and Technology. During his graduate studies he held positions of graduate research assistant and graduate teaching assistant in the Department of Civil, Architectural, and Environmental Engineering. Piyush completed his Masters of Science in Civil Engineering with a Structural and Material emphasis in May, 2018.